Chem Soc Rev

Activation and catalytic transformation of methane under mild conditions

Journal:	*Chemical Society Reviews*
Manuscript ID	CS-REV-08-2021-000783
Article Type:	Review Article
Date Submitted by the Author:	18-Aug-2021
Complete List of Authors:	Tang, Yu; Fuzhou University, Li, Yuting; University of Kansas, Department of Chemical and Petroleum Engineering Tao, Franklin; University of Kansas,

Activation and catalytic transformation of methane under mild conditions

Yu Tang,[a]* Yuting Li,[b] and Franklin (Feng) Tao [b]*

Institute of Molecular Catalysis and In-situ/operando Studies, College of Chemistry, Fuzhou University, Fujian, 350000 China [a]

Department of Chemical and Petroleum Engineering, University of Kansas, KS 66045, USA[b]

* To whom all correspondence should be addressed to. Email: tangyu.zju@gmail.com and frankin.tao.2017@gmail.com

Authors' biographies

Yu Tang

Professor Yu Tang received his Bachelor and Master's degrees in chemistry from Zhejiang University and PhD degree from University of Kansas. His expertise is in-situ and operando studies of catalysts and fundamental studies of molecular catalysis including transformation of methane. He was offered a faculty position by Fuzhou University for building the Institute of molecular catalysis and in situ/operando studies of catalysts. Currently, he is a professor in chemistry and leading the Institute of Molecular Catalysis and In-situ/operando Studies at College of Chemistry at Fuzhou University. He has co-authored over 60 publications in international journals of chemistry.

Yuting Li

Dr. Yuting Li received her Bachelor degree from Tianjin University and PhD degree from University of Kansas. Her expertise is in-situ and operando studies of catalysis and fundamental studies of transformation of small molecules to value-added chemicals through heterogeneous catalysis at high temperature and under mild conditions. Her research interests are heterogeneous catalysis through in situ and operando characterization and development of catalysts for chemical transformation through chemical synthesis.

Franklin (Feng) Tao

Professor Franklin (Feng) Tao received his PhD from Princeton University. He worked as a postdoctoral research fellow at University of California at Berkeley in Prof. Gabor Somorjai group and Prof. Miquel Salmeron group before starting his independent career. He was elected as a fellow of Royal Society of Chemistry (RSC) in 2013 and a fellow of American Association for the Advancement of Sciences (AAAS) in 2017. His research interests are fundamental understanding of catalysis at a molecular level including single atom catalysis, bimetallic catalysis, reducible oxide catalysis, and in-situ/operando characterizations. He co-authored about 190 articles in important international journals.

Abstract

In the last a few decades, scientists were motivated by the goal of producing chemicals from the widely available, tremendous amount of low-cost resource, methane (CH_4). To achieve this goal, a whole library of catalytic chemistries of transforming CH_4 to various products is requested to develop. Worldwide scientists have made significant efforts to reach this goal. These significant efforts have demonstrated the feasibility of oxidation of CH_4 to value-added intermediate compounds including but not limited to CH_3OH, HCHO, HCOOH, and CH_3COOH *under mild conditions*. Fundamental understandings of these chemical and catalytic transformations of CH_4 under mild conditions have been achieved to some extent although currently neither a catalyst nor a catalytic process could be used for chemical production under mild conditions at a large scale. In academic community, over ten different reactions were developed for converting CH_4 to different types of oxygenates under mild conditions in terms of a relative low activation or catalysis temperature. However, there is still lack of molecule-level understanding of activation and catalysis processes performed in extremely complex reaction environment under mild conditions. This review was launched for discussing these achievements obtained so far and exploring any prospective in efficient chemical production from CH_4 in the future. In this review, different oxidative activations of CH_4 or catalytic transformations toward chemical production under mild conditions were reviewed in parallel, by which the track of developing catalysts for a specific reaction was identified and insights of designing these catalysts were deposited. As a whole this review focuses on discussing profound insights gained through endeavours of scientists in this field. It aims at presenting a relatively complete picture for activation and catalytic transformations of CH_4 to value-added chemicals under mild conditions. In this review, suggestions of potential explorations for production of chemicals from CH_4 under mild conditions are made. Challenges being faced by the community in the efforts to achieve the goal are highlighted and possible solutions to tackle them are briefly proposed.

1. Introduction

1.1 Availability of worldwide methane and chemical transformation of methane at high temperature versus low temperature

Methane has been used for production of numerous chemicals through thermal catalysis at high temperature or relatively high temperature for decades (Figure 1). Unfortunately, these practices exhibit significant disadvantages. One is the high cost of transportation of natural gas in liquid due to its extremely low boiling point at -164^{o}C. The other is heavy consumption of energy in current high-temperature catalytic conversions of CH_4 in industries as these currently conversion processes are mostly performed at high temperature.[1, 2] For instance, both steam and dry reformings of CH_4 are heavily endothermic and thus production of one mole of CO through CH_4 reforming request a heat supply of at least 206-247 kJ.[1] In addition, short lives of catalysts working at high temperature have largely increased the cost of CH_4-based production of value-added chemicals. To break these limits, transformation of CH_4 to valuable chemicals *under mild conditions* have been explored in the last decades toward efficient utilization of CH_4 economically and environmentally friendly. Here a mild condition is defined to an activation or a catalytic transformation of CH_4 at a temperature lower than 250^{o}C. In general, it covers biocatalysis at room temperature, homogeneous catalysis at near room temperature and heterogenous catalysis mostly at a low temperature (<150^{o}C) or sometimes at a relatively low temperature (150-250^{o}C).

The enormous advantage of transformation of CH_4 to value-added chemicals under mild conditions has attracted significant efforts in the last decades. Scientists have made significant progress in formation of high value chemicals from CH_4 under mild conditions. Feasibility of transforming CH_4 to important intermediate compounds under mild conditions has been demonstrated. Through these efforts numerous new catalysts have been developed although neither an acceptable durability nor a reasonably high activity has been exhibited from these catalysts. From fundamental science point of view, significant amount of knowledge on noncatalytic oxidation and catalytic transformation have been obtained. Thus, it is the time to review this vital topic, activation and catalytic transformation of CH_4 *under mild conditions* from fundamental science point of view. In this review article, we will discuss the progresses on this topic achieved recently, review the fundamental understanding of reaction mechanisms in these transformations, deposit insights gained in developing new catalysts, present grand challenges our community are still faced, and brief promising solutions to tackle them.

1.2 Brief of catalytic transformation of CH_4 at high temperature

Figure 1 presents these catalytic routes for producing important intermediate compounds in chemical industries by starting from CH_4 for production of valuable chemicals. These high temperature transformations of CH_4 can be primarily categorized into direct and indirect conversions. Through a direct conversion, CH_4 is transformed to important intermediate compounds such as ethylene, benzene, toluene, xylene, and oxygenates. In terms of an indirect conversion, CH_4 is first transformed to syngas, a mixture of CO and H_2; then the syngas is converted to several types of intermediate compounds or valuable chemicals including alcohol, different hydrocarbons, alcohols, dimethyl ether, and oxygenates typically through Fisher-Tropsch synthesis.[3-20]

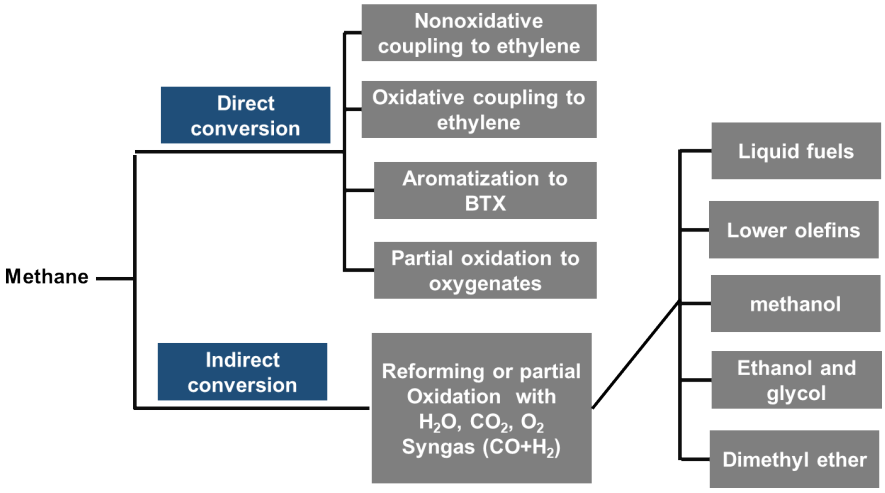

Figure 1. *Developed main production routes using* CH_4 *as the starting material to produce important intermediate compounds or value-added chemicals through direct or indirect transformations at high temperature.*

Alternatively, these high temperature catalytical reactions of CH_4 presented in Figure 1 can be classified into oxidation and dehydrogenation. Through oxidative process, CH_4 can be transformed to alcohol, aldehyde, acid, ester and many other organic oxygenates. In general, catalytic oxidations of CH_4 include steam reforming,[21-25] dry reforming[1, 26-36] and partial oxidation[37-42] to form syngas, oxidative coupling of CH_4 to form ethylene,[43-47] and even complete oxidation to form CO_2 and H_2O.[48-52] Notably, partial oxidation of CH_4, oxidative coupling of CH_4, or oxidative dehydrogenation of C_2H_6 or C_3H_8 at high temperature involves both catalysis reactions performed on surface of catalysts and radical-based reaction occurred in gas phase at high temperature. Typically, these high-temperature radical-based steps are more out of control; thus, there has been very limited understanding to these high-temperature

radical reactions.[45, 47, 53, 54] Inspiringly, characterisation methods of radicals formed at high temperature were developed recently[53, 55] and have been successfully used in fundamental studies of high-temperature transformations of CH_4.[53, 55] As complete oxidation is always more thermodynamically favourable compared to partial oxidation, oxidative coupling and oxidative dehydrogenation, CO_2 and H_2O are typically by-products of incomplete oxidation occurred at high temperature.

Different from oxidative transformation, another category of high temperature catalysis is dehydrogenation. Compared to the exothermic nature of incomplete oxidation of CH_4, C_2H_6, and C_3H_8, direct dehydrogenation of CH_4 to C and H_2 or C_2H_6 and C_3H_8 to unsaturated hydrocarbons and H_2 is endothermic. With dehydrogenation paths, hydrogen, benzene, toluene, xylene, ethylene, and even carbon can be produced. Unfortunately, these dehydrogenation reactions are mostly performed at quite high temperatures. Coke formation is a prevailing problem for these dehydrogenations performed at high temperature although complete dissociation of CH_4 to carbon and H_2 on liquid-metal catalysts was demonstrated as a promising route of efficient use of CH_4 at high temperature.[56-59]

Most productions of important intermediate compounds involve at least one of or many of these high-temperature catalytic processes as listed in Figure 1. For instance, CH_3OH and CH_3COOH are two of the most important intermediate compounds for chemical production. As shown in Figure 2 the production chain of CH_3OH suffers from high energy cost and ready deactivation of catalysts in the production process.[60-63] The first step of this process is CH_4 reforming at high temperature to produce syngas, mixture of CO and H_2. Then, CH_3OH can be synthesized from CO and H_2 at a high temperature. Catalyst of the high temperature reforming step are readily deactivated through formation of coke on the catalyst surface.

Although development of catalysts with long durability and high thermal stability active for selective production of important intermediate compounds or valuable chemicals is a significant field and even a dominate topic in heterogeneous catalysis, this review does not cover the topic of high-temperature catalytic conversion of CH_4 listed in Figure 1. Excellent review on this topic published by Bao *et al* on this topic can be found in literature.[64]

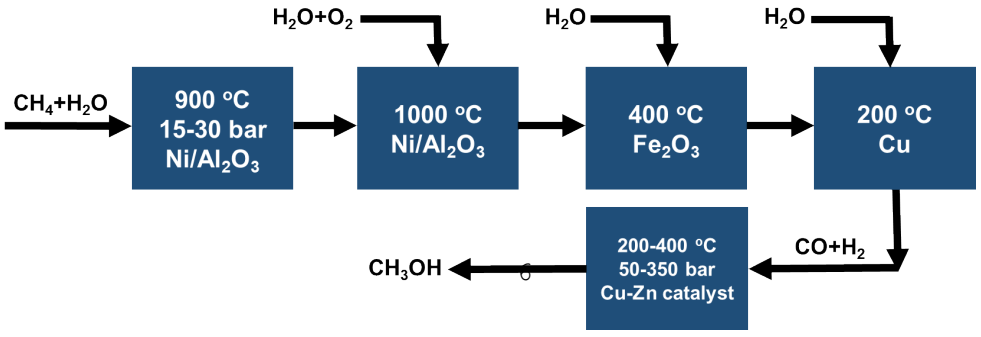

Figure 2. *Industrial high-temperature catalytic processes for synthesis of CH_3OH by using CH_4 as raw material. Reproduced from Ref. 199, copyright 2013, with permission from Springer Nature.*

1.3 Limit to activation of CH_4 at low temperature

CH_4 is one of the most inert molecules due to its strong C-H bonds with a C-H dissociation energy of 438.8 kJ/mol, high ionization energy of 1206.1 kJ/mol, low proton affinity of 424.5 kJ/mol, and low acidity (pK_a=48).[65, 66] From electronic structure point of view, the inertness of CH_4 results from the localized C-H bonds, which makes it lack of high-energy occupied orbitals and low-energy unoccupied orbitals to couple with other molecules or a catalytic site electronically. Direct dissociation of C-H of CH_4 is endothermic. A quite high temperature is typically requested as demonstrated in preparation of carbon materials and molecular hydrogen on high-temperature liquid catalysts as reported in literature.[56]

Design of a catalyst with high activity for oxidation of CH_4 to organic oxygenates under mild conditions has been challenging although tremendous efforts have been made in the last decades. Here a mild condition is defined in terms of temperature. It is in the temperature range of 20-250^{o}C. From surface science point of view, one reason for the existence of this challenge is that active surface of a catalyst active for oxidation of CH_4 at low temperature can be readily poisoned through oxidation of the active catalyst by O_2 or H_2O since they are most commonly available oxidant or impurity in reactant gas or/and solvent. For instance, even at a low temperature O_2 and H_2O can readily inactivate catalytic sites through immediate oxidation of supported metal clusters by O_2 or H_2O.[67-69] From this point of view, support metal catalysts are not advantageous for oxidative transformation of CH_4 using O_2 or H_2O under mild conditions since they cannot remain their high surface energy state in environment containing O_2 or/and H_2O. Compared to nake metal clusters supported on oxide particles, encapsulation of active sites in microporous environment could be a better choice for oxidative transformation of CH_4 under a mild condition.[61] In fact, majority of catalysts reported in literature have catalytic sites of metal atoms encapsulated in micropores of zeolites. Alternatively, preservation of nake metal or oxide nanoclusters in inset gas or high vacuum is another approach to avoid poisoning them by O_2 or/and H_2O; preservation of active sites in high vacuum has been used in early exploration how CH_4 could be activated at room temperature; this approach is reflected in recent discovery of activation of CH_4 on iridium oxide at a temperature as low as 150 K.[70-74] From this point of view, a balance between the high reactivity of a catalytic site and its resist to potential poisonous molecules plays an important role in design of new catalysts active for

CH_4 transformation under mild conditions..

1.4 Organization of this article

Both activation and catalytic transformation of CH_4 are covered in this review as both of them chemically transform CH_4 to valuable-added chemicals. Here activation of CH_4 is referred to a chemical reaction between CH_4 and oxidant; the oxidant could be oxygen atoms in MO^+ clusters in gas phase, oxygen atoms anchored in micropores of a zeolite, oxygen atoms of a reactant in solute of aqueous solution such as H_2SO_4, or oxygen atoms of dissolved molecules such as O_2 in solvent. In terms of catalytic transformation of CH_4, this review covers biocatalysis, homogeneous catalysis and heterogeneous catalysis but focuses on heterogeneous catalysis. Notably, there has been increasing effort in transformation of CH_4 through electrocatalysis and photocatalysis in the community of catalysis. Due to the limited space, this review does not discuss any results of electrocatalysis and photocatalysis.

There have been a great number of catalysts designed for transformation of CH_4 to value-added chemicals under mild conditions in literature. From reaction point of view, scientists have studied many transformative chemical reactions including these reactions adopted from other fields of chemistry for producing value-added chemicals from CH_4 under mild conditions. Instead of arranging materials to be reviewed by different categories of catalysts, this review was organized by discussing materials *on the basis of different reactions* transforming CH_4 to value-added chemicals. We started by introducing biocatalysis in converting CH_4 to CH_3OH on soluble CH_4 monooxygenase (sMMO) and particulate CH_4 monooxygenase (pMMO), briefed molecular catalysis toward transforming CH_4 to chemicals in solution, discussed oxidative activation of CH_4 with MO^+ existing in inert gas or vacuum, reviewed formation of CH_3OH through oxidation of CH_4 by active oxygen atoms bound to metal atoms anchored in zeolites, and discussed catalytic production of oxygenates including CH_3OH, acetic acid, and aldehydes through catalytic oxidation of CH_4 with H_2O_2. In each section reviewing a specific chemical reaction, its subsections were arranged according to different catalysts or samples performing oxidative activation. One feature of this review is the inclusion of comparison of different catalysts active for the same reaction and comparison of the same catalyst for different reactions. Another feature is the offers of specific suggestions on some topics provided to readers; these suggestions are shown in italic in the text.

Although significant efforts were made in the last decades, actually there has been lack of a catalyst and a catalytic process which can be utilized for production of oxygenate under

mild conditions at a large scale. The current status results from several challenges to be tackled. At the end of this review, these challenges were presented and promising solutions for them were discussed.

2. Feature and advantage in transformation of CH_4 under mild conditions

The current industrial processes of utilizing CH_4 are mainly catalytic transformations at high temperature performed on supported metal or oxide catalysts.[75] Disadvantage of these transformations performed at high temperature is the formation of coke and rapid deactivation of catalysts.[22, 23, 31] In addition, these transformations performed at high temperatures consume significant amount of energy.[1] In terms of significant amount of heat input in the current high-temperature catalytic process, it can be exemplified by at least 8.0×10^{13} kJ heat needed for the production of 6.5 million metric tons of CH_3COOH in USA in 2017 based on the endothermic nature of steaming reforming of CH_4 to produce CO ($\Delta H_r = 206\ kJ/mol$) which is the reactant to synthesize CH_3OH ($CO+2H_2\rightarrow CH_3OH$) and the following methanol carbonylation ($CH_3OH+CO\rightarrow CH_3COOH$).

Chemical transformation of CH_4 under mild conditions is chemical conversion of CH_4 to valuable chemicals at low temperature (≤150°C) or relatively low temperature (150-250°C). Thermodynamically, a transformation through partial, selective or even complete oxidations at a temperature lower than 300°C is feasible. Thus, most transformations of CH_4 under mild conditions are oxidative reactions of CH_4. Compared to the current high temperature processes (>600°C), one important feature of the transformation of CH_4 under mild conditions is the low energy cost. Another feature of these transformations of CH_4 under mild conditions is that pressure of reactants such as CH_4 or O_2 is high, typically several to tens of bars. High pressure is necessary since more molecules of reactants at a higher pressure can be dissolved in solvent to access active sites of catalyst particles at solid (catalyst)-liquid (solvent) interface.

Such chemical transformations under mild conditions offer significant advantages. Low temperature catalysis can save tremendous amount of energy compared to the current high-temperature catalysis processes.[1] The footprint cost of catalysis processes performed under mild conditions is compellingly lower in contrast to the facilities of currently high temperature reactors and related maintenance needed for the current high temperature catalytic processes. In addition, as low temperature oxidative catalysis is expected to prevent ideal products from being further oxidized, a higher selectivity for forming an ideal product under mild conditions of CH_4 transformation is highly promising in contrast to CH_4 transformation through high

temperature catalytic processes. In addition, low-temperature catalysis can avoid deactivation as coke could not form under mild condition.

3. Important experimental methods

3.1 Brief of characterization for exploring reaction mechanism at a molecular level

Identification of catalytic sites at atomic scale is vital for fundamental understanding of mechanisms of catalytic reactions. Characterization is an essential component of catalysis studies. To provide information on structure and chemistry of a catalyst, characterization is typically performed under an ex-situ condition. An ex-situ characterization could be performed through two routes. One is the characterization of an as-prepared catalyst or a used one at room temperature in high vacuum; another route is the characterisation of an as-prepared catalyst or a used one at room temperature in air. Compared to in-situ or operando characterization, an ex-situ characterization does not request complicated instrumentation and sample preparation. However, to reach a fundamental understanding of catalysis at a molecular level, relationship between a measured catalytic performance and information obtained from an ex situ characterization does not necessarily reflect the intrinsic correlation between the authentic catalyst structure during catalysis and its corresponding function in terms of catalytic activity, selectivity and durability.[76-82] A theoretical simulation based on this relationship may not rationalize how a catalytic reaction is performed.

Characterisation of a catalyst during catalysis has always been a challenging task. It would never be as simple as an advertisement of an equipment manufacturer that a turn-on key machine of in situ/operando characterisation is ready and the only thing to do for a researcher is to just push a button to collect data. In truth, there are numerous issues existing in characterizations of oxidation and catalytic transformation of CH_4 under mild conditions. Lack of appropriate methods and techniques to characterize catalysts under working conditions of the catalyst or even semi-working conditions is still one major challenge in the community of catalysis science.

Regarding to characterisations of catalysts of CH_4 transformations under mild conditions, X-ray absorption (XAS), vibrational spectroscopy and nuclear magnetism resonance (NMR) are three of these main techniques valuable in characterization of metal atoms anchored on a solid catalyst surface or encapsulated in micropores of a solid catalyst distributed in liquid environment under a gas phase at high pressure. Integration of isotope labelling methods into mass spectrometry, vibrational spectroscopy, and NMR can largely assist the endeavour in

achieving profound understanding of reaction mechanisms at a molecular level. Other than these characterisation techniques, UV-vis spectroscopy and X-ray photoelectron spectroscopy are important characterizations on the topic of CH_4 catalytic transformation. In addition, computational study has play increasing role in fundamental understanding of catalysis at a molecular level.

3.2 Quantitative analysis of products through NMR

In general, ^1H NMR is the technique to identify the products such as methanol, formaldehyde, formic acid, ethanol, acetic acid and other oxygenates. Here quantitative analysis of methanol with NMR was used to demonstrate how NMR identify and quantify products of CH_4 formed under mild conditions.[202] After a catalytic transformation of CH_4 under a mild condition, the reactor contains both solid catalyst powder and solution of solvent and products. The first step is to filtrate the mixture of catalyst and solution before a test solution is prepared. The test solution can be a part of the original filtrate collected from the reactor after a filtration. Alternatively, it can be a part of a diluted filtrate if the concentration of the chemicals in the original filtrate is too high. For the purpose of calibrating the chemical shift of these chemicals to be analysed, 3-(trimethylsilyl)-1-propanesulfonic acid sodium salt (DSS) is used as a chemical shift standard. Its peak was set at $\delta = 0.0$ ppm. A solution of 0.020 wt% DSS was made by diluting DSS in D_2O solvent. 0.10 mL of solution of 0.020 wt% DSS was mixed with a test solution, typically 0.70 ml in an NMR tube for analysis. To measure the concentration of a product such as methanol in test solution, a standard curve of the product such as methanol needs to establish. The concentration range of the standard curve should cover the concentration of all test solutions. To establish a standard curve of methanol, a series of standard solutions with different concentrations of methanol but the same concentrations of solvent and all other solutes were prepared. NMR spectra of these standard solutions are collected by using the exactly same parameters of NMR measurements. For each standard solution, the ratio of the area of methanol peak to DSS peak in the spectrum was calculated. Ratios obtained from these standard solutions were plotted as a function of the known concentration of methanol in these solutions. Fitting these data points in the plot gives a linear equation. Thus, the concentration of a test solution can be readily measured by introducing the ratio of the methanol NMR peak of the test solution to its DSS peak into this linear equation. If the concentration of the test solution is beyond the range of the standard curve, another standard curve needs to be established. If the test solution is taken from a solution obtained

through dilution of the original filtrate, a dilution factor should be multiplied to calculate the concentration of the original filtrate. Through multiplying the obtained concertation of the original filtrate by its volume, the amount of methanol formed in the reactor in mol or mass in gram is measured. Furthermore, reaction rate in terms of the amount or mass of methanol produced per hour can be calculated under an assumption that this reaction is performed under a kinetics-controlled regime. The amount in mol or mass of the CH_4 in gram introduced to the batch reactor before the reaction can be evaluated with the ideal gas law. Thus, yield of methanol through this transformation of CH_4 under the mild condition can be evaluated through dividing the amount of produced methanol by the amount of CH_4 introduced to the batch reactor before a reaction. With the same method, yields of other products can be readily calculated. Selectivity can be calculated through either dividing the amount in mol of produced methanol by the amount of the converted CH_4 or dividing the amount (in mol) of carbon atoms in the produced methanol by the total amount (in mol) of carbon atoms in all products. With the same method, the selectivities of other products can be measured readily.[202]

3.3 XANES and EXAFS for revealing electronic state and coordination environment of metal atoms

X-ray absorption spectroscopy, including X-ray absorption near edge structure (XANES) spectroscopy and Extended X-Ray Absorption Fine Structure (EXAFS) spectroscopy, has been used in studies of catalysis since the modern understanding of post edge absorption oscillation was proposed by Sayers, Stern, and Lytle in 1970s'.[83-87] It uses X-ray with energy typically higher than 7 keV to excite sample and then the transmitted X-ray or generated fluorescent X-ray is collected after the catalyst absorbs certain amount of X-ray at a specific energy window. The high energies of incident X-ray and collected X-ray make this spectroscopy capable of studying catalyst particles in gas or liquid phase. Particularly, it is an appropriate technique for identifying specific chemical and coordination environments of metal atoms of catalytic sites of single-atom catalysts, catalyst of nanoparticles with a size smaller than 3 nm, and catalysts of supported sub-nanometre clusters. Comprehensive review of using XAS in catalysis studies can be found in literature.[82, 88-92]

XANES is a technique identifying oxidation state of elements in a sample and even crystal structure; EXAFS is a technique uncovering chemical and coordination environments of metal atoms.[93-96] EXAFS often provides key information for building an appropriate structural model before simulating reaction pathway of a catalytic reaction with computational studies. It is

widely acknowledged that obtaining coordination number of atoms A around an atom M at high temperatures is challenging due to temperature-depending Debye-Waller factor.[97-99] Thus, most in situ or operando characterization published in literature were performed through a *semi*-in situ or *semi*-operando approach. In other words, most reported XAS studies termed in situ or operando studies were performed in fact by collecting data at room temperature or a relatively low temperature <200^{o}C in a gas phase of reactants after catalysis was performed at a high catalysis temperature. Thus, the catalyst was not catalysing a reaction when chemical and structural information of the catalyst was being extracted with XAS in such a *semi*-in situ or *semi*-operando approach. From this point of view, development of analytical method to extract chemical and structural information of metal atoms from XAS data collected *during catalysis at catalysis temperature* instead of a low temperature of data collection is needed for uncovering catalyst structure *during catalysis* toward establishing a direct structure-catalysis correlation. Notably, some valuable modifications of reaction cell have been made in literature[100-105] for collection of spectra for XANES and EXAFS while catalysis is performed in liquid under a gas phase of high pressure. These modifications are valuable for characterizing catalytic sites of catalysts during CH_4 transformation under mild conditions.

3.4 NMR for identifying adsorbate and catalytic sites

NMR is a technique extensively used in catalysis.[106-108] Other than its quantification of products briefed in Section 3.2, it can characterize catalysts, adsorbates or intermediates on a catalyst during catalysis in terms of operando approach other than routine characterizations of a catalyst under an ex-situ condition. Significant efforts in instrumentation and development of methodology were made in the last decades for characterizing a catalyst in a batch reactor mode[108-114] or a flowing reaction cell mode.[115-122] Some applications of this technique were well developed including the identification of Bronsted acid site with ^{1}H MAS NMR by adsorption of different probing molecules including deuterated pyridine and perfluorotributyl amine, the observation of Lewis acidic site with ^{31}P MAS NMR through adsorption of trimethylphosphine oxide[123, 124] or trimethylphosphine,[125-127] and the differentiation of Bronsted and Lewis acidic sites through ^{1}H, ^{31}P, ^{15}N, ^{13}C MAS NMR by choosing appropriate probing molecules.[108] Bao et al reviewed how solid-state NMR can be used in studies of catalysts under in situ conditions .[108]

As discussed in the next sections of this article, zeolite-based catalysts are the main players of chemical transformations of CH_4 to value-added chemicals under mild conditions. MAS

NMR has been widely used in tracking evolution of Bronsted acid sites of a zeolite along change of pre-treatment or catalysis conditions such as temperature.[128] In situ MAS NMR can be used to observe active sites. One example is the use of ^{95}Mo MAS NMR in tracking the chemical environment of Mo atoms in MoO_3/ZSM-5 during aromatization of CH_4 [129-131] and even distinguishing different Mo species with ultrahigh field ^{95}Mo NMR.[132, 133] Definitely, NMR is an excellent technique in studying deactivation mechanism of catalysts.[134-136] Another type of important application is the investigation of reaction kinetics using ^{1}H,[137] ^{13}C,[138] or ^{129}Xe,[134] providing important information for understanding catalytic mechanisms at a molecular level. As represented in some of the following sections of this review, NMR has been a vital approach in accomplishing fundamental understanding of catalytic transformation of CH_4 at a molecular level.

3.5 Vibrational spectroscopy

Vibrational spectroscopy is the most widely used in situ/operando technique in the field of catalysis. It mainly includes infrared and Raman spectroscopies. They can provide significant information on adsorbates and catalytic sites on surface of a catalyst. As they are photon-in and photon-out techniques, in situ and operando studies have been readily performed by using different types of reaction cells developed a few decades ago.[139-142] Recently, a unique cell was reported for studying catalyst particles in a liquid phase and adsorbates at a solid-liquid interface.[143] In situ/operando studies using transmission infrared spectroscopy can track vibrational signatures of reactants and products, analyse composition and study kinetics during catalysis. Its instrumentation is relatively straightforward.[144, 145] It is an integration of an optical path mainly including window for introduction and exit of infrared light with an assured sealing of liquid at certain temperature, typically 200^{o}C or lower in a high-pressure reaction cell.

Compared to transmission infrared spectroscopy, attenuated total reflection (ATR) spectroscopy exhibit a great advantage.[139, 143, 146-149] It can study adsorbates on a catalyst surface during catalysis at a solid-liquid interface even while the liquid phase is below a high-pressure gas phase in a high-pressure reactor. One function of this spectroscopy is analysis of adsorbates on a catalyst surface while the signal of liquid containing reactant, products, by-products, spectator is collected under a catalytic condition. Thus, it exhibits a significant potential in exploration of mechanism of a reaction performed at solid-liquid interfaces while the liquid phase is under a high-pressure gas phase. We have to acknowledged that it is challenging to directly study a heterogeneous catalytic reaction occurring at the interface *between* dispersed

catalyst particles in liquid *and* the liquid phase containing solvent, liquid reactants and dissolved gaseous molecules by using the attenuated total reflection spectroscopy although the applications of ATR spectroscopy to in situ or operando studies of catalysis have been demonstrated in literature.[145] [139, 143, 146-149] To use ATR spectroscopy to perform in situ or operando studies of catalysis at a solid-liquid interface, catalyst particles are *immobilized* on an internal reflection element (IRE) crystal, typically germanium or diamond. In the ATR spectroscopy, it is assumed that the catalytic reaction performed at the interface of liquid phase and the *immobilized* catalyst particles is similar to the catalytic reaction on catalyst particles *freely dispersed* in the liquid. Reactors were built for fundamental understanding of catalysis performed at solid-liquid interface in liquid phase under high-pressure gas phase. For instance, Baiker et al built a high-pressure reactor with integrated view cell for in situ studies of catalysis performed at solid-liquid interface in liquid under high-pressure gas phase.[145] It can provide valuable information on this type of catalysis at a temperature up to 200^{o}C under a gas phase up to 200 bars. It has been used for in situ studies of hydrogenation of ethyl pyruvate on Pt/Al_2O_3 catalyst particles (heterogenous catalysis) and formylation of morpholine with CO_2 and H_2 on a bidentate ruthenium complex (homogeneous catalysis).[145] More information on how to use ATR spectroscopy to study of catalysis in liquid phase can be found from the reviews.[139, 143, 146-149] Even some works relevant to the chemical transformation of CH_4 on active sites anchored in microporous aluminosilicate were done. For instance, IR spectroscopy and mapping were used to identify Si-O-B vibrational signature of boron in partially substituted zeolite particles MFI through an ex-situ model.[150] Unfortunately, very limited studies have used ATR spectroscopy to in-situ or operando studies of chemical transformation of CH_4 at solid-liquid interface under the high-pressure reactants during catalysis. One reason could be the difficulty in using the complicated instrument.[145] It is expected to see more in situ studies of activation and catalytic transformation of CH_4 in high-pressure gas phase or liquid phase under a high-pressure phase for providing insights of activation or catalytic transformation of CH_4 under these conditions.

Noteworthy emphasis is the significance of infrared and Raman spectroscopic imaging techniques which have been used in in situ studies of catalysis.[151] For instance, IR microscopy can track the evolution of a specific species such as CH_3 and CH_2 groups in MFI crystal along the increase of probation temperature.[152] Weckhuysen et al early demonstrated that Coherent anti-Stokes Raman scattering (CARS) can be used to track catalytic conversion of thiophene on ZSM-5 particles, in which the H-C= stretching vibrational signature appeared at 3115 cm^{-1} in Raman band was used to represent the reactant thiophene.[153] The intensity of this signature

was taken as a measure of the local concentration of thiophene, by which 3-D concentration profiles of concentration of reactant were successfully constructed for helping understanding catalytic conversion of thiophene.

3.6 UV-vis spectroscopy

UV-vis spectroscopy is a photon-in photon-out technique which examines electronic transitions of catalyst or reactants and products under reaction or catalytic conditions. It can measure a catalyst in the presence of a fluid.[154, 155] In general, it can provide information on oxidation states, band gaps of semiconducting support, particle size, dispersion of supported oxide moieties through measuring electron transitions. UV-vis spectroscopy has been used in characterisation of catalysts through ex situ or in situ model.

UV-vis spectroscopy has been used in investigations of catalysts under catalytic conditions in terms of in-situ or operando UV-vis spectroscopy. For instance, heteropoly acids containing Mo and V in the mixture of CH_3OH and O_2 were investigated with UV-vis with a setup containing a homemade quartz cell combined with an integrating sphere;[154, 155] this in situ study revealed that the degree of reduction of V^{4+}-O-Mo^{6+} was a function of the O_2/CH_3OH ratio. Another example is the in-situ study of ethane and O_2 system at 723 K on VO_x species supported on ZrO_2, Al_2O_3 and SiO_2; the intensities of the d-d transitions of V^{4+}/V^{3+} (17,000 cm^{-1}) in VO_x species supported on different oxides were tracked; it is found that the degree of reduction is influenced by support of VO_x; it increases in the ordering of $SiO_2<Al_2O_3<ZrO_2$. In addition, several other catalytic reactions on supported VO_x were studied with in situ UV-vis spectroscopy.[156-162] Other than the supported VO_x, this technique has been used in identifications of catalysts under catalytic conditions of many different reactions including $CaCO_3$ for ethene or propene oxidation at 473K,[163] MnO_4^{2-} -exchanged layered double hydroxides for decomposition of H_2O_2.[164] Relevant to the topic of transformation of CH_4 by aluminosilicate microporous catalysts under mild conditions, UV-vis spectroscopy was used in identifying the state of iron in Fe@ZSM-5 under catalytic oxidation of NH_3; the in situ UV-vis studies found that isolated Fe^{3+} ions in ZSM-5 was reduced in the mixture of 0.1% NH_3 and 0.1% NO.[165] More examples of UV-Vis studies of catalysts under reaction and catalytic conditions were discussed in these published reviews.[166-168]

Another important application of in situ UV-vis spectroscopy is acquisition of data of catalysts and products for establishing a direct correlation between a catalyst structure and its corresponding catalytic performance for understanding catalysis. Weckhuysen et al investigated butane dehydrogenation on chromium supported on silica alumina by using a

Harrick setup.[169-173] In these studies, the conversion of butane was measured under the same condition on catalysts with different loadings of chromium, by which the correlation between catalytic activity and the amount of reduced chromium was established and it is concluded that Cr^{3+} is the most active species for oxidation of butane.[169-173] Similarly, this approach was used for establishing correlation between catalytic performance and catalyst structure of chromium supported on alumina for propane dehydrogenation,[166, 167, 174] or sulphated zirconia for *n*-butane isomerization, WO_3 supported on ZrO_2 for *n*-pentane isomerization.[175] More examples can be found in the published review.[176]

Though introduction of UV-vis with a fibre optical probe, UV-vis spectroscopical imaging was realized.[177, 178] For instance, with time-resolved measurements, it has been used in studies of kinetics of both redox of supported oxides VO_x on TiO_2 and reduction of WO_x/ZrO_2 by H_2.[179, 180] Temporarily, there has been lack of in situ studies using UV-vis spectroscopy or spectroscopic imaging techniques for in situ or operando studies of chemical transformation of CH_4 under mild conditions during catalysis.

3.7 X-ray photoelectron spectroscopy

X-ray photoelectron spectroscopy (XPS) is a routine analytical method for surface of a materials. It can qualitatively identify elements in the surface region, quantitatively analyse surface composition or atomic fraction of one element, characterize oxidation state or even deduce electronic transfer between different atoms. As the mean free paths of photoelectrons generated with soft X-ray ($h\nu$<1000 eV), Mg Kα or Al Kα are in the range of 0.5-2 nm, the signal of XPS data is mainly contributed from the surface region with a depth of about 1.5-6 nm. In addition, as the contribution to the signal decays exponentially as a function of depth, atoms at a region closer to the surface have much more contributions to the overall signal. Thus, XPS is an analytic technique with high surface sensitivity.

Ambient pressure X-ray photoelectron spectroscopy (AP-XPS) is the XPS spectroscopy specific for studying surface buried in gas phase. Its development can be tracked back to 1970's. The continuous development in the last decades has made it a highly value analytic method for a sample in gas phase with a pressure in Torr pressure range, particularly for a catalyst in a gas phase at Torr pressure or even higher. A catalyst can be remained in either a static gaseous environment by filling gas to an existing chamber or a dynamic gaseous environment by flowing gas through a reaction cell where a catalyst is placed in. In terms of AP-XPS, X-ray source is isolated from either the reaction chamber through an aluminium foil

transparent for X-ray or a reaction cell having a thin window transparent for X-ray. Different from the electrostatic energy analyser of a vacuum XPS, an aperture has to be installed *between* a reactive cell or reaction chamber of AP-XPS *and* an electrostatic energy analyser; in addition, additional focusing lenses working at near ambient pressure have to be added at front of an electrostatic energy analyser. AP-XPS has exhibit significant value in uncovering active surface of a catalyst under a reaction condition and during catalysis. More information on the instrumentation of AP-XPS and application of AP-XPS to fundamental studies of catalysis and surface science can be found from literature.[78, 181-184] For instance, AP-XPS using Al Kα has been used to track surface of catalysts during activation of CH_4 by a catalyst in gas phase. For active catalytic sites encapsulated in the microporous materials, however a hard X-ray source is necessary for generating high-energy photoelectrons from the buried metal atoms in micropores of catalyst particles. Hard X-ray AP-XPS instruments have been available in some synchrotron centres. It has been applied to explore various materials [185] although no studies of activation and catalytic transformation of CH_4 to CH_3OH with hard X-ray AP-XPS were reported in literature. [185] It is expected a hard X-ray AP-XPS will be used in uncovering chemical and electronic state of metal atoms anchored in micropores of zeolite catalysts during transformation of CH_4 in gas phase under mild conditions.

The community of photoelectron spectroscopy has made efforts in tackling challenging task in terms of using XPS to characterize surface of catalyst particles in liquid in the last few years.[186-188] This challenging task has been feasible by remaining or even flowing a liquid containing well dispersed catalyst particles through a graphite membrane;[187, 188] in these methods, a portion of photoelectrons generated from surface of catalyst particles can penetrate the liquid layers between the catalyst particles and graphite membrane and then transmit the graphene membrane to enter the vacuum environment where photoelectrons were collected by a routine energy anlzyer.[186-188] As the catalytic transformation of CH_4 to CH_3OH is typically performed at a solid-liquid interface while the liquid phase is under a *high-pressure* gas phase of CH_4, it is extremely challenging if not impossible to use XPS to observe surface of catalyst in liquid under a high-pressure gas during catalysis.

3.8 Incorporation of isotope labelling method into characterizations

Isotope labelling is a powerful approach in identification of products, stable intermediates, catalytic sites through its incorporation with mass spectrometry, NMR and vibrational spectroscopy. By replacing ${}_{1}^{1}H$ with ${}_{1}^{2}D$, ${}_{6}^{12}C$ with ${}_{6}^{13}C$, or ${}_{8}^{16}O$ with ${}_{8}^{18}O$ for a specific

atom of a reactant molecule or catalytic sites of a catalyst, whether these replaced atoms participate into the catalytic reaction can be readily elucidated. For instance, integration of isotope substitution into mass spectrometry can assist identification of active sites of a catalytic reaction. Whether lattice oxygen atoms of surface of $NiCo_2O_4$ catalyst directly participate into complete oxidation of CH_4 can be elucidated by using an isotope labelled catalyst, $NiCo_2{}^{16}_{8}O_{4-x}{}^{18}_{8}O_x$ which can be prepared through annealing $NiCo_2O_4$ in ${}^{18}_{8}O_2$.[48] If surface lattice oxygen participates into oxidation of CH_4 ($CH_4+2O_2\rightarrow CO_2+2H_2O$), $C{}^{16}_{8}O\,{}^{18}_{8}O$ (m/e=46) and $C\,{}^{18}_{8}O_2$ (m/e=48) must be observed in spectra of mass spectrometry. Through tracking the formation of products with mass spectrometry, whether surface lattice oxygen atoms of $NiCo_2O_4$ catalyst participates into the reaction was checked.[48]

Integration of isotope labelling into NMR analysis can help to identify reaction pathway. For instance, Rh_1O_5 single atom site encapsulated in ZSM-5 can catalyse the coupling of CH_4, CO and O_2 to form acetic acid.[188] One of the potential reaction paths is oxidation of CH_4 by O_2 to form CH_3OH and then carboxylation of CH_3OH to generate acetic acid. In order to elucidate whether this is a reaction path taken by this catalyst (Rh_1O_5@ZSM-5), an isotope substituted methanol, $CH_3{}^{18}_{8}OH$was added into aqueous solution containing the catalyst particles under the mixture of CH_4, CO and O_2. If the reaction path taken by Rh_1O_5@ZSM-5 is the carboxylation of methanol, $CH_3C^{16}_8O^{18}_8OH$ should be produced in this isotope experiment. If no $CH_3C^{16}_8O^{18}_8OH$ could be observed in NMR, the path of CH_3OH carboxylation should be excluded.

Incorporation of isotope substitution into infrared spectroscopy can assist to identify whether C-Y bond of X-C(R_2)-Y is activated or dissociated. In this case, Y of X-C(R_2)-Y can be labelled by isotope of Y′. Then, the isotope-labelled X-C(R_2)-Y′ is used to replace X-C(R_2)-Y to perform the same catalytic reaction. If shift of vibrational peak of C-Y′ could be observed with IR or Raman spectroscopy, activation of C- Y′ would be confirmed. If no shift of C- Y′ vibrational peak could be observed, it shows that C-Y of X-C(R_2)-Y cannot be activated.

Isotope labelling method plays a unique role in testing binding strength of molecules on surface of a catalyst. For instance, binding strengths of CO on a single-atom catalyst (Pt_1/SiO_2) and a nanoparticle catalyst (Pt NP/SiO_2) were investigated experimentally through isotope-labelled IR experiments.[189] Pt_1/SiO_2 and Pt NP/SiO_2 were exposed to ^{12}CO gas to reach equilibrium of chemisorption at 100°C. Then, the two Pt catalysts with chemisorbed ^{12}CO at 100°C were exposed to ^{13}CO gas phase to allow exchange between chemisorbed ^{12}CO and free

^{13}CO of gas phase. The number of replaced ^{12}CO molecules pre-chemisorbed on a catalyst can be quantized with the intensity of ^{13}CO chemisorbed on the catalyst since $\nu(^{13}C\text{-}O)$ of ^{13}CO is ~ 50 cm^{-1} lower than that of ^{12}CO. As the ratio of peak intensity of $\nu(^{13}C\text{-}O)$ to $\nu(^{12}C\text{-}O)$ for single-atom catalyst, Pt_1/SiO_2 is obviously lower than the ratio for nanoparticle catalyst, Pt NP/SiO_2, it is concluded that the binding strength of CO on Pt_1/SiO_2 is much stronger than Pt NP/SiO_2. This difference in binding of CO confirmed by isotope-labelling IR studies rationalized the distinct difference in catalytic activity for CO oxidation on Pt_1/SiO_2 and Pt NP/SiO_2. Thus, incorporations of isotope labelling into mass spectrometry, NMR, infrared spectroscopy have largely strengthened the functions of these spectroscopies in fundamental studies of oxidation and transformation of CH_4 under mild conditions.

3.9 Computational study for simulating reaction pathway

Computational study using density function theory (DFT) has become a significant approach in fundamental understanding of catalytic reactions at a molecular level. It searches transition states and optimizes structure of intermediates. Though systematic simulations, a complete catalytic cycle comprising all elementary steps and a corresponding energy profile can be proposed. These simulations can also offer an energy profile of all elementary steps from reactants to products. Through this energy profile, the rate-determining step(s) can be identified. If the active sites of the catalyst can be identified experimentally, a correlation *between* the activation barrier of the transition state of the rate-determining step *and* its corresponding chemical and coordination environments of a catalytic site can be established. With this intrinsic correlation, the descriptor of this catalytic performance can be proposed. Based on this descriptor, a new catalytic site offering a higher activity can be uncovered. Then, such a new favorable catalytic site "proposed" through the integration of experimental and computational studies is significantly valuable for experimentalists. Experimentalists can design a synthetic route to prepare a catalyst consisting of such catalytic sites to test this prediction. Thus, definitely theoretical simulation plays significant role in interpreting catalytic performance of a tested catalyst and proposing a new catalyst for transformation of CH_4 under mild conditions. Significant part of this review is devoted to the molecular understanding of the CH_4 transformation under mild conditions based on computational studies.

4. Brief of catalytic conversion of CH_4 by enzymes at ambient condition

In contrast to the currently high-temperature catalytic processes with low selectivity for

ideal products and facile deactivation of catalysts, CH_4 monooxygenase (MMO) enzymes can oxidize CH_4 to CH_3OH at room temperature at ambient pressure. Understanding of the efficient biocatalysis of producing methanol from CH_4 is significant for designing artificial catalysts mimicking this amazing biofunction of the Nature. In the Nature, methanotrophic bacteria can oxidatively activate C-H of CH_4 under an ambient condition since these bacteria contain MMO.[190] Methanotrophs of such bacteria can metabolize CH_4 with MMO by oxidation of CH_4 to CH_3OH. Two types of MMOs were reported being active for this oxidation at room temperature. They are in soluble and particulate forms and thus called sMMO and pMMO, respectively. sMMO is in bacterial cytoplasm in environment with low concertation of iron. Catalytic activity of pMMO requires copper-based catalytic sites.

Methylococcus capsulatus (Bath) and methylosinus trichosporium OB3b belong to sMMO. They were studied well in literature.[191-197] sMMO consists of three components including reductase (MMOR), hydroxylase (MMOH), and regulatory protein (MMOB). It is found that all the three components are necessary for aerobatic oxidation of CH_4.[198] Electron transfer between CH_4 and O_2 is performed between hydroxylase and reductase. Figure 3a presents the main components of a sMMO enzyme system having a dimeric structure with feature of an $(\alpha\beta\gamma)_2$ dimer architecture.[199] These studies[198] suggested that the active sites of the hydroxylase are responsible for reduction of O_2 and activation and oxidation of CH_4. The sMMO in Figure 3 has a dimeric structure consisting of two $\alpha\beta\gamma$-promoters. The feature of each $\alpha\beta\gamma$-promoter is its nearly complete α-helical secondary structure. Each α-subunit has a four-helix bundle. The bundle is the di-iron active site in hydroxylase responsible for hydroxylation. The di-iron site within hydroxylase is the catalytic site where O_2 is activated and reduced and CH_4 is oxidized. Notably, MMOB in Figure 3a, a protein cofactor can tailor the structure and activity of the di-iron site of MMOH in terms of activation of MMOH. MMOR in Figure 3a is responsible for transferring electrons from electron donor NADPH/NADH to MMOH.[200] Obviously, MMOH, MMOR, MMOB are consolidated to form a well-functioned enzyme to selectively transport four species including molecular CH_4, molecular O_2, electrons, and protons to the catalytic centre, di-iron site. The hydroxylase-regulatory protein controls the pathways of delivering CH_4 to the active site of sMMO. Figure 3b schematically presents the proposed mechanism of sMMO.

The MMOH complex containing an active di-iron site consists of four glutamates (E114, E144, E209 and E243) and two histidines (H147 and H246). As seen in the oxidation form of MMOH (Figure 3c), two OH ligands bridge the two Fe atoms in an oxidation state and the coordination sphere of Fe atoms contains solvent H_2O molecules. The confirmed structure of di-iron site bridging two OH groups has driven significant efforts in designing catalysts containing a di-μ-oxo structure which were discussed in sections 9 and 13 of this article. The di-μ-oxo structure encapsulated in zeolite was found to be reactive in oxidative activation of C-H of CH_4 to form CH_3OH at a temperature of 50-100°C in aqueous solution. Upon electrons are transferred to oxidation form of MMOH, it is changed to reduction form (Figure 3d); in the reduction form of MMOH, the bridging OH groups depart and one oxygen atom of E243 likely coordinate with two Fe atoms, by which the distance between the two Fe atoms increase and thus an open coordination shell in reduction form is formed for being ready accessed by O_2. Activation of molecular O_2 by the reduction form of MMOH results in breakage of O-O bond and also the restructuring of the di-iron site, by which the restructured di-iron site is ready for activation of C-H of CH_4 to form CH_3OH. More details of oxidation of CH_4 to CH_3OH by sMMO can be found in literature.[200-202]

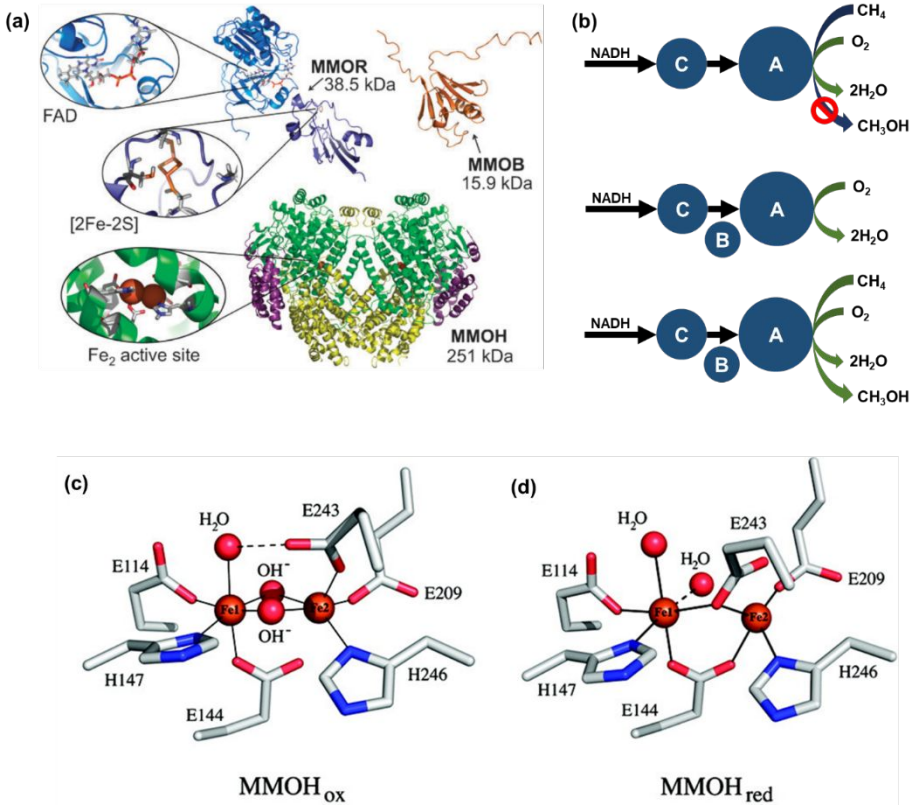

Figure 3. *Representation of mechanism of catalytic oxidation of CH_4 to CH_3OH by sMMO. (a) Structure of sMMO enzyme obtained from methylococus capsulatus (Bath).[200] It consists of three components including (1) a hydroxylase [MMOH (PDB reference 1MTY)]. (2) an oxidoreducase*

[MMOR consisting of FAD domain (PDB reference 1TVC) and [2Fe2S]-Fd domain (PDB reference 1JQ4)], and (3) a regulatory protein [MMOB (PDB reference 1CKV)]. Reproduced from Ref. 200 with permission from the Royal Society of Chemistry. (b) Schematic showing mechanism of oxidation of CH_4;[198] A, B, and C in the schematic are three components of a soluble CH_4 monooxygenase of methylococcus capsuhtus which was reported in literature.[203-207] Reproduced from Ref. 198, copyright 1985, with permission from Elsevier. (c) Oxidation form of di-iron site with coordination different from the oxidation form in (c).[202] (d) Reduction form of di-iron structure.[202] Reproduced from Ref. 202, copyright 2011, with permission from ACS.

In contrast to sMMO, less understanding was achieved for pMMO.[208-210] pMMO is an integral membrane protein with the function of transformation of CH_4 to methanol in methanotrophic bacteria. Although Nature does have more pMMO than sMMO, it is more difficult to purify pMMO than sMMO. The difficulty in purification of pMMO results from the instable lipid bilayer and easy loss of metal cofactors. Rosenzweig et al reported the crystal structure of pMMO.[211] Compared to sMMO, the transformation of light alkanes on pMMO is highly regiospecific and stereoslective.[212-214] For synthesis of biomimic catalyst with function similar to pMMO of the Nature, significant effort in identifying structure of the active site of pMMO was made in the last two decades.[209]

Figure 4 presents the architecture of pMMO. pMMO consists of pmoA, pmoB, pmoC in a trimer ($\alpha_3\beta_3\gamma_3$) of $\alpha\beta\gamma$ monomers. Each monomer has three copper ions and one zinc ion. The three units including pmoA, pmoB, pmoC in Figure 4 are shown in yellow, green, and pink, respectively. How Cu atoms and their ligands coordinate the oxy-transfer chemistry was a crucial question extensively explored a decade ago.[209, 215-218] It was suggested that a tri-copper structure located in pmoB subunit should be the catalyst site. Recently, Martinho et al indicated that a nonheme di-iron center is also active for this transformation although Fe/Cu atomic ratio is only 1:80.[219, 220] As later studies suggested that all 14-15 Cu atoms in a purified pMMO participate into elementary step of CH_4 oxidation, the early proposal of the direct participation of di-iron centre into hydroxylation of CH_4 is implausible.[209]

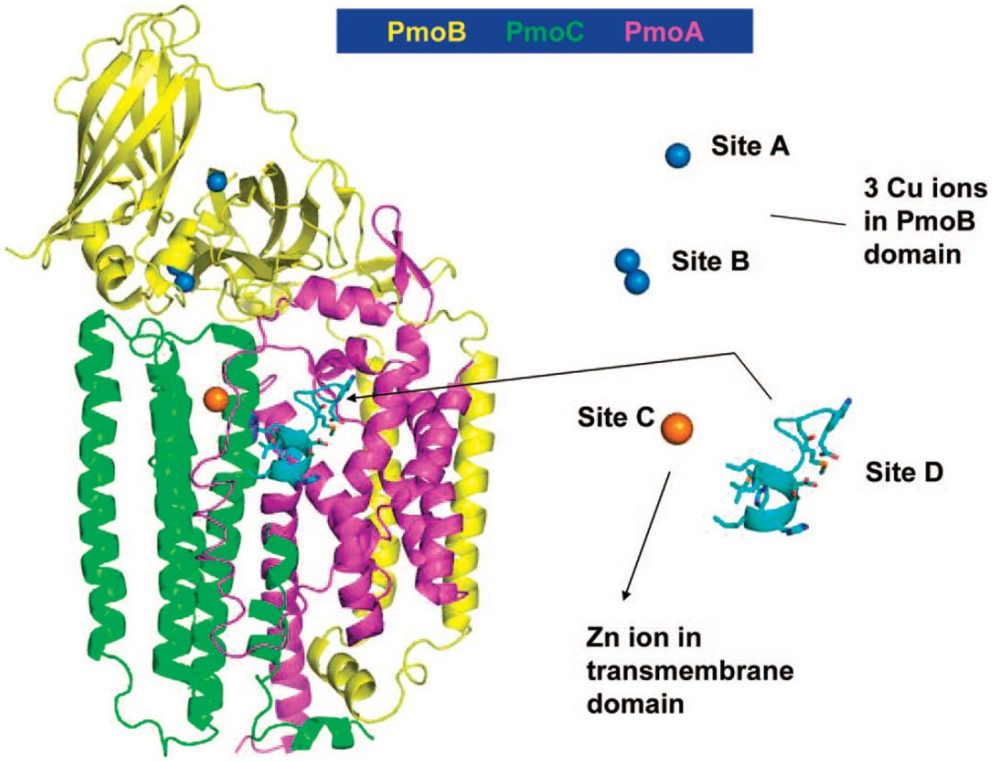

Figure 4. *Representation of architecture of pMMO. PmoA, PmoB, and PmoC are shown in pink, yellow and green, respectively.* [209] [211] *Reproduced from Ref. 211, copyright 2008, with permission from ACS.*

Chan et al divided the 14-15 Cu atoms in pMMO into two groups since 6 of them are oxidized by O_2 and the other 9 Cu atoms remain reduced.[221] The group of the 6 Cu atoms and their surroundings were assessed as catalytic clusters as they are active in activation of both O_2 and hydroxylation. The 6 Cu atoms related to the catalytic sites are two trinuclear copper clusters.[218, 221, 222] The existence of Cu_3 clusters was supported by studies using electron paramagnetic resonance (EPR).[223] In the proposed mechanism,[218, 221, 222] one Cu_3-cluster is responsible for both activation of O_2 and hydroxylation of CH_4 but the other Cu_3-cluster only plays a role in activation of O_2. As shown in Figure 4, PmoA and PmoC are transmembrane primarily. Based on the reported enzyme crystal structure,[211] the N- and C-terminal subdomains in PmoB are surrounding by cytosol and are buried at water-membrane interface. Remarkably, there is a cavity comprising a hydrophilic cluster in the transmembrane domain at site D. Notably, early study did not consider this hydrophilic cluster of residues as a site to bind metal atom.[211] Chan et al suggested that site D should bind to metal ions as electrostatic energy of the cavity of hydrophilic residues could be exceptionally high.[217] Studies of Chan et al using redox potentiometry provided unambiguous evidence for the existence of Cu^{II} Cu^{II} Cu^{II} in

pMMO (Figure 5).[217] The existence of $Cu^{II}Cu^{II}Cu^{II}$ in pMMO was further confirmed by the fact that the EPR observed from pMMO is the same as the tricopper complexes synthesized by Chan *et al.*[217] Surprisingly, the synthesized $[Cu^{I}Cu^{I}Cu^{I}(L)]^{+}$ complex can couple with molecular O_2 to form an intermediate beneficial to addition of oxygen atoms to C-C bond at room temperature.[217] In addition, Chan et al found that $[Cu^{I}Cu^{I}Cu^{I}(L)]^{+}$ complex can accelerate the transfer of atomic oxygen to C-H bond of CH_3. These obviations strengthened the hypothesis that the Cu_3 cluster of pMMO is responsible for oxygen activation.

Computational study was performed for modelling the trinuclear $Cu^{II}Cu^{II}Cu^{II}$ cluster in order to fundamentally understand the role of this Cu_3 cluster at site D in pMMO. Through considering structural parameters of species in the widely defined coordination environment, the geometries of the residues and metal ions were optimized for minimizing total energy of the Cu_3 site as shown in Figure 5. Distances of Cu-O and Cu-Cu provided by this optimization show that accommodation of a Cu_3 cluster at site D is reasonable. Modelling suggests that the amino acid side chains coordinating to Cu ions are PmoA His38 and PmoC Glu154 for $Cu_{1'}$ ion, PmoA Asp47 and Met41 for $Cu_{2'}$ ion, and PmoA Asp49 and Glu100 for $Cu_{3'}$ ion.[217] Definitely, site D in pMMO holding hydrophilic cluster without Cu ions is clearly unstable, exhibiting high activity.

Based on the assumption that oxidation of CH_4 is performed through a direct concerted O-atom insertion mechanism, Chan et al expected a binding pocket near to the Cu_3 cluster for CH_4.[209] In addition, a hydroxylation site must include the copper site and the hydrophobic cavity since Cu site can activate molecular O_2 and hydrophobic cavity can host CH_4 molecules. They used a pentane molecule as a probe for identifying any possible binding sites of hydrocarbon molecules in the $\alpha\beta\gamma$ monomer. Their studies show that the most probable site binding a hydrocarbon molecule is the hydrophobic channel lined by the aromatic residues Trp48, Phe50, Trp51 and Trp54 of PmoA. Thus, this binding site of hydrophobic substrate plays a role in direct concerted O atom insertion into a C-H bond of light hydrocarbon.[209, 211, 216, 217] It is proposed that the active site catalysing the insertion of O atom to C-H of light hydrocarbons is the intermediate $[Cu^{II}Cu^{II}(\mu\text{-}O)_2Cu^{III}]^{3+}$, as shown in Figure 6a.[215] This intermediate is formed through oxidation of the reduced $[Cu^{I}Cu^{I}Cu^{I}]^{3+}$ cluster.

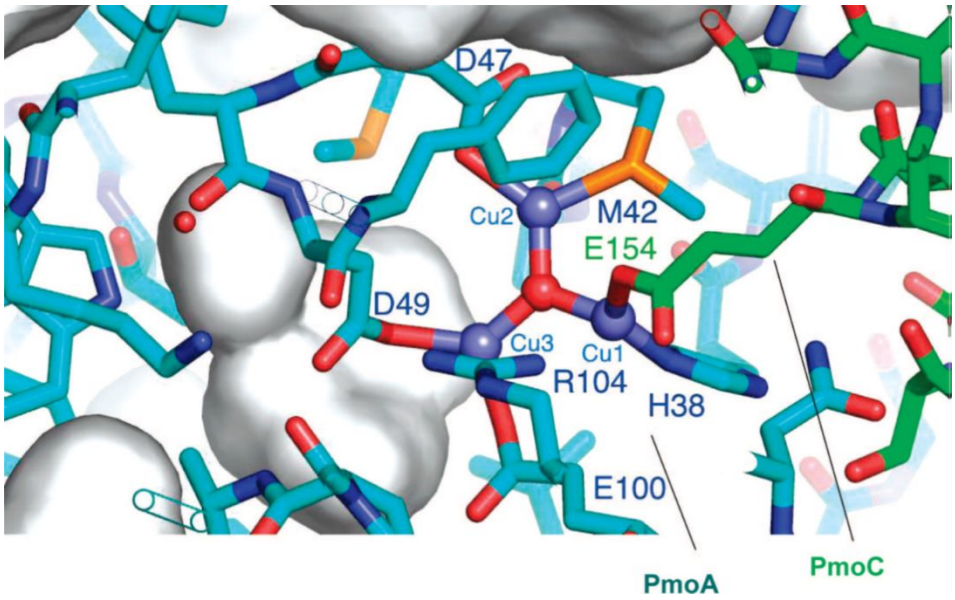

Figure 5. *Representation of environment of Cu^{II} Cu^{II} Cu^{II} with capping "oxo" in site D. PmoA His38 and PmoC Glu154 coordinate Cu_1 ion; PmoA Asp47 and Met41 surround Cu_2 ion; PmoA Asp49 and Glu100 coordinate Cu_3 ion.[217] Reproduced from Ref. 217, copyright 2007, with permission from John Wiley and Sons.*

It is reported that a di-nuclear copper cluster, bis(μ-oxo)Cu^{III}-Cu^{III} species (2 in Figure 6b) can catalyse the transfer of O atom to a C-H bond.[216, 217, 220, 224] A singlet oxene could transfer from bis(μ-oxo)Cu^{III}-Cu^{III} to a light hydrocarbon when the μ-oxo atom is at an appropriate position for forming a transition state complex to couple with C-H of a light hydrocarbon.[217] However, DFT calculation suggested the μ-oxo atom has to stretch much to form a transition state with high activation barrier. Notably, the energy barrier for activating C-H on bis(μ-oxo)Cu^{III}-Cu^{III}-based intermediate (2 of Figure 6b) is much higher than that of the $[Cu^{II}Cu^{II}(\mu\text{-}O)_2Cu^{III}]^{3+}$-based intermediate (1 of Figure 6b).[215] DFT calculation suggested three most probable models including mono-valent bis(μ-oxo)$Cu^{III}Cu^{III}$ complex, multi-valent bis(μ-oxo)$Cu^{II}Cu^{III}$ complex, and $[Cu^{II}(Cu^{II}(\mu\text{-}O)_2Cu^{III}]^{3+}$ in Figure 6b.[215] Obviously, the calculated rate constant of CH_4 consumption in transformation of CH_4 to CH_3OH on $[Cu^{II}(Cu^{II}(\mu\text{-}O)_2Cu^{III}]^{3+}$ (1 in Figure 6b) at room temperature is 2.91×10^4 s^{-1} which is much larger than 0.57 s^{-1} of bis(μ-oxo)$Cu^{III}Cu^{III}$ (2 in Figure 6b) and is 119 times of the rate constant of bis(μ-oxo)$Cu^{II}Cu^{III}$ (3 in Figure 6b). Clearly, trinuclear cluster (1 in Figure 6b) is most kinetically favourable.[209, 218] Overall, these DFT calculations support that trinuclear Cu clusters (1 in Figure 6b) in site D play a crucial role of hydroxylation of CH_4 in pMMO.

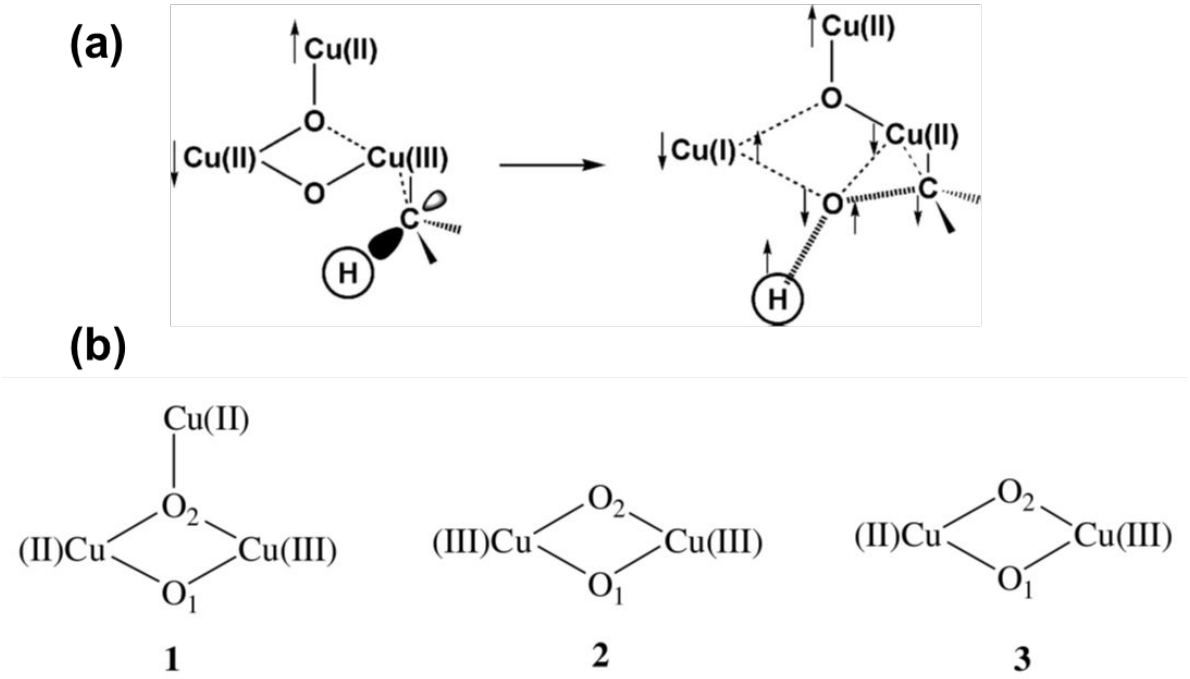

Figure 6. *Representation of details of the adiabatic "singlet oxene" transfer from a dioxygen activated Cu_3 cluster to CH_4 and formation of transition state. (a) The O_2 activated tricopper cluster and its transition state predicted by DFT calculation.[218] The arrows show the up and down directions of the unpaired electron spins. Reproduced from Ref. 218, copyright 2004, with permission from ACS. (b) Three possible structural models of the activated pMMO considered in DFT calculation.[215] Reproduced from Ref. 215, copyright 2006, with permission from Elsevier.*

In terms of using metabolic process of methanortrophic bacteria to transform CH_4 to CH_3OH, there is an issue of selectivity in producing methanol in the oxidation. This is because formaldehyde instead of methanol is the final product of metabolites of bacteria.[202] Thus, if natural bacteria are the "catalyst", it must be challenging to produce large scale of methanol due to the limit of selectivity in production of CH_3OH. Based on this fact, it is necessary to engineer or modify the structure of CH_4 monooxygenase to prevent a further oxidation of methanol to formaldehyde. However, such an engineering must be based on a deep understanding of the mechanism of enzyme-catalysed oxidation of CH_4. For instance, understanding of the pathway that CH_4 accesses the di-iron site within hydroxylase of sMMO is a prerequisite for developing an efficient biocatalyst with high selectivity for producing CH_3OH. Similarly, deep understanding of oxidation of CH_4 by pMMO is a requirement for developing a biocatalyst with high selectivity for producing CH_3OH. Upon deep understanding

of the CH_4 oxidations by sMMO and pMMO, modifications of MMO structures could be done through chemical or/and biological approaches toward developing biocatalysts for production of CH_3OH with high selectivity. Due to the low selectivity and the limited available amount of MMO and the high cost of MMO, it is too early to claim production of CH_3OH from CH_4 at large scale with biocatalytic process. Inspired by these insights gained from experimental exploration and computational analysis, it is expected that numerous efforts in synthesizing artificial catalysts for mimicking the trinuclear Cu clusters will be made in the near future.

5. Brief of organometallic approach and related homogeneous catalysis

Compared to the activations of O-O of O_2 and C-H of CH_4 to generate CH_3OH with sMMO and pMMO, CH_4 can be activated and oxidized in many reactions accelerated with molecular catalysis in liquid. Periana and his colleagues published a comprehensive review on how CH_4 can be functionalized through homogeneous reactions.[225] They categorized all homogeneous functionalizations reported in literature into 12 types of reactions based on (1) the specific consideration in terms of whether O_2 can be directly utilized and (2) the reaction mechanism of elementary step reacting with CH_4 with regard to whether the CH_4-involved elementary step is proceeded with chain or no-chain reactions, with stoichiometric reagents or catalytic species.[225] Here we only briefed C-H activation of CH_4 with organometallic approaches in homogeneous systems under mild conditions. Progress and achievement in catalytic transformation of CH_4 can be found in this excellent review.[225]

As reviewed in literature,[226] C-H activation of light alkanes can be performed through σ-bond metathesis, electrophilic activation, oxidation addition, 1,2-addition, and metalloradical activation. Regarding to oxidative addition, it is performed on $[L_nM^y]$. M atom is coordinatively unsaturated in $[L_nM^y]$ as it needs to bond to additional alkyl (-R) and H atom. $[L_nM^y]$ is typically generated from a stable precursor such as $L_nM^{y+2}H_2$. Figure 7a represents oxidation activation of light alkane by $[L_nM^y]$. For this type of activation, M is typically a metal atom with rich d electrons such as Rh, Ir, and Pt and at low valence.

Figure 7b represents reaction of electrophilic activation performed on $L_nM^{y+2}X_2$. $[M^{y+2}]$ in Figure 7b is typically late transition metal such as Pd^{2+} or Pt^{2+}. In this activation, an intermediate $[L_nM^{y+2}(R)(X)]$ is first formed by coupling $[L_nM^{y+2}X_2]$ with alkane. Then, R and X atoms on $[L_nM^{y+2}(R)(X)]$ couple each other to form R-X, releasing and regenerating $[L_nM^y]$.

Electrophilic activation is typically performed in a highly polar solvent.

Regarding to σ-bond metathesis (Figure 7c), it is performed on L_nM^y. M is commonly an early 3d transition metal such as Sc. This reaction is more like an interchange of alkyl fragments (R and R′) instead of net alkane activation.

In respect of 1,2-addition, it is the addition of R and H groups of alkane RH to a double bond of M=Y (M: transition metal, Y: non-metal element such as C and N) (Figure 7d). Literature reported addition of R-H to M=C and M=N.[227] However, how this activation could be used to produce value-added chemicals need to be explored definitely.

(a)

$$[L_nM^y] + R{-}H \rightarrow L_nM^{y+2}\begin{matrix}H\\R\end{matrix}$$

(b)

$$L_nM^{y+2}X_2 + R\text{-}H \rightarrow [L_nM^{y}] + R\text{-}X + H\text{-}X$$

(c)

$$L_nM^y{-}R + R'\text{-}H \leftrightarrow L_nM^y{-}R' + R\text{-}H$$

(d)

$$(R'NH)_2Zr = NR' \xrightarrow{CH_4} (R'NH)_3ZrCH_3$$

Figure 7. *Representation of promising organometallic reactions for activation of C-H of light alkanes.[226] (a) Oxidative addition. (b) Electrophilic activation. (c) σ-bond metathesis. (d) 1,2-addition. Reproduced from Ref. 226, copyright 2002, with permission from Springer Nature.*

Although there are limited examples in catalytic conversion of CH_4 or C_2H_6 to value-added chemicals through these organometallic approaches of C-H activation, they are promising paths to catalytically transform CH_4 under mild conditions through homogeneous catalysis. An example of electrophilic activation of alkanes and oxidation was early proposed by Bercaw et al.[228] In this activation, $[PtL_3Cl]$ complex replaces a proton of light alkane H-R, forming a $[Pt^{II}L_3R]$ complex (1 in Figure 8). Then, $[Pt^{II}L_3R]$ is reduced to form Pt^{IV} complex (2 in Figure 8) upon reaction with $[Pt^{IV}Cl_6]^{2-}$; in this step, $[Pt^{II}L_3R]$ transfers two electrons to $[Pt^{IV}Cl_6]^{2-}$ which binds with two additional Cl atoms, forming complex 2 in Figure 8, $[Pt^{IV}L_3RCl_2]$. Then, H_2O molecule performs nucleophilic attack to complex 2; the nucleophilic attack produces a CH_3OH molecule and releases a HCl molecule; meanwhile, the molecular catalyst, $[Pt^{II}L_3Cl]$ is regenerated. The electrophilic activation follows

nonoradical path, similar to C-H activation of alkenes in organometallic chemistry. As $[Pt^{IV}Cl_6]^{2-}$ is transferred to $[Pt^{II}Cl_4]^{2-}$, it acts as an oxidant instead of a recoverable catalyst; therefore, a regeneration of $[Pt^{II}Cl_4]^{2-}$ to $Pt^{IV}Cl_6]^{2-}$ needs another reaction. This route was illustrated in transformation of CH_4 to CH_3OH by Shilov et al.[229] Notably, the relatively low selectivity and quite low activity in oxidation of CH_4 to CH_3OH through this electrophilic activation make this route a more model instead of a promising application. Efforts in replacing $[Pt^{IV}Cl_6]^{2-}$ with an economic oxidant such as copper salts[230] or even electrochemical approach were made.[231]

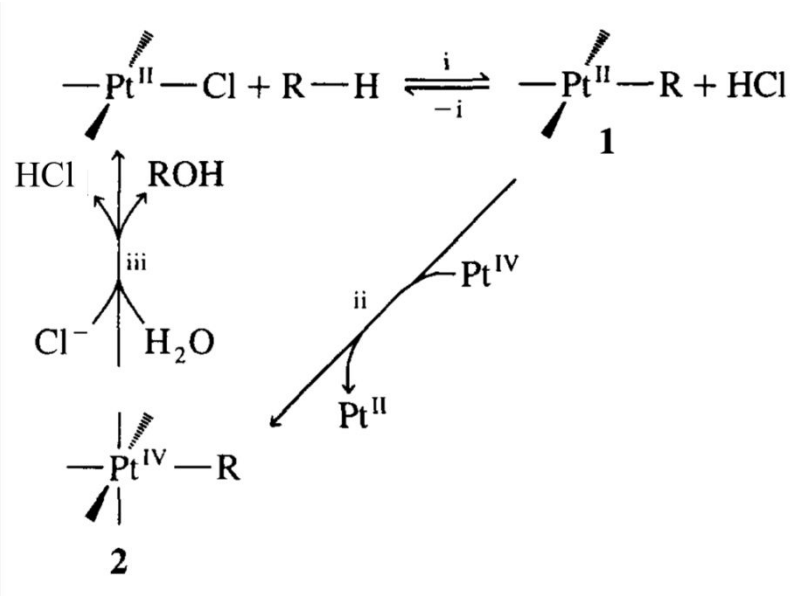

Figure 8. *Representation of activation and oxidation of alkanes.* [228] *Reproduced from Ref. 228, copyright 1995, with permission from Elsevier.*

One successful example of oxidation of CH_4 through electrophilic activation with high activity and selectivity is the catalytic oxidation of CH_4 to CH_3OSO_3H by the oxidant H_2SO_4 and the catalyst, (bpym)$Pt(OP)_2$ (bpym: 2, 2′-bipyrimidine) at 100°C reported by Perianan et al.[232] The key role of bpym is the increase of solubility of Pt species. One reason for using H_2SO_4 is the protection of bi-sulphate group which is a ligand inert for being oxidized. Although the product of organometallic chemistry, CH_3OSO_3H is not a value-added chemical without further hydrolysis, this close catalytic cycle of oxidation of CH_4 with H_2SO_4 to CH_3OSO_3H with high activity and selectivity distinctly demonstrated success of organometallic approach in transformation of CH_4 to value-added chemicals under mild conditions. Figure 9 represents the proposed reaction mechanism for oxidation of CH_4 through (bpym)$Pt(OP)_2$ to form CH_3OSO_3H.[232] Periana et al concluded the C-H activation on (bpym)$Pt(OP)_2$ is performed through electrophilic activation and occurs with the highly

electrophilic, largely uncoordinated, 14-electron complex with T-shape (Figure 9). The product, methyl bisulfate CH_3OSO_3H play steric and electronic effects for preventing it from being further oxidized. [232] The -OSO_3H group of CH_3OSO_3H prevents C-H of CH_3 of CH_3OSO_3H from being accessed. More importantly, the electronic drawing effect of OSO_3H group makes CH_3 of CH_3OSO_3H electronically deficient. Thus, an electrophilic attack of metal complex to electron-density deficient C-H bond of CH_3 unfavorable. In other words, using H_2SO_4 as the specific oxidant can effectively prevent CH_3 from being further oxidized since the control oxidation of CH_4 is key for transformation of CH_4 to CH_3OH with high selectivity. The formed CH_3OSO_3H can be transformed to CH_3OH through additional hydrolysis.

Significant advance in catalytic oxidation of C-H of CH_4 with molecular catalysis in liquid phase has been made in the last decades. All these transformations catalyzed by molecular catalysis are performed under mild conditions. More information on this approach can be found from the comprehensive review published by Periana et al.[225]

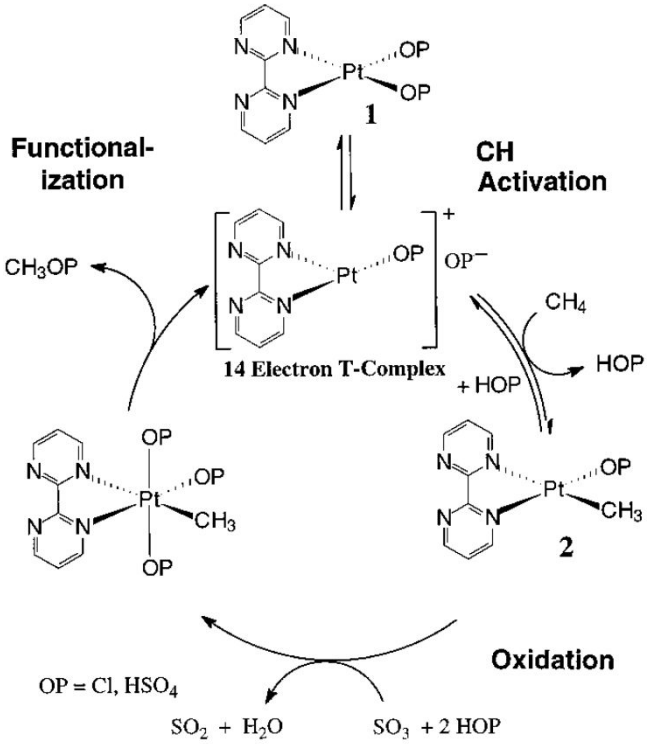

Figure 9. *Representation of proposed reaction mechanism of oxidation of CH_4 to methyl bisulfate CH_3OSO_3H by methyl bisulfate CH_3OSO_3H at 100°C through electrophilic activation. This mechanism consists of C-H activation, oxidation, functionalization. [233] Reproduced from Ref. 233, copyright 1998, with permission from AAAS.*

6. Activation and oxidation of CH_4 on bare MO^+ to CH_3OH

Some bare transition-metal cations (M^{n+}) in gas phase[234-236] can activate C-H and C-C cleavages of light alkanes. Oxidation of bare transition-metal cations forms bare transition-metal oxide cations (MO^+). Similar to the ligand effect in tuning reactivity of metal centre of a molecular catalyst discussed in Section 5, bare transition-metal oxide cations (MO^+) exhibit high activity in oxidation of organic molecules. Here MO^+ acts as an oxidant.

Dirven by the significance of low-temperature oxidation of light hydrocarbons, oxidative reactions of CH_4 on bare transition-metal oxide cations (MO^+)[237-241] such as FeO^+,[71, 242-248] CoO^+,[72, 249] and OsO^+ [250] in gas phase, were studied extensively.[73] These studies of oxidation of light alkanes by MO^+ in gas phase offered insights of reactivity patterns, roles of ligands on transition metal atoms, chemo- and regioselectivities, and potential intermediates at a molecular level. [250,73] These insights are significant for developing catalysts active and selective in oxidative transformation of CH_4 to value-added chemicals. It built the foundation for later exploration of single atom cluster M_1O_n anchored in zeolites which was reviewed in later sections.

In general, MO^+ clusters were generated with ion cyclotron resonance mass spectrometry.[73] The theoretical base for generation of MO^+ clusters with this spectrometry was reported in literature.[251] MO^+ clusters were trapped in a magnetic field of an ion cyclotron setup and then they were selected with modulable radio-frequency pulses on the basis of their masses. The mass-selected ions can be slowed to an ideal kinetic energy before using them for reaction with CH_4. Once a type of specific MO^+ clusters with a specific kinetic energy was created, they were leaked into a glass chamber containing CH_4 at a low pressure in the range of 10^{-2} -0.5 Torr; the reason to remain pressure of CH_4 low is to minimize multiple molecule-ion scatterings. This reaction between MO+ clusters and CH_4 molecules is the direct oxidation of CH_4 by MO^+ such as $CH_4 + CoO^+ \rightarrow CH_3OH + Co^+$. The temperature of CH_4 is remained at room temperature. Thus, exothermic or nearly thermoneutral reactions can occur under this condition. The products formed in the glass chamber were collected by a quadruple mass filter for identifying their masses and analysing their intensities.[73]

These oxidations reviewed in Section 6 or to be reviewed in Sections 7-13 can be categorized into three types of oxides including oxidation by MO^+ clusters in gas phase of CH_4 at sub-Torr pressure, oxidation by active oxygen atoms bound to micropores of zeolites in 1 bar pressure of CH_4, and oxidation by catalytic sites anchored in zeolites dispersed in liquid under high-pressure gas phase of CH_4. The operational condition of the oxidative activation of CH_4 by MO^+ clusters is very similar to catalytic oxidation of CH_4 by PtO^+ to be reviewed in

Section 7. In both cases, the pressure of reactant CH_4 is in sub-Torr pressure or lower for minimization of multiple molecule-ion scatterings. Different from the operational condition used in Sections 6 and 7, the oxidative activation of CH_4 by oxygen atoms bound to metal atoms anchored in micropores of zeolite or oxygen atoms on metal oxide particles to be reviewed in Sections 8-10 was performed by introducing reactant CH_4 at ambient pressure to a zeolite at room temperature or a temperature in the range of 20°C-250°C. Obviously, the operational condition of oxidative activation and catalytic oxidation of CH_4 on MO^+ clusters is different from the oxidative activation of CH_4 through active oxygen atoms in zeolite or on metal oxide.

The operational conditions of oxidation of CH_4 by MO^+ clusters (Sections 6 and 7) and oxygen atoms in micropores or on surface of metal oxide (Sections 8-10) are different from the operational conditions of catalytic oxidation of CH_4 at solid-liquid interface to be reviewed in Sections 11-13. The oxidation of CH_4 in Sections and 7 is performed in gas phase at a pressure of sub-Torr of CH_4 where the oxidant in terms of MO^+ clusters is dispersed in gas phase of CH_4. Different from the operational conditions of oxidation of CH_4 by MO^+ clusters, oxidation of CH_4 by modified zeolites in Sections 9 and 10 is performed at solid-gas interface at 100-250°C in gas phase of CH_4 at 1 bar; an important feature is that the zeolite needs to be regenerated through oxidation at 300-500°C. Different from these non-catalytic oxidizations of CH_4 to be reviewed in Sections 9 and 10, these catalytic oxidation of CH_4 under mild conditions to be discussed in the Sections 11-13 are actually performed at solid-liquid interfaces in the temperature range of 20°C-250°C; in these catalytic oxidation, only dissolved CH_4 molecules can access to the catalytic site of catalyst particles dispersed in solvent. This is why the liquid phase containing catalyst particles must be under a gas phase of CH_4 with high pressure (1-100 bars).

Compared to those oxidations of CH_4 to be reviewed in the sections 8-13, the oxidations of CH_4 by MO^+ clusters dispersed in gas phase are performed at 25°C in the gas phase of CH_4 at low pressure of 10^{-2}-0.5 Torr. Obviously, the oxidation of CH_4 by MO^+ clusters at low pressure gas of CH_4 is not a track leading to produce CH_3OH at large scale. In addition, the oxidation of CH_4 by oxygen atoms bound to metal atoms anchored in zeolites is a noncatalytic process; it needs regeneration of the oxygen atom after the consumption of those active oxygen atoms; thus, it is not a feasible process to produce value-added chemicals at a large scale potentially. It is expected that the catalytic oxidation of CH_4 at solid-liquid interface by catalyst dispersed in liquid under a high-pressure gas phase of CH_4 is a potential process for transformation of CH_4 to oxygenates at a large scale in the future. From the point view of

fundamental understanding of the science behind oxidation of CH_4 to CH_3OH, oxidation of CH_4 by MO^+ clusters is significant as MO^+ clusters can be well characterized for elucidating reaction mechanism at atomic scale and its insight gained from these studies can inspire the design of catalysts for producing CH_3OH.

CH_4 can be transformed to oxygenates by MO^+ in gas phase. Here transformation of CH_4 to CH_3OH on MO^+ is taken as an example to demonstrate the approach of converting hydrocarbons to organic oxygenates by free MO^+ in gas phase. Experimental exploration showed that late 3d-metal oxide clusters including MnO^+,[74] FeO^+,[71] CoO^+,[72] NiO^+ [73]are active for this reaction. However, the MO^+ clusters of early 3d transition metals such as ScO^+,[252-254] ZrO^+,[255] CrO^+,[256] are not active for oxidation of CH_4 to CH_3OH. Based on theoretical simulations,[237] such an oxidation is processed through adsorbed CH_4 on MO^+, a four-membered ring-like transition state (TS1), an intermediate, a three-membered ring transition state (TS2), formed CH_3OH on MO^+ before desorption to gas phase, $CH_4+MO^+\rightarrow(CH_4)MO^+\rightarrow[TS1]^{\#}\rightarrow CH_3\text{-}MO^+\text{-}OH\rightarrow[TS2]^{\#}\rightarrow(CH_3OH)M^+\rightarrow CH_3OH+M^+$.

Electronic structure of these MO^+ clusters active in oxidation of CH_4 to CH_3OH varies largely from the early to late 3d metals (Figure 10a).[237] M-O distance increases along the increase of d-electrons of M metal and dissociation energy of M-O bond decreases with the increase of d-electrons. As shown in Figure 10a, electron configurations of ScO^+ and FeO^+ are d^0 and d^5. At $^1\Sigma^+$ ground state of ScO^+, four pairs of electrons of ScO^+ occupy a nonbonding 1σ and three bonding orbitals (2σ and 1π) and thus form a strong triple bond similar to N_2, resulting in a high dissociation energy of Sc-O bond, rationalizing the low reactivity in activation of C-H and oxidation of CH_4 on ScO^+.[252-254] However, in terms of FeO^+, the bonding orbitals are doubly occupied and each 2π orbital is singly occupied (Figure 10b), similar to electronic configuration of a triplet O_2. Thus, the dissociation energy of Fe-O is definitely lower than Sc-O, responsible for the higher activity of FeO^+ in contrast to ScO^+. The difference in electronic states of ScO^+ and FeO^+ vindicated the observed difference in activity in oxidation of CH_4 to CH_3OH between ScO^+ and FeO^+.

The activity of MO^+ cluster of late 3d metals in transformation of CH_4 to CH_3OH origins at the orbital interaction of MO^+ and CH_4 in $[TS1]^{\#}$ and the change of fragment molecular orbital of C-H of CH_4 upon the formation of $[TS1]^{\#}$. As shown in Figure 10b, MO^+ fragments have high-lying-d-block orbitals of 3σ, 1σ, 2π and low-lying ligand of 2σ and 1π; CH_4 fragment has three C-H bonding orbitals resulting from 3-fold degenerate HOMO of T_d of CH_4. Molecular orbital of $[TS1]^{\#}$ (Figure 10b) can be constructed from these fragment

molecular orbitals. As shown at the left in Figure 10b, unfortunately the high-lying 3σ of ScO^+ cannot interact with C-H bonding orbitals. It makes sense that ScO^+ is not active for activation of C-H of CH_4.

Different from MO^+ of early 3d metal, there is significant interaction between molecular orbitals of MO^+ of late 3d metal and CH_4. This is because that the d-block orbital, 3σ of FeO^+ and CuO^+ are not fully occupied but they are lower in energy than ScO^+ (Figure 10b). Thus, the interaction between low-lying 3σ orbitals of late 3d metal MO^+ and CH_4 is effective, leading to energetical stabilization of the $[TS1]^{\#}$. Compared to the four-electron-two-orbital interaction in $[TS1]^{\#}$ formed from the coupling between ScO^+ and CH_4, the formed two-electron-two-orbital interaction between the low-lying 3σ orbital of FeO^+ and HOMO of the CH_4 fragment can stabilize the $[TS1]^{\#}$ formed from FeO^+ and CH_4. Similarly, the interaction between the 3σ orbital of CuO^+ and HOMO of CH_4 fragment is significant, making the formed orbitals in $[TS1]^{\#}$ low-lying.

Molecular orbital overlap population (MOOP) analysis can qualitatively explain why the MO^+ of late 3d metals can weaken C-H bond but the MO^+ of early 3d metals cannot. The weakening of C-H in $[TS1]^{\#}$ is evidenced by pushing the highest occupied level of C-H up or down. Be specific, if the C-H bonding orbitals in $[TS1]^{\#}$ are unoccupied or partially unoccupied, the C-H bond have been effectively weakened. As shown on the left of Figure 10c, the energy level of the highest C-H level in the $[TS1]^{\#}$ of ScO^+ is below the energy level of HOMO of ScO^+ and thus they are still fully occupied in the $[TS1]^{\#}$. Consequently, the interaction of orbitals of ScO^+ and CH_4 does not vary the occupancy of electrons in HOMO of CH_4; thus, such an interaction is not effective in activation of CH_4. Different from ScO^+, the orbital interaction between FeO^+ and CH_4 pushes the energy level of C-H up and thus make HOMO of CH_4 half-occupied (Figure 10c). In terms of the orbital interaction between CuO^+ and CH_4, in the formed orbitals of $[TS1]^{\#}$, C-H orbitals at -9 eV and -12 eV are completely unoccupied and half-occupied, respectively. Since the energy level of C-H bonding in the $[TS1]^{\#}$ of CuO^+ and CH_4 is definitely above E_{HOMO}, these highest levels of CH_4 are unoccupied or partially occupied. It further suggests that the C-H bond of CH_4 has been effectively weakened.

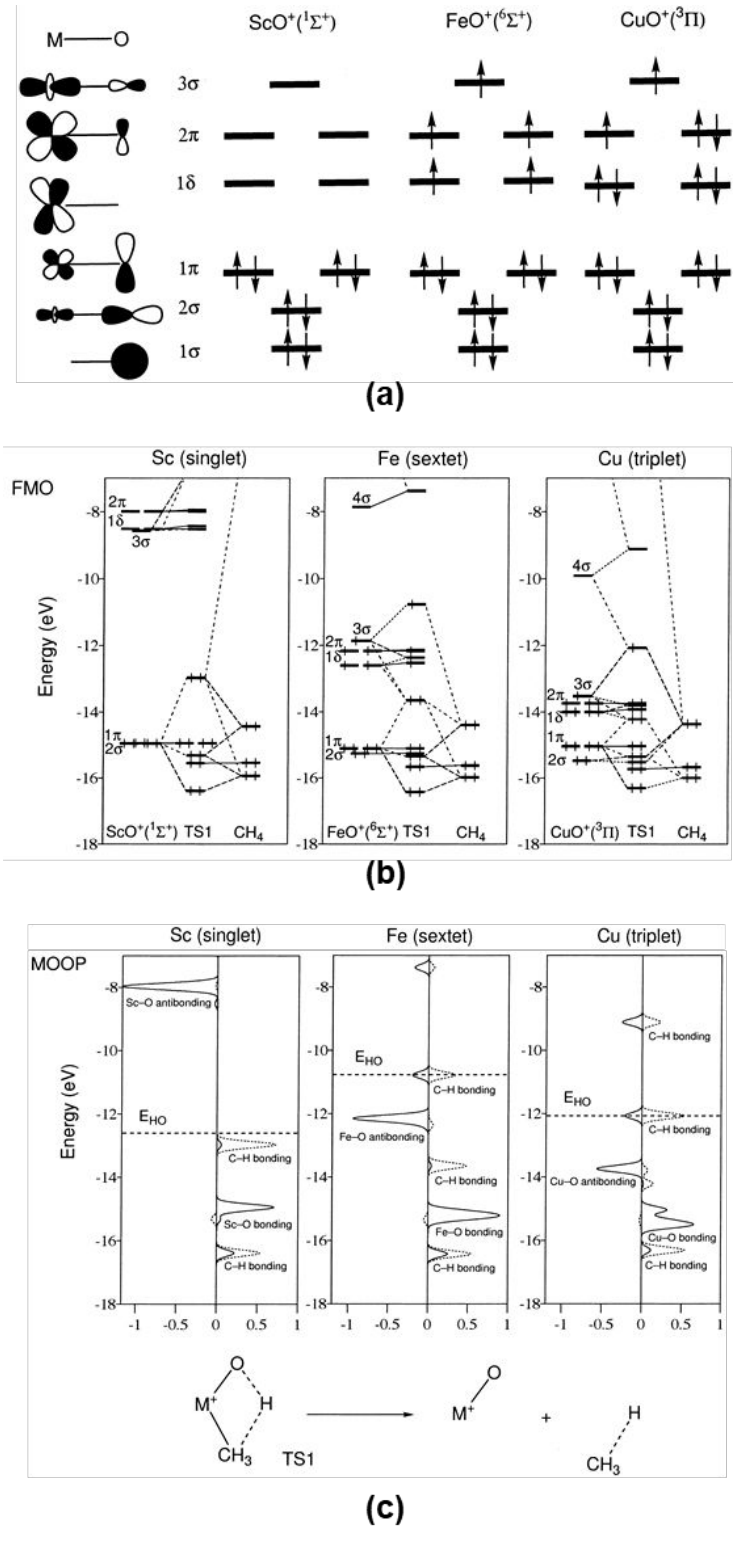

Figure 10. *Representation of interaction of free MO^+ clusters and CH_4 in transformation of CH_4 to CH_3OH in gas phase. (a) Molecular orbital of MO^+ clusters. (b) Analysis of fragment molecular orbital (FMO) of CH_4 and representative MO^+ including ScO^+, FeO^+ and CuO^+. (c) Analysis of molecular orbital overlap population (MOOP) of $[TS1]^\#$ formed from CH_4 and representative MO^+ including ScO^+, FeO^+ and CuO^+.[237] Reproduced from Ref. 237, copyright 2000, with permission from ACS.*

These analyse of molecular orbitals of MO^+, CH_4 and their $[TS1]^{\#}$ provided profound understanding of the lack of activity in activation of CH_4 on MO^+ of early 3d metals but active on MO^+ of late 3d metals. The high activity of CuO^+ and FeO^+ for oxidation of CH_4 to form CH_3OH is in good agreement with the later finding that Fe-O and Cu-O clusters encapsulated in zeolite are active in oxidation of CH_4 to CH_3OH under mild conditions. The oxidations of CH_4 to CH_3OH by Fe-O and Cu-O clusters encapsulated in zeolite were reviewed in Section 9. These insights gathered from experimental and computational studies at level of molecular orbitals provided foundation for understanding activity of Fe-O and Cu-O clusters anchored in zeolite in oxidation of CH_4 to CH_3OH.

These systematic studies of free MO^+ clusters of all 3d metals have rationalized the evolution of activity of free MO^+ clusters in oxidation of CH_4 to CH_3OH at the level of molecular orbitals. *However, there are lack of experimental studies for M-O clusters of all 3d metals anchored in zeolite such as Sc@ZSM-5, Ti@ZSM-5, V@ZSM-5, Mn@ZSM-5 and lack of exploration of potential evolution of activity in oxidizing CH_4 to CH_3OH by M@ZSM-5 (M=Sc, Ti, V, Cr, Mn, Fe, Co, Ni, Cu) as a function of electronic structure and molecular orbitals of M-O clusters. Such studies are highly recommended as they will allow for uncovering correlation between electronic state of anchored M-O clusters and their reactivities in oxidizing CH_4 to CH_3OH.*

7. Catalytic oxidation of CH_4 on bare MO^+ and M^+

Early studies suggested that MO^+ can catalyse oxidation of hydrocarbons to form oxygenates including alcohols and aldehydes.[71, 243, 237-241] One example of catalytic oxidation involving MO^+ is the catalytic oxidation of CH_4 by O_2 on Pt^+ ions with a turnover rate of about 6.0 for the Pt^+-mediated oxidation of methane to produce multiple products including CH_3OH, formaldehyde and formic acid.[73, 257] PtO^+ is not an initial reactant. But PtO^+ clusters are formed based on the temporal evolution of the species involved (Figure 11a).[257] Thus, PtO^+ clusters do play an important role the catalytic oxidation of CH_4. In addition, $Pt[CH_2]^+$ complex was formed in the catalytic oxidation of CH_4 by Pt^+. Thus, three sequential reactions involving Pt^+, $[PtCH_2]^+$, and PtO^+ are proposed (Figure 11b).[257] Reaction III includes two parallel reactions; one is the direct oxidation of CH_4 by PtO^+ to form methanol. In fact, this catalysis is more complicated than simply understanding it into three sequential reactions because all three Pt-

based species can activate CH_4 molecules as shown in Figure 11b. In addition, as reaction II in Figure 11b is the slowest step in this catalytic oxidation, a large excess of O_2 has to be used if a high turn-over rate of CH_4 is requested. In the study of Figure 11a, an O_2:CH_4 ratio of 1:20 was used. A consequence while a high O_2/CH_4 ratio is used is the high selectivities for deeper oxidations of CH_4 in terms of formations of formaldehyde and formic acid in this catalytic oxidation process.

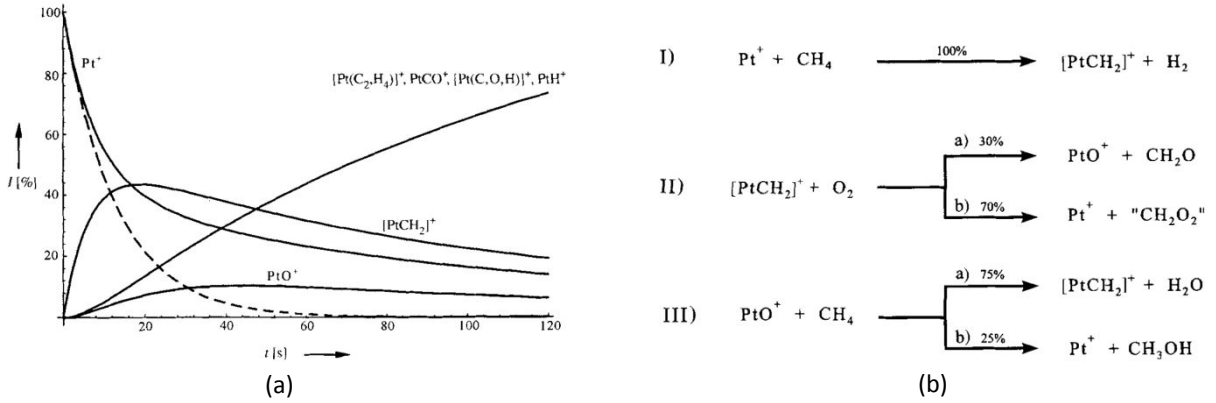

Figure 11. Catalytic oxidation of CH_4 to methanol, formaldehyde, and formic acid through Pt^+ involving formation of PtO^+ and oxidation of CH_4 to form CH_3OH by PtO^+.[257] (a) Temporal evolution of intensities of Pt-based species including Pt^+, $[PtCH_2]^+$, and PtO^+ in the mixture of O_2 and CH_4 with molar ratio of 20:1. (b) Three reactions involved in the catalytic oxidation of CH_4. *Reproduced from Ref. 257, copyright 2003, with permission from John Wiley and Sons.*

8. Activation and oxidation of CH_4 on M-O cluster anchored on oxide

Bare MO^+ such as MO^+ (M=Mn, Fe, Co, Ni, Cu, Pt) exhibit high reactivity in activation or oxidation of CH_4 as reviewed in Section 6. As discussed in Section 7, some of them can even oxidize light alkanes including CH_4 to oxygenates such as CH_3OH through a close cycle of catalysis. In such activations or catalysis, MO^+ cations are free standing and distributed in gas phase. Consistent with high reactivity of *free* or called *free standing* FeO^+ or NiO^+ in oxidation of CH_4 at room temperature reviewed in Section 6,[71, 242-248 72, 249] oxidation of CH_4 by NiO species *anchored* on surfaces of $NiCo_2O_4$ and $NiFe_2O_4$ was reported recently.[48, 49]

Ni cations were introduced to Co_3O_4 through partial replacement of cobalt ions. Thus, surface of this catalyst consists of Ni-O and Co-O species. As shown in Figure 12a, the anchored NiO cations can activate C-H of CH_4 at a temperature as low as 60°C. [95, 96] Surface of $NiCo_2O_4$ during catalysis was tracked with AP-XPS. C 1s photoemission features of carbon-containing species on $NiCo_2O_4$ during oxidation of CH_4 in the temperature range of 60-400°C

were presented in Figure 12a. Two carbon-containing species were clearly observed on the basis of the two C 1s peaks at 288.5 eV and 285.8 eV (Figure 12a). As there is lack of any carbon species of potential contaminants before exposure to mixture of CH_4 and O_2, the surface of $NiCo_2O_4$ is carbon free before the introduction of CH_4. The two carbon-containing species must result from the activation of CH_4 by $NiCo_2O_4$ surface. Peak 2 of Figure 12a was assigned to an OCHO species based on in situ infrared spectroscopy.[95] As the evolution of C 1s intensity as a function of temperature of catalyst $NiCo_2O_4$ exhibits a volcano-like evolution, OCHO is the intermediate which was formed at low temperature and observed by infrared spectroscopy.[95]

This observation of OCHO species at 60°C on $NiCo_2O_4$ surface suggests that CH_4 can be activated under a mild condition even at a temperature as low as 60°C. Computational studies show that Ni-O on surface is active for activating CH_4 to form OCHO and CH_3 bonded to surface of $NiCo_2O_4$.[95] Thus, the high activity of charged Ni-O cluster *anchored* on Co_3O_4 is consistent with the reported high activity of *bare* NiO^+ for activation of CH_4. Similarly, the charged Ni-O species anchored on surface of Fe_3O_4 are active for oxidation of CH_4 at a temperature as low as 60°C.[96] Similar to $NiCo_2O_4$, the activation of CH_4 on $NiFe_2O_4$ forms similar OCHO and CH_3 species.

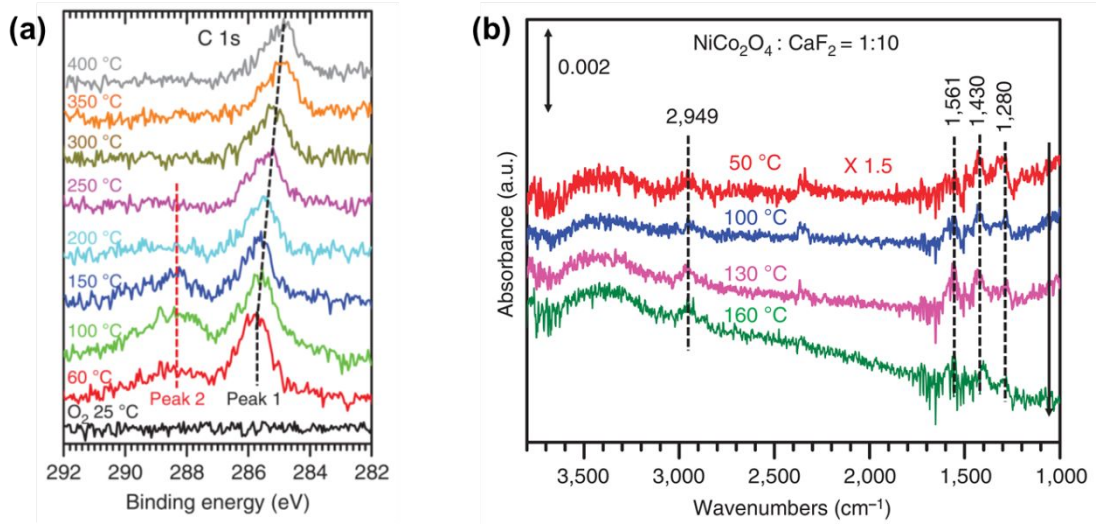

Figure 12. *Representation of photoemission features of C 1s collected from Ambient Pressure X-ray Photoelectron Spectroscopy (AP-XPS) and vibrational signatures collected with Diffuse Reflectance Infrared Fourier Transform (DRIFT) spectroscopy from surface adsorbates formed through activation of CH_4 on charged Ni-O species anchored on surface of $NiCo_2O_4$.[48] (a) C 1s spectra of surface adsorbates formed on $NiCo_2O_4$ at 60°C in CH_4 . (b) Vibrational spectrum of adsorbate after exposing $NiCo_2O_4$ at 60°C to CH_4. Reproduced from Ref. 48, copyright 2015, with permission from Springer Nature.*

9. Activation and oxidation of CH_4 by M-O cluster anchored in zeolite

To generate organic oxygenates by activation and oxidation of CH_4, source of oxygen atoms can be the free-standing MO^+ cations in gas phase or the anchored MO^+ on surface of oxide nanoparticles. From thermodynamic point of view, these activation and oxidation to transform CH_4 to CH_3OH can be performed under mild conditions or even at room temperature. Upon transformation of these pre-anchored oxygen atoms to CH_3OH, this type of specific oxygen atoms has to be regenerated before more CH_4 molecules can be oxidized. Strictly speaking, they are an oxidative reaction instead of a close cycle of catalysis. Notably, these transformations discussed in Sections 6-8 and this section use pre-existing oxygen atoms of M-O clusters freely in gas phase or anchored on support instead direct use of any routine oxidant of chemical reactions such as O_2, H_2O_2 or H_2SO_4. Other than these free-standing MO^+ and supported M-O clusters supported on Co_3O_4, a few transition metal cations including Cu, Fe, and Ni can form unique oxide clusters with specific structures such as μ-oxo structure in ZSM-5 upon pre-treatment in O_2 or N_2O at high temperature. Notably, these reactions reviewed in this section are activation and oxidation of CH_4 instead of catalytic oxidation. They are different from catalytic oxidations of CH_4 with H_2O_2 on catalysts such as zeolite with anchored metal oxide clusters reviewed in Section 13.

9.1 Confinement effect of microporous aluminosilicate on activation of molecules in micropore

As confinement effect is an important concept in understanding activation of C-H of CH_4 in M-O clusters anchored in ZSM-5, it is briefed here. Olson et al reported that sub-nanometre pores of ZSM-5 exhibit spatially limit effect for molecules with kinetic diameter larger than about 7.0 Å.[258] CH_4 with kinetic diameter of about 3.7 Å can readily diffuse in this micropores since the pore size of 10-membered-ring of ZSM-5 is 5.4-5.6 Å. Based on Zicovich-Wilson and Corma's reports,[259, 260] different from a molecule in gas phase, orbitals of the molecule encapsulated in a micropore of zeolite do not extend over all space, which was called confinement effect by Zicovich-Wilson and Corma.[259, 260]

One consequence of the confined effect is the large distortion of bond geometry. As shown in Figure 13c, this confinement effect was supported by the difference b bond angle *between* the 85°-111° of ∠OMC (M: metal atom) such as ∠OFeC, ∠OCoC, ∠ONiC, and ∠OCuC in the optimized geometry of CH_4 adsorbed on metal atoms anchored in confined

space of ZSM-5 *and* the nearly 180° on an metal oxide cluster in open space.[261]

A surprising consequence of this confinement effect[261] is the low binding energy of CH_4 on a MO^+ confined in microporous silicate such as CuO^+-ZSM-5 is only -1.1 kcal/mol which is much lower than the -45.8 kcal/mol for adsorption of CH_4 on free-standing CuO^+ in gas phase.[237] In addition, systematic DFT calculations on different MO^+ clusters encapsulated in ZSM-5 show that binding energies of CH_4 on MO^+ clusters in ZSM-5 are correlated with the configurations of O-M-C atoms;[237] a smaller ∠OMC angle on the adsorbed CH_4 on MO^+ in ZSM-5 in terms of a large distortion of molecular geometry of adsorbed CH_4 corresponds a lower binding energy of CH_4 in terms of a larger confinement effect. In other words, the limited extension of molecular orbital of CH_4 in the sub-nanometre porous space forces CH_4 to take a bent configuration which is at an unstable state in terms of having higher energy than that in open space.

A very favourable consequence of the confined effect of the micropore of zeolite to CH_4 molecule is the low activation barrier for cleaving C-H of CH_4. The computational studies suggest that the activation barrier for C-H of CH_4 on a confined CuO^+ in ZSM-5 is only 6.4 kcal/mol[261] which is much lower than 26.4 kcal/mol on bare CuO^+.[237] This consequence is also supported from a comparison to the activation of C-H of CH_4 on the open surface of CuO. The activation barrier for cleaving the first C-H of CH_4 in CuO^+ confined in ZSM-5, 6.4 kcal/mol, is obviously lower than the activation barrier, 11.3 kcal/mol for cleaving the first C-H of CH_4 on the open surface of CuO(110) where C atom of CH_4 in the transition state binds to cationic Cu atom of CuO(110) surface.[262]

Other than the distortion of binding configuration of a reactant molecule and the decrease of activation barrier of the molecule confined in zeolite, another significant impact from confinement of micropores of zeolite is the largely increased repulsion *between* the reactant molecule *and* O and Si atoms of sub-nanometre pore. Thus, these consequences of confinement effect of zeolite to molecules adsorbed on MO^+ encapsulated in ZSM-5 suggest the significance of anchoring MO^+ clusters in micropores for a facile activation of CH_4 under mild conditions.

9.2 Computational studies for transformation of CH_4 to CH_3OH by MO^+ in ZSM-5

Transformation of CH_4 to CH_3OH on free standing first-row transition metal oxide ions (MO^+) in gas phase was investigated with computational approach (M=Sc, Ti, V, Cr, Mn, Fe, Co, Ni, and Cu).[237] Although no experimental studies for activity for oxidation of CH_4 on MO^+

anchored in ZSM-5 were performed, Yoshizawa et al performed parallel computational studies of MO^+@ZSM-5 (M=Fe, Co, Ni, Cu) for investigation of the influences of different metals on oxidation of CH_4 to CH_3OH.[261] They proposed that this transformation is performed through three intermediates including reactant complex, hydroxyl and product complex and two transition states (Figure 13a). Energy profiles of the four "catalysts" are very different (Figure 13b). The binding energy of the reactant complex in terms of adsorbed CH_4 on CuO^+@ZSM-5 is highest among the four analogous "catalysts", MO^+@ZSM-5 (M=Fe, Co, Ni, Cu). This high binding energy originates at the significant interaction between the low-lying 3σ orbitals of CuO^+ and HOMO of CH_4 fragment.[237, 261] Figure 13a illustrates the catalytic cycle for catalytic oxidation of CH_4 with N_2O to form CH_3OH and N_2. The activation barriers of the two transition states on CuO^+@ZSM-5 are lowest compared to the other three catalysts (Figure 13b). In terms of TS1, the lowest activation barrier on CuO^+@ZSM-5 among MO^+@ZSM-5 (M=Fe, Co, Ni, Cu) results from the shortest O-C distance and smallest ∠OMC in the configuration of transition state among the four catalysts (Figure 13c). Regarding to TS2, the lowest activation energy to cross TS2 on CuO^+@ZSM-5 can be rationalized with the shortest M-C bond (2.50 Å for Fe catalyst, 2.30 Å for Co catalyst, 2.13 Å for Ni catalyst, 2.08 Å for Cu catalyst) (Figure 13d).

As pointed out by Shiota et al, the number of *d*-electrons and the energy of the *d*-block orbitals are two dominant factors affecting the barrier of C-H activation of CH_4 on *free standing* MO^+.[237] In terms of activation of C-H of CH_4 on *anchored* MO^+ in ZSM-5, we predict that the number of *d*-electrons and the energy of the *d*-block orbitals to be the descriptors playing controlling roles in governing the barrier of C-H activation of CH_4. Thus, here a computational study is suggested to investigate whether the two descriptors of free-standing MO^+ reported in literature[237] could be applied to MO^+ anchored in ZSM-5. In addition, such a proposed computational study can help to elucidate whether the confinement effect of ZSM-5 on MO^+ could dominate the descriptors of the C-H activation of CH_4 on MO^+ (M=Fe, Co, Ni, Cu) anchored in ZSM-5 upon comparing descriptors of *anchored* MO^+ in ZSM-5 to those of *free-standing* MO^+.

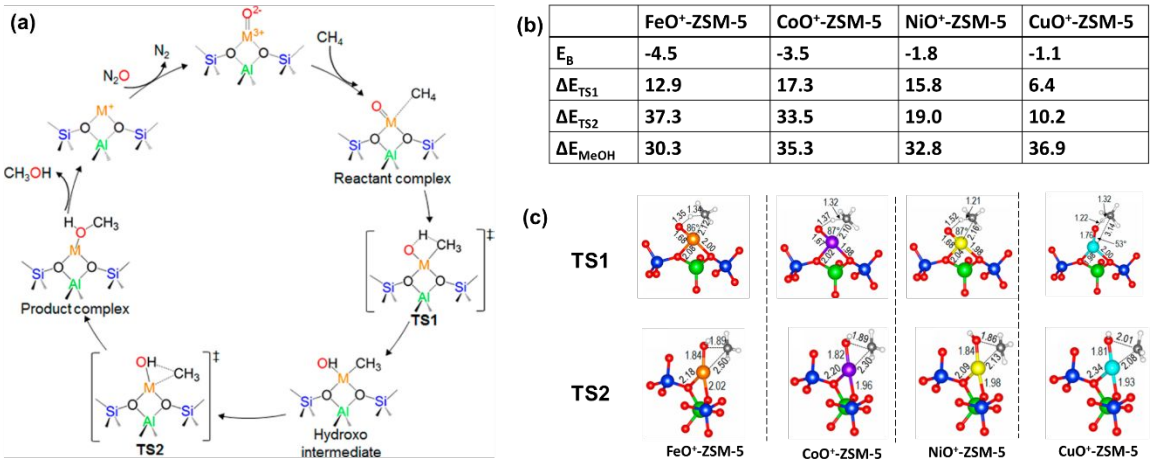

(b)	FeO^+-ZSM-5	CoO^+-ZSM-5	NiO^+-ZSM-5	CuO^+-ZSM-5
E_B	-4.5	-3.5	-1.8	-1.1
ΔE_{TS1}	12.9	17.3	15.8	6.4
ΔE_{TS2}	37.3	33.5	19.0	10.2
ΔE_{MeOH}	30.3	35.3	32.8	36.9

Figure 13. *Representation of computational studies of oxidation CH_4 by MO^+ (M=Fe, Co, Ni and Cu) anchored in ZSM-5 to CH_3OH.[261] (a) Proposed catalytic cycle. (b) List of energies of intermediates and transition state in oxidation of CH_4 by MO^+ anchored in ZSM-5 to CH_3OH. (c) Optimized structures of TS1 and TS2 on the four catalysts. Reproduced from Ref. 261, copyright 2016, with permission from ACS.*

9.3 Anchored bis(μ-oxo)diiron in ZSM-5 for activation of CH_4

The early studies reported oxidation of CH_4 at high temperature by anchored oxygen atoms on Fe-ZSM-5 which was prepared through pre-treatment of precursor in N_2O; oxidation of CH_4 by Fe-ZSM-5 formed different products.[263] [264-268] Among these studies, CH_3OH was produced from oxidation of CH_4 at room temperature by anchored oxygen atoms on Fe^{III} in Fe-ZSM-5.[267, 268] Notably, the formed CH_3OH was strongly adsorbed in micropores of ZSM-5. The strong adsorption results from van de Waals forces, particularly the hydrogen bonding of CH_3OH in micropores enhanced by confinement effect of aluminosilicate pores. In general, the formed CH_3OH is extracted from the micropores with a mixture of acetonitrile and water[269] or through water steam.[60] A creative method developed by van Bokhoven is that CH_3OH formed in Cu-MOR can be extracted in an on-line mode in steam.[270]

The activity of activated Fe-ZSM-5 origins at oxygen atom bonded to Fe^{III}, which was called α-oxygen in literature.[264-266, 271, 272, 273] $(Fe^{II})_\alpha$ complex, sometime called α-site, can be formed through calcination of Fe-ZSM-5 at a temperature higher than 500°C in O_2. Based on literature,[274] Fe^{III} of Fe-ZSM-5 is evolved to Fe^{II} at 500°C along releasing O_2. Some Fe^{II} atoms were stabilized in the zeolite matrix,[275] making oxidation of this species unfavourable thermodynamically even at a temperature higher than 700°C.[276] Thus, an appropriate activation temperature in O_2 is key for gaining reactivity in oxidation of CH_4 to CH_3OH. In addition,

active Fe-ZSM-5 with $(Fe^{III}\text{-}O\cdot)_\alpha$ sites can be prepared through oxidation of precursor in terms of Fe loaded ZSM-5 in N_2O at 200°C-250°C since the O_α desorbs in the form of molecular O_2 at a temperature higher than 300°C. Based on the measured stoichiometric ratio of O_α to Fe never exceeding 1:2,[277] driven by the coincidence of Mossbauer spectroscopy of Fe in sMMO and Fe in ZSM-5[268], inspired by the modelling of oxygen activation on CH_4 monooxygenase,[278] and supported by the computational studies of Fe-ZSM-5,[277] Panov et al suggested that Fe atoms in Fe-ZSM-5 could exist in the form of a binuclear complex, bis(μ-oxo) in which two Fe atoms are linked through bis(μ-oxo) although there was lack of EXAFS data to support.[277] The first successful construction of the structural model of the active site of Fe-ZSM-5 in terms of oxo-bridged di-iron complex can be tracked to the early study in 1993.[273] Analysis of electronic structure of the oxo-bridged di-iron complex shows the lowest unoccupied molecular orbital (LUMO) has a very low eigenvalue (-0.79 eV), suggesting that this complex is a strong oxidant. This low-lying LUMO is mainly contributed from d-orbitals of one Fe atom and has admixtures of orbital centred on adjacent oxygen atoms.[277] Thus, the Fe atom in oxo-bridged di-iron complex efficiently acted as the actual oxidizing site at atomic scale.

Yoshizawa et al simulated the reaction mechanism of CH_4 hydroxylation on α-oxygen of a simplified structure model (Figure 14a).[279] This study suggests that the coordinatively unsaturated iron-oxo is the species activating C-H, which is consistent with the analysis of electronic structure of a derivative of bis(μ-oxo)diiron in terms of the contribution of LUMO.[277] Based on this computation represented in Figure 14, a CH_4 complex is formed; in this complex, CH_4 weakly binds to Fe (III) which coordinates with three oxygen atoms. Upon formation of the CH_4 complex, one C-H bond is cleaved through a Fe-C-H-O four-member-ring-like transition state shown in Figure 14b, which is similar to the first intermediate formed on FeO^+ in activation CH_4 on free FeO^+.[237] Upon traversing this first transition state, the hydroxy intermediate is formed; it binds to the Fe^{III} atom (Figure 14b). Subsequently, the CH_3 and OH groups bound to the same Fe^{III} atom couple each other, forming a three-centre transition state (TS2 in Figure 14b). Upon dissociation of Fe-O bond, a CH_3OH molecule adsorbed to the Fe atom is formed. Figure 14c is the energy profile of the direct CH_4 hydroxylation on Fe-O_α in ZSM-5 (Figure 14c)[279] which is very similar to that of the gas phase reaction between CH_4 and free FeO^+.[280, 281] Notably, the reaction mechanism of formation of CH_3OH through *direct oxidation* of CH_4 by Fe-O_α of ZSM-5[279] is distinctly different from the radical mechanisms in *catalytic oxidation* of CH_4 by H_2O_2 on di-iron species anchored in ZSM-5 which was reviewed in Section 13.

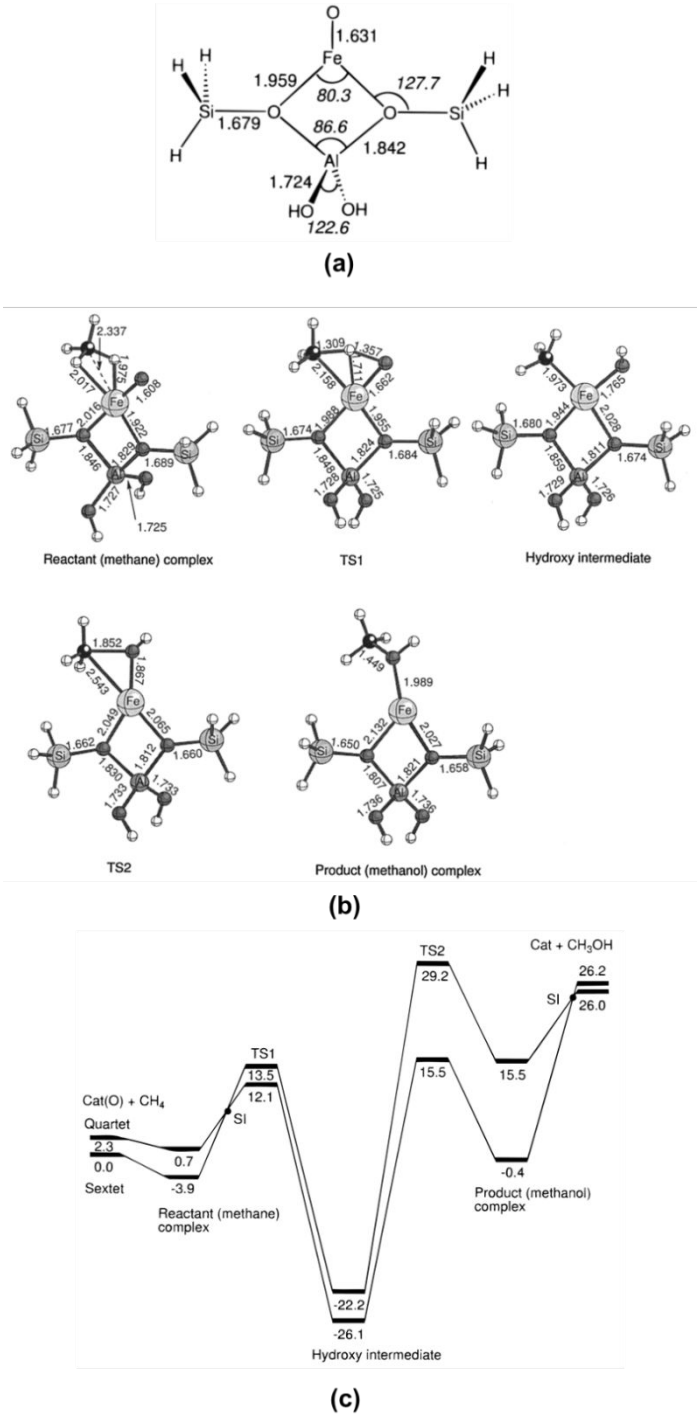

Figure 14. *Representation of results of computational studies of the mechanism for oxidation of CH_4 with α-oxygen of Fe-ZSM-5 to form CH_3OH.[279] (a) Scheme of $(Fe\text{-}O)_\alpha$. (b) Optimized intermediates and transition state for reaction of CH_4 with α-oxygen to form CH_3OH molecule. (c) Energy profile for direct CH_4 hydroxylation on the structural model (a) of α-oxygen of Fe-ZSM-5 in sextet and quartet states. Reproduced from Ref. 279, copyright 2000, with permission from ACS.*

9.4 Anchored oxygen over Cu sites for activation of CH_4

9.4.1 $Cu_nO_n^{2+}$ in ZSM-5

Zeolite loaded with Cu was early used for selective oxidation of hydrocarbons with molecular O_2 and deNO_x for diesel combustion engine.[282-285] Groothaert early reported successful oxidation of CH_4 to CH_3OH in micropore of Cu-ZSM-5 at 100°C or so.[269] They proposed that bis(μ-oxo)dicopper species can be formed through annealing Cu-ZSM-5 in N_2O or O_2 at a temperature high than 350°C. The bis(μ-oxo)dicopper species contributed to the characteristic peak at 22700 cm^{-1} in UV-vis spectra.[269] This assignment was supported by the correlation between oxidation of more CH_4 and simultaneous decay of intensity of 22700 cm^{-1} was clearly shown in Figures 14a and 14b. Formation of this bis(μ-oxo)dicopper species was supported by other characterizations including EXAFS, TEM, and EPR.[286] More importantly, the time-dependent attenuation of the intensity of peak at 22700 cm^{-1} during reaction with CH_4 clearly shows that the Cu complex is the site to oxidize CH_4. With the extraction method using solution of 1:1 water/acetonitrile, 82 μmol of CH_3OH was generated from 1 gram of Cu-ZSM-5 with Si/Al=12 and Cu/Al=0.58 (CZ-12-0.58).[269]

The selectivity for producing CH_3OH on the CZ-12-0.58 is as high as 98%. Different from the low selectivity for producing CH_3OH in catalytic oxidation of CH_4 with H_2O_2, the high selectivity for producing CH_3OH by non-catalytic oxidation benefits from the lack of excessive oxidant since only these oxygen atoms anchored to metal atoms in zeolite are oxidant for oxidation of CH_4. Similar to Fe-ZSM-5,[267, 268] the formation of CH_3OH in through oxidation of CH_4 by Cu-ZSM-5 is not a catalytic process as Cu-ZSM-5 was not exposed to CH_4 and an oxidant and CH_3OH was not be produced continuously. Section 13 extensively discussed *catalytic* oxidation of CH_4 to form CH_3OH by using H_2O_2 as an oxidant under mild conditions.

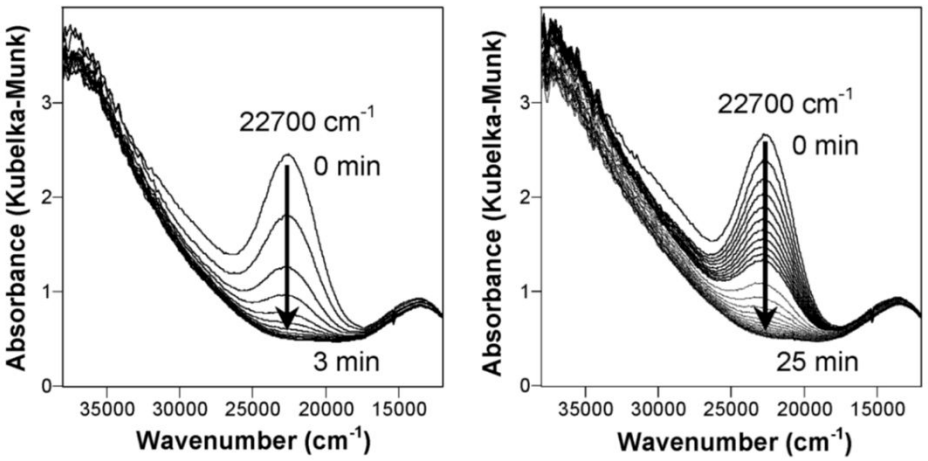

Figure 15. *Representation of fibre-optic UV-vis spectra of O_2-activated CZ-12-0.58 during reaction with CH_4 (5% in N_2; 25 mL min^{-1}) at 448 K (a) and at 398 K (b).[269] Reproduced from Ref. 269, copyright 2005, with permission from ACS.*

The chemical and coordination environments of Cu atoms in the micropores of Cu-ZSM-5 is quite complicated. Many endeavours were made in elucidation of the structure of the Cu-based active sites at an atomic scale. It is suggested that the reactivity of Cu-ZSM-5 for oxidation of CH_4 to form CH_3OH mainly stems from anchored binuclear oxygen-containing Cu complex, $[Cu(\mu\text{-}O)Cu]^{2+}$.[287-291] However, early studies proposed that the active site could be a bis(μ-oxo)dicopper, $[Cu(\mu\text{-}O)_2Cu]^{2+}$, which is an analogue of a catalytic site of pMMO hypothesized early without approval.[292-297] These ambiguous assignments probably resulted from the challenges in experimentally distinguishing bis(μ-oxo)dicopper, $[Cu(\mu\text{-}O)_2Cu]^{2+}$, and binuclear species $[Cu(\mu\text{-}O)Cu]^{2+}$. In fact, analysis of lobes of HOMO of $[Cu(\mu\text{-}O)_2Cu]^{2+}$ and $[Cu(\mu\text{-}O)Cu]^{2+}$anchored in 10-membered rings suggest (1) both of them are a hybridization of μ-O atom(s), two Cu atoms and two O atoms between Cu and Al, and (2) both of them have a complicated *d-type* bonding.[298] In addition, bis(μ-oxo)dicopper, $[Cu(\mu\text{-}O)_2Cu]^{2+}$ and binuclear species, $[Cu(\mu\text{-}O)Cu]^{2+}$ exhibit very similar stability. Despite of these early studies, the recent resonance Raman spectroscopy studies of Cu-ZSM-5 suggested that binuclear species $[Cu(\mu\text{-}O)Cu]^{2+}$ plays a significant role in oxidation of CH_4 to form CH_3OH.[299]

Inspired by the importance of multi-nuclear Cu species (Cu_3O_4) (1 in Figure 6b) in oxidation of CH_4 in pMMO,[218, 300-302] and the significant heterogeneity of extra-framework species formed in cation-exchanged microporous aluminosilicate, Pidko et al proposed that multi-nuclear Cu complexes are active sites for oxidation of CH_4 to form CH_3OH in their computational study combining periodic DFT calculations and ab initio thermodynamic analysis.[303] This computational study shows that the formation of Cu complexes depends on conditions of activation of Cu-ZSM-5 in terms of the temperature and gas phase composition used for activation, particularly partial pressure of O_2.[303] As shown in Figure 16a, a low partial pressure of O_2 is favourable for formation of binuclear $[Cu(\mu\text{-}O)Cu]^{2+}$ species, and trinuclear Cu complex $[Cu_3(\mu\text{-}O)_3]^{2+}$ can be formed at a relatively high oxygen pressure. Figure 16b suggests that $[Cu_3(\mu\text{-}O)_3]^{2+}$ exhibits a higher stability than mono-nuclear $[Cu(\mu\text{-}O)]^{2+}$ and binuclear $[Cu(\mu\text{-}O)Cu]^{2+}$ from thermodynamic point of view. In addition, the calculated Bader atomic charges of binuclear $[Cu(\mu\text{-}O)Cu]^{2+}$ shows the nature of an anion radical of the μ-O (-0.77 e). Similarly, the Bader charge on O atom of $[Cu_3(\mu\text{-}O)_3]^{2+}$ is about -0.70e – -0.73 e,

exhibiting the nature of an anion radical.[303]

Activations of C-H on $[Cu(\mu\text{-}O)Cu]^{2+}$ and $[Cu_3(\mu\text{-}O)_3]^{2+}$ were simulated with DFT approaches. These computational studies suggested these activation of C-H of CH_4 on $[Cu(\mu\text{-}O)Cu]^{2+}$ is performed through homolytic C-H bond dissociation with a followed direct radical rebound.[299] The dissociated H atom binds to μ-O, forming a OH group bridging on the two Cu atoms. The activation energy for the homolytic C-H dissociation step is 68-78 kJ/mol.[299, 303] Alternatively, a heterolytic dissociation results in H and CH_3 bond to Cu and μ-O, respectively, forming $[CH_3\text{-}Cu(\mu\text{-}OH)Cu]^{2+}$. Other than the two paths, a more thermodynamically favourable path is homolytic on one lattice oxygen atoms of zeolite neighbouring to the Cu complex (Figure 16c), forming a framework-anchored CH_3O group. [299, 303] Unfortunately, formation of CH_3OH from this framework-anchored CH_3O group is unfavourable since transfer of OH group to CH_3 in this case is significantly endothermic. For the radical rebound route, as shown in Figure 16c, about 156 kJ/mol energy is needed to desorb CH_3OH adsorbed on two Cu atoms through O atoms of the CH_3OH molecule. Definitely, this is a strong chemisorption of CH_3OH. The strong adsorption is unfortunately favourable for further oxidation to form formaldehyde or formic acid or even CO_2.

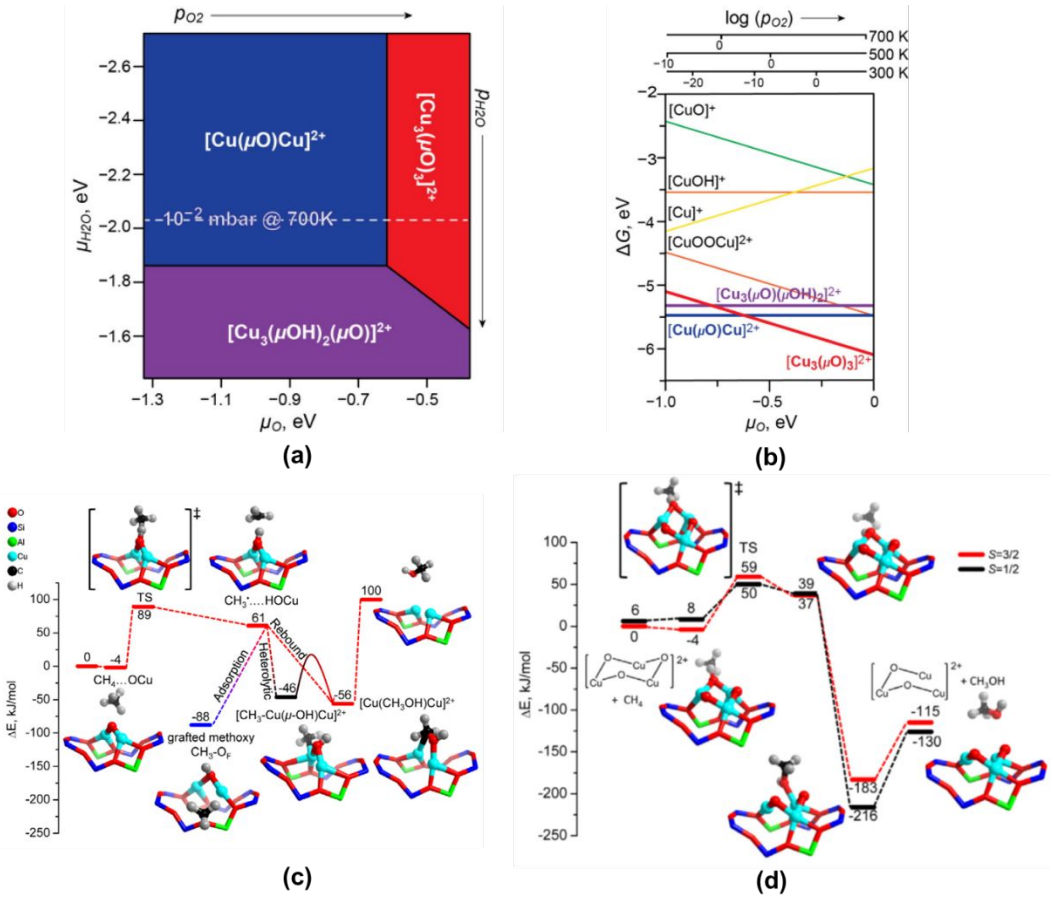

Figure 16. *Representation of ab initio thermodynamic analysis of Cu complexes formed at different conditions. (a) 2D projection of the lowest Gibbs free energy $Cu_xO_mH_n$ species in ZSM-5 (DG (eV/U.C.), $\Delta G(T,p) = \Delta E - \frac{2m-n-2x+2}{2}\Delta\mu_O - \frac{n-2}{2}\Delta\mu_{H_2O}$ as a function of oxygen $(\Delta\mu_O)$and water $\Delta\mu_{H_2O}$ chemical potentials. (b) A cross section of the 3D phase diagram at a fixed $\Delta\mu_{H_2O}$ (indicated with a dashed line in (a)), corresponding to 10^{-2} mbar H_2O at 700K. (c) Reaction path an energy profile for selective oxidation of CH_4 with binuclear $[Cu(\mu\text{-}O)Cu]^{2+}$ to form CH_3OH. (d) Reaction path an energy profile for selective oxidation of CH_4 with trinuclear $[Cu_3(\mu\text{-}O)_3]^{2+}$ to form CH_3OH.*[299, 303] *Reproduced from Ref. 303, copyright 2016, with permission from Elsevier.*

In terms of $[Cu_3(\mu\text{-}O)_3]^{2+}$, direct rebound route, absorption and heterolytic routes on trinuclear $[Cu_3(\mu\text{-}O)_3]^{2+}$ were investigated for oxidation of CH_4 to form CH_3OH. Compared to the strong binding of CH_3OH to Cu atoms of $[Cu(\mu\text{-}O)Cu]^{2+}$ (156 kJ/mol in Figure 16c), the binding energy of CH_3OH on trinuclear $[Cu_3(\mu\text{-}O)_3]^{2+}$ in the rebound route and heterolytic routes is 86 kJ/mol (Figure 16d). It suggests that oxidation of CH_4 with $[Cu_3(\mu\text{-}O)_3]^{2+}$ is thermodynamically favourable. Kinetically, on the basis of computational studies of Li et al.,[303] the activation barrier for C-H cleavage by trinuclear $[Cu_3(\mu\text{-}O)_3]^{2+}$, 10 kJ/mol is much lower than that of binuclear $[Cu(\mu\text{-}O)Cu]^{2+}$, 64-68 kJ/mol.[303] These DFT studies [299, 303] predicted that $[Cu_3(\mu\text{-}O)_3]^{2+}$ formed in ZSM-5 is an active site for selective oxidation of CH_4 to form CH_3OH although exclusive experimental evidences to support this prediction has not reported.[303] The reactivity of tri-nuclear $[Cu_3(\mu\text{-}O)_3]^{2+}$ anchored in MOR reported by Grundner et al[304] supported this suggestion that $[Cu_3(\mu\text{-}O)_3]^{2+}$ in ZSM-5 is the active site for oxidation of CH_4 to CH_3OH made by Pidko et al.[303]

The inconsistence between structure suggested from experimentalists and that proposed by theoreticians very likely results from (1) the heterogeneity of sites of sample prepared experimentally, (2) the lack of information on the authentic sites of due to the limited access of current characterisation technique, (3) difficulty in differentiating $[Cu(\mu\text{-}O)Cu]^{2+}$ and $[Cu_3(\mu\text{-}O)_3]^{2+}$. Further effort of experimental side is necessary for elucidating the reaction mechanism of oxidation of CH_4 to CH_3OH on Cu@ZSM-5 under mild conditions.

9.4.2 $Cu_nO_n^{2+}$ in MOR

Another set of extensively studied catalyst is Cu-MOR. Cu-MOR has been greatly studied for catalytic reductions of NO with CO, hydrocarbons or NH_3 for decades.[305] Efforts toward elucidation of active sites of Cu-MOR in these catalytic reactions at atomic scale have not concluded.[285, 306] The coordination environment of Cu atoms in Cu-exchanged ZSM-5 was suggested to be the form of bis(μ-oxo)dicopper complex.[307] As most characterizations of

catalysts before late 1990's were performed under ex-situ condition and the low spectral resolution of vibrational spectroscopy in 1990's could have made the identification of active sites at atomic scale challenging, elucidation of chemical and coordination environments of Cu atoms in Cu-MOR had remained significant interest in the last two decades.

Inspired by the reported activity for oxidation CH_4 to CH_3OH on Cu-ZSM-5,[269] test of activity for oxidation of CH_4 on Cu-MOR was done by Schoonheydt et al in 2005[293] although elucidation of chemical and coordination environments of Cu atoms of Cu-MOR was quite challenging. Cu-MOR is active for oxidation of CH_4 to form CH_3OH. The yields of CH_3OH are in the range of 1-7 μmol per gram of Cu-MOR.[293] In this early study, the Cu-MOR was activated with O_2 and then CH_4 was introduced to react with the activated Cu-MOR. The formed CH_3OH was extracted. The close correlation between the amount of CH_3OH produced and the intensity of UV-Vis peak at 22700 cm^{-1} was established, suggesting that the activity of Cu-MOR originates at species contributing to this peak.[293]

The peak at 22700 cm^{-1} observed in UV-vis results from transition of $O_{bridge} \rightarrow Cu$ charge transfer.[293] A few $Cu_xO_y^{2+}$ complexes including mono (μ-oxo) dicopper species, bi(μ-oxo) dicopper species, or even tri(μ-oxo)dicopper species could contribute to the 22700 cm^{-1} band. In fact, a later study using resonant Raman spectroscopy and other approaches propounded that the active Cu-based species is a bent mono(μ-oxo)dicopper complex.[299] As intensity of this peak decaies rapidly along the reduction by CH_4, a Cu-based species containing Cu-O-Cu bridge structure must be the active oxidant to transforming CH_4 to CH_3OH. This deduction was further supported by the reinstallation of this active bridge structure through calcination of a used Cu-MOR in O_2 at 500°C.

Although UV-vis and resonant Raman spectroscopy could not provide the atomic-scale structure of the Cu-based sites, $Cu_xO_y^{2+}$ in MOR, extensive XAS studies on evolution of chemical and coordination environments of Cu in MOR have provided significant insights toward understanding active sites for partial oxidation of CH_4 to CH_3OH.[296, 308] Smeets *et al* suggested that activation of Cu-exchanged MOR in O_2 at 450°C results in the formation of (μ-η^2: η^2-peroxo)dicopper species which is interchangeable to mono(μ-oxo)dicopper with involvement of two electrons provided by Cu(I) species.[296] Figure 17a schematically shows the evolution of chemical and coordination environments of Cu atoms of Cu-exchanged MOR along the increase of activation temperature in O_2.[296, 308] The in situ observation of structural parameters of Cu coordination environment derived from the features of energy space spectra and r-space spectra of Cu K-edge as a function of activation temperature in 30-450°C in O_2 or

helium was plotted in Figure 17b-16e. One important experimental finding in r-space spectra is the contribution of one additional fractional oxygen. The coordination numbers of the fractional O to Cu and O-Cu distance are 0.3 and 2.42 Å, respectively. The additional fraction oxygen atom was observed in O_2 in the temperature range of 300-450°C (Figures 16b and 16c). Notably, contribution of this additional fractional oxygen was not observed when the Cu-exchanged MOR was treated at 300-450°C in 1 bar helium (Figures 16d and 16e). These extensive XAS studies suggest that the high-temperature treatment (300-450°C) of Cu-MOR in O_2 is necessary for formation of μ-oxo dicopper species although whether μ-oxo dicopper species could be an active phase of oxidation of CH_4 to form CH_3OH was not concluded.

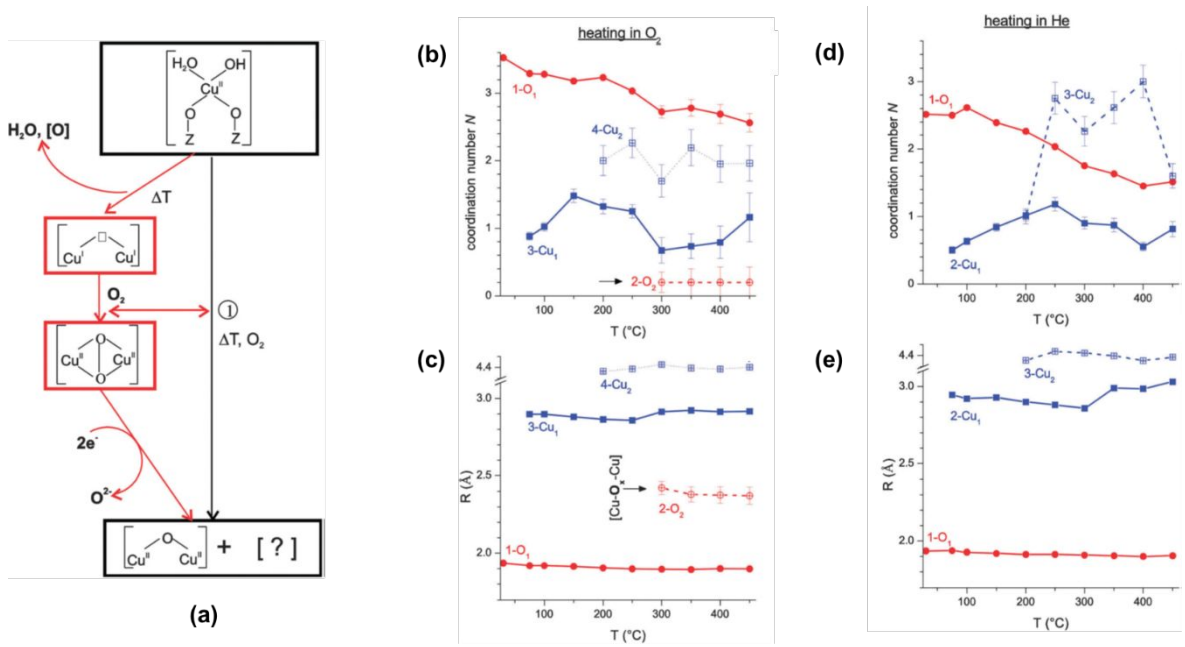

Figure 17. *Representation of schematic showing changes of chemical and coordination environments during activation of Cu-exchanged MOR in O_2 at 450°C and in situ observation of coordination environment of Cu during activation in O_2 and H_2 in the temperature range of 30-450°C. (a) Schematic of the chemical change. (b) Coordination number of O around Cu during activation of Cu-exchanged MOR in O_2 at different temperature. (c) Distance between O and Cu during activation of Cu-exchanged MOR in O_2 at different temperature. (d) Coordination number of O around Cu during activation of Cu-exchanged MOR in helium at different temperature. (e) Distance between O and Cu during activation of Cu-exchanged MOR in helium at different temperature.*[296, 308] *Reproduced from Ref. 308, copyright 1999, with permission from Royal Society of Chemistry.*

Due to the intricate factors, the atomic details of the sites responsible for activation and oxidation of CH_4 to CH_3OH on Cu-MOR was not conclusively identified. A very recent work

of Lercher et al made an exclusive assignment to the Cu_xO_y site responsible for activity they exhibited.[304] A single-site trinuclear copper oxygen cluster $Cu_3O_3^{2-}$ anchored in pocket channel of MOR was reported as an active site for oxidation of CH_4 to form CH_3OH with unprecedented activity by Lercher et al.[304] Their preparation of single type of $Cu_3O_3^{2-}$ was realized by strictly following two requirements. Firstly, species of Cu precursor must not form $Cu(OH)_2$ in aqueous solution. Secondly, the anchoring sites should be homogeneous. They chose MOR instead of ZSM-5 to anchor Cu atoms since protons of BAS sites in the more constrained side pockets of MOR can preferentially exchange with cations of a solution.[309] The formation of $Cu_3O_3^{2-}$ in MOR was confirmed with comparative fittings of k^2-weighted Fourier transformed EXAFS with potentially structural models of binuclear $[Cu(\mu\text{-}O)Cu]^{2+}$ and $[Cu_3(\mu\text{-}O)_3]^{2+}$. In fact, the r-space spectrum of Cu K-edge can be better fit when $[Cu_3(\mu\text{-}O)_3]^{2+}$ was used as the structural model of fitting. This fitting shows that $[Cu_3(\mu\text{-}O)_3]^{2+}$ instead of $[Cu(\mu\text{-}O)Cu]^{2+}$ is formed through this specific preparation protocol.[304]

Fitting of the r-space spectra of Cu K-edge of the Cu-O clusters anchored in MOR, $[Cu_3(\mu\text{-}O)_3]^{2+}$ suggests that there are two types of oxygen atoms in the second shell of Cu (Figure 18a); two of them are extra-framework oxygen atoms (O_{EF}); the other two are framework oxygen atoms (O_F). These parameters are quite consistent with the coordination environment of the structure provided by DFT calculation.[304] Figure 18a is the optimized structure of $[Cu_3(\mu\text{-}O)_3]^{2+}$ localized in side-pocket of MOR. In fact, the two paired type I (Al^I) atoms at the pocket mouth shown in yellow anchored the cluster $[Cu_3(\mu\text{-}O)_3]^{2+}$ (Figure 18b). The formation of Cu-O-Cu through activation in O_2 at 450°C was confirmed by the appearance of the peak at ~2.4 Å (distance before phase correction) in the red spectrum in Figure 18c. In the black spectrum in Figure 18c, the preservation of this peak at 200°C in CH_4 suggests that product molecule is adsorbed on the cluster after the O atom(s) of $Cu_3O_3^{2+}$ participated into the formation CH_3OH. Upon desorption of CH_3OH through steam treatment at 135°C (blue spectrum), the disappearance of the peak at ~2.4 Å suggests the removal of oxygen atoms of $[Cu_3(\mu\text{-}O)_3]^{2+}$. Upon consumption of oxygen atoms bonded to Cu atoms, $[Cu_3(\mu\text{-}O)_3]^{2+}$ clusters can be regenerated through activation at 500°C in O_2. Catalytic activity of the catalyst recovered after seven tests exhibited the same activity in production of CH_3OH as the original catalyst. Lercher et al. proposed that C-H activation of CH_4 on the extra framework $[Cu_3(\mu\text{-}O)_3]^{2+}$ cluster is facilitated through coupling of C-H bond with a formally radical-anionic extra-framework oxygen centre.[304, 310] They further suggested that electron transfer from molecular orbital of $Cu_3O_3^{2+}$ to antibonding C-H orbital of CH_4 weakens C-H bond of CH_4 and thus leads

to C-H cleavage under mild conditions.[304, 310]

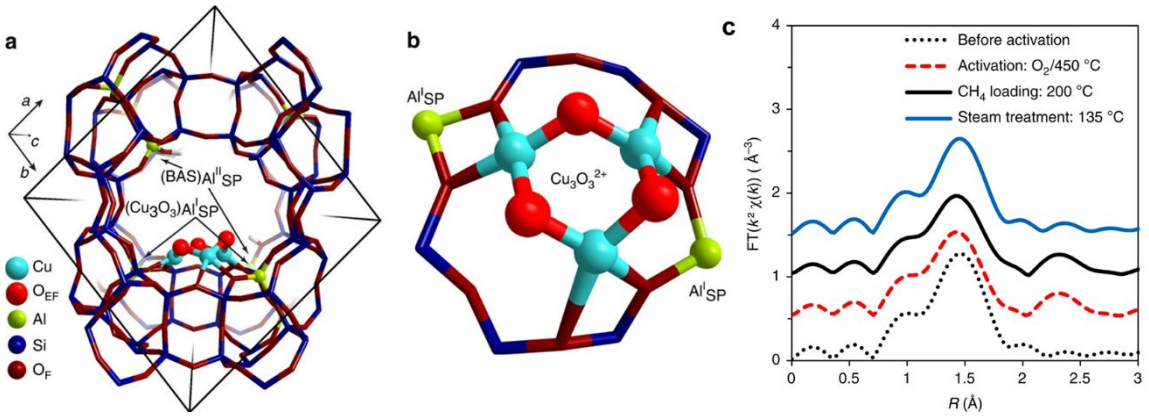

Figure 18. *Representation of optimized structure of $[Cu_3(\mu\text{-}O)_3]^{2+}$ in MOR and in-situ EXAFS of Cu K-edge of catalyst precursor during pre-treatment and catalyst during catalysis.[304] (a) MOR encapsulated with a $[Cu_3(\mu\text{-}O)_3]^{2+}$ cluster; two types of Al atoms are marked; type I (Al^{I}) is paired Al atoms which anchor $[Cu_3(\mu\text{-}O)_3]^{2+}$; type II ($Al^{II}$) is the isolated Al atoms. (b) $[Cu_3(\mu\text{-}O)_3]^{2+}$ stabilized by two anionic centres formed on two Al^{I} lattice sites at the entrance of the side pocket of MOR. (c) r-space spectra of Cu K-edge of catalyst precursor during activation and catalysis. Reproduced from Ref. 304, copyright 2015, with permission from Springer Nature.*

9.4.3 Transformation of CH_4 to CH_3OH under a low-temperature, isothermal condition

A breakthrough in oxidative transformation of CH_4 to CH_3OH under mild conditions was the low-temperature, isothermal production of CH_3OH at an elevated pressure of CH_4 reported by van Bokhonven *et al*.[311] In this study, low temperature is defined to 200°C. This isothermal approach is schematically shown in Figure 19a. Through this approach, CH_3OH is generated by a stepwise activation by Cu-MOR at 200°C in 1 bar O_2, reaction with CH_4 at 200°C and extraction with water steam at room temperature through off-line or on-line method.[311] One feature of this approach is that the yield of CH_3OH largely increases along the increase of CH_4 pressure upon activation of the catalyst at 450°C although yield of CH_3OH is basically independent from pressure of O_2 used in activation (Figure 19c). At 37 bars of CH_4, the yield of CH_3OH reaches about 56 μ mol per gram of catalyst (Figure 19d). With this approach, similar yields were still achieved after several cycles of reaction.

An intriguing finding of this study[311] is the exclusion of mono-μ-oxo dicopper complex as active sites of Cu-MOR in oxidation of CH_4 to form CH_3OH because there is lack of the signature of mono-μ-oxo dicopper complex (22700 cm^{-1}) in UV-vis spectrum after activation of Cu-MOR before using it for oxidizing CH_4 to CH_3OH.[311] Previous studies confirmed that mono μ-oxo dicopper complex was formed from either activation of Cu-exchanged ZSM-5 in

N_2O at a temperature higher than 350°C or activation of Cu-exchanged MOR in O_2 at a temperature ***higher than 350°C***[269, 270, 293, 312, 313] although it has been continuously debating whether μ-oxo dicopper complex(es) could be the active site for oxidation of CH_4 to CH_3OH. The observation of evolution of chemical and coordination environments of Cu atoms by using in-situ EXAFS suggests that mono μ-oxo dicopper complex species are formed from Cu-exchanged MOR in O_2 ***at 300°C*** or higher.[308] To check whether mono-μ-oxo dicopper complex is a necessary site for oxidizing CH_4 to CH_3OH, the Cu-exchanged MOR was activated ***at 200°C*** in O_2 before being used for oxidation of CH_4 to CH_3OH.[311] Clearly, this Cu-exchanged MOR did not have any mono-μ-oxo dicopper complex since it was activated at a temperature lower than 300°C. However, notably this specific Cu-exchanged MOR which does not have mono-μ-oxo dicopper complex in fact exhibited high activity in oxidative transformation of CH_4 to CH_3OH. Thus, these studies concluded that mono-μ-oxo species is not a necessary site for the activity of Cu-MOR in the isothermal approach.[311] Actually, control experiments designed by van Bokhonven *et al* suggested the active sites for oxidation of CH_4 to CH_3OH in the isothermal approach is the dehydrated copper oxide clusters which are less active at low pressure of CH_4 but quite active at high pressure CH_4.[311]

The conclusion of the active sites of oxidizing CH_4 to CH_3OH by Cu-MOR at 200°C suggests the high complexity of active sites of Cu-MOR in oxidation of CH_4 to CH_3OH. The complication results from multiple interacting factors determining reactivity in activation and oxidation of CH_4 to CH_3OH. These factors are closely related to preparation step and temperature of activation of Cu-MOR.

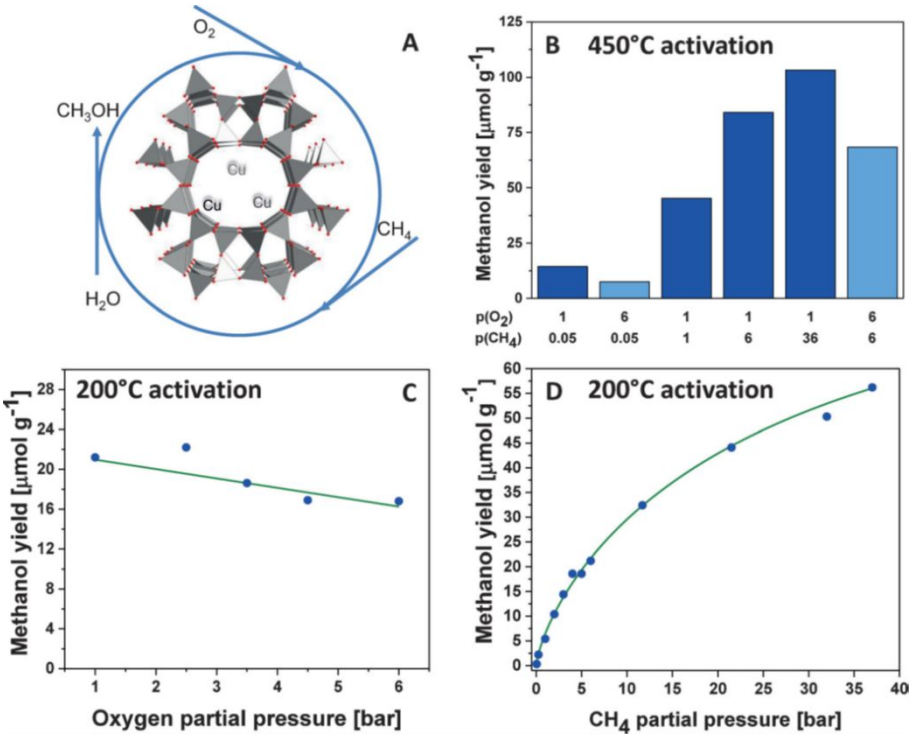

Figure 19. *Representation of schematic of isothermal approaches and influence of partial pressures of O_2 and CH_4 on yields of CH_3OH from Cu-MOR (Si/Al=6, 4.7 wt%Cu).*[311] *(a) Schematic showing the main step of isothermal approach of continuous production of CH_3OH from Cu-MOR without off-line extraction of CH_3OH. (b) Yields of CH_3OH after activation at 450°C, reaction and off-line extraction as a function of partial pressures of O_2 and CH_4. (c) Influence of partial pressures of O_2 used in activation at 200°C on yield of CH_3OH. (d) Influence of partial pressure of CH_4 used in reaction on yield of CH_3OH (activation was done in 1 bar O_2 at 200°C). Reproduced from Ref. 311, copyright 2016, with permission from John Wiley and Sons.*

9.4.4 Size-dependent stability and activity for CH_4 oxidation on $Cu_nO_n^{2+}$ loaded to zeolite

Computational studies suggested the both stoichiometric clusters $Cu_nO_n^{2+}$ and nonstoichiometric clusters $Cu_nO_{n-1}^{2+}$ formed in 8-membered ring of MOR exhibit the same size-dependent stability which is the increase of stability of $Cu_xO_y^{2+}$ along the increase of size of nonstoichiometric $Cu_xO_y^{2+}$ clusters in MOR.[298] This dependence is in good accordance with the increase of stability along the increase of size of stoichiometric $Cu_nO_n^{2+}$ clusters (n=2-9) of Cu-SSZ-13.[314]

Other than the size-dependent stability of $Cu_nO_n^{2+}$ clusters, a size-dependent reactivity in activation of C-H of CH_4 was suggested in computational studies. Formation of a Cu-O-H and CH_3 species is the first step in oxidative transformation of CH_4 to CH_3OH. For a mono(μ-oxo)dicopper cluster in MOR and ZSM-5, free total energies of the formed Cu-O-H and CH_3 species are higher than reactants by 76 kJ/mol for MOR and 61 kJ/mol for ZSM-5, respectively.[303, 315] Interestingly, in terms of a trimer cluster $[Cu_3(\mu\text{-}O)_3]^{2+}$ in ZSM-5, the formation of Cu-O-H and CH_3 species only results in increase of free energy by 37 kJ/mol. In other words, the Cu-O-H and CH_3 species formed on $[Cu_3(\mu\text{-}O)_3]^{2+}$ in ZSM-5 is more stable than that on a mono(μ-oxo)dicopper cluster, $[Cu(\mu\text{-}O)Cu]^{2+}$ in ZSM-5.[298] Similarly, cost of free energy for formation of Cu-O-H and CH_3 species on dimer ($Cu_2O_2^{2+}$), trimer ($Cu_3O_3^{2+}$), tetramer ($Cu_4O_4^{2+}$), and pentamer ($Cu_5O_5^{2+}$) in MOR are 11.6 kJ/mol, 41.4 kJ/mol, 34.7 kJ/mol, and 28.9 kJ/mol, respectively;[298] it suggests the increase of reactivity of $Cu_nO_n^{2+}$ clusters along the increase of size. [298] [317] [317] [317] [315] [314] [305] [300] [294] [287] [285] [284] [284] [284] [282] [281] [280] [276] [276] [275] [273] [272] [269] [266] [250] [248] [247] [245] [241] [240] [241] [241] [232] [231] [229] [224] [222] [213] [211] [210] [209] [209] [208] [202] [201] [198] [194] [194] [186] [184] In other words, the higher stabilization of a larger cluster make it better stabilize the formed HO and CH_3 upon C-H activation. The predicted higher activity of a larger cluster $Cu_nO_n^{2+}$ suggests the origin of activity of Cu-MOR and even Cu-ZSM-5 in activation of C-H of CH_4 could be more complicated than what hypothesized or even deduced in literature. The complexity was supported by the proposal of Tomkins et al that activity of CH_4 oxidation to form CH_3OH on

Cu-exchanged MOR could result from some copper oxide clusters which have not been identified.[311] An excellent review published by van Bokhoven et al summarized these insights and highlighted the complexity of oxidative transformation of CH_4 to CH_3OH on Cu-ZSM-5 and Cu-MOR.[60]

9.4.5 Other Cu-exchanged zeolites for activation of CH_4

Other than extensive studies of Cu-MOR and Cu-ZSM-5, reactivity of Cu loaded to S-1, FER, EMT, BEA, FAU, SAPO-34 and SSZ-13 for oxidative transformation of CH_4 to CH_3OH were investigated. Cu-SAPO-34 and Cu-SSZ-13 with anchored Cu cations are active for oxidative transformation of CH_4 to CH_3OH.[293, 316] The yields of CH_3OH from CS-1-2.0, CY-2.7-0.45, CU-2.75-0.34, and CE-4-0.36 and CA-1-1.7 are lower than 1 μmol CH_3OH per gram of sample, actually suggesting lack of activity.[197] Here notation CX-Y-Z denotes different zeolite. X is the first letter of the zeolite such as Z=ZSM-5, M=MOR, U=USY, Y=Y, B=BEA, F=FER, and E=EMT; Y is the Si/Al ratio; Z is the Cu/Al ratio. Table 1 represents the characteristics of the zeolites with encapsulated Cu^{2+}. The lack of activity of these Cu-zeolites is basically consistent with the lack of a peak at 22000cm^{-1} – 22700 cm^{-1} in UV-vis spectra.

Table 1. List of characteristics of the zeolites with encapsulated Cu^{2+}. Reproduced from Ref. 293, copyright 2005, with permission from Elsevier.

Sample	Source	Topology	Si/Al	#mL 0.01M Cu Solution per gram	Cu/Al	Cu wt%
CZ-12-0.54	ALSI-PENTA	MFI	12	63	0.54	4.3
CZ-25-0.51	PQ-zeolites	MFI	25	32	0.51	2.0
CZ-30-0.47	ExxonMobil	MFI	30	25	0.47	1.5
CZ-77.5-0.55	PQ-zeolites	MFI	77.5	97.5	0.55	0.68
CZ-120-0.88	PQ-zeolites	MFI	120	6.3	0.88	0.77
CM-5.3-0.39	Norton	MOR	5.3	144	0.39	6.2
CM-8.0-0.50	TRICAT	MOR	8.8	78	0.50	5.1
CE-4-0.36	ExxonMobil	EMT	4	189	0.36	7.3
CF-6.2-0.42	Toyo Soda	FER	6.2	126	0.42	5.9
CB-9.8-0.50	ZEOCAT™	BEA	9.8	100	0.50	4.7
CY-2.7-0.45	ZEOCAT™	FAU	2.7	664	0.45	11
CU-13.5-0.32	PQ-zeolites	FAU	13.5	500[a]	0.32	2.3
CU-14.5-0.42	ZEOCAT™	FAU	14.5	500[a]	0.42	2.9
CU-27.5-0.34	PQ-zeolites	FAU	27.5	500[b]	0.34	1.2
CU-36.9-0.34	PQ-zeolites	FAU	36.9	500[c]	0.34	0.9

Compared to the inactive CS-1-2.0, CY-2.7-0.45, CU-2.75-0.34, and CE-4-0.36 and CA-1-1.7, CF-6.1-0.42 and CB-9.8-0.50 are obviously active in oxidation of CH_4 to CH_3OH. Yields of CH_3OH of 12 μmol/g and 4.2 μmol/g yields were obtained from CF-6.1-0.42 and CB-9.8-0.50 upon their reactions with CH_4 at 200°C. Surprisingly, no band in the region of

22000 cm^{-1} – 22700 cm^{-1} was observed for the Cu-exchanged CF-6.1-0.42 and CB-9.8-0.50. Thus, the observation of high yields from CF-6.1-0.42 and CB-9.8-0.50 and the absence of a peak in the region of 22000 cm^{-1} – 22700 cm^{-1} in UV-vis spectra clearly show that both CF-6.1-0.42 and CB-9.8-0.50 must have another type of active sites which can provide oxygen atoms to partially oxidize CH_4 to form CH_3OH.[293] This finding has urged further exploration of chemical and coordination environments of Cu atoms in the Cu-based catalytic sites anchored in CF- and CB-type zeolites.

9.5 Anchored oxygen atoms over Co sites for activation of CH_4

Other than zeolite loaded with Fe or Cu, the O_2-activated Co-ZSM-5 was reported being reactive in oxidative transformation of CH_4 to CH_3OH at 150°C.[317] The Co-ZSM-5 was prepared through impregnation or ion exchange. Co-ZSM-5 exhibits activity for oxidizing CH_4 to form CH_3OH and formaldehyde although it is much lower than Cu-ZSM-5. The yield of CH_3OH on Co-ZSM-5 is in the range of 0.1-0.6 μmol per gram of catalysts.[316, 317]Although the chemical and coordination environments of Co atoms in Co-ZSM-5 have not been characterized thoroughly, it is extrapolated that the Co atoms in Co-ZSM-5 prepared with impregnation mainly exist in the form of CoO or Co_3O_4 and cobalt oxide clusters are responsible for activity in production of CH_3OH through oxidation of CH_4.[317, 318] It even further propounded that the activity in oxidation of CH_4 to form CH_3OH on Co-ZSM-5 does not originate at μ-oxo dicobalt species. More studies on this system are necessary for uncovering the origin of the activity on Co-ZSM-5. In addition, it would be valuable if structure and activity in oxidative transformation of CH_4 to CH_3OH on Co-MOR and even other zeolites loaded with Co can be studied in a comparative manner toward gaining fundamental understanding of the correlation between chemical and coordination environment of Co atoms in different zeolites and their corresponding activity in activation and oxidation of CH_4 to CH_3OH.

9.6 Anchored mono(μ-oxo)dinickel site for activation of CH_4

As reviewed in Section 6-8, Ni atoms in forms of free standing NiO^+ cations and anchored Ni-O species on support oxide are quite active in oxidative transformation of CH_4 o CH_3OH. Consistent with them, Ni-based mono(μ-oxo)dinickel species anchored in ZSM-5 exhibits high reactivity in oxidization of CH_4 to CH_3OH under mild conditions.

Microporous aluminosilicate consisting of bent mono(μ-oxo)dinickel species on the internal wall was prepared through first impregnation and then filtration.[319] In the filtration

step, the sample precursor obtained upon impregnation were washed with distilled water for several cycles. Figure 20b is 2.5 wt % Ni-ZSM-5 catalyst which does not have NiO nanoparticles formed on external surface of microporous aluminosilicate particles. TEM images excluded the formation of NiO nanoparticles on microporous aluminosilicate. The lack of NiO nanoparticles on surface of microporous aluminosilicate particles is further supported by the lack of satellite peaks of Ni $2p_{3/2}$ which are $3d^{10}L^{-2}$ and $3d^{9}LL_{far}{}^{-1}$ (Figure 20c). The absence of satellite peaks must be related to an unusual bonding environment of the Ni atom anchored to ZSM-5 [mono(μ-oxo)dinickel in Figure 20d]. It is widely acknowledged that the satellite peaks of Ni $2p_{3/2}$ of Ni^{2+} of NiO originates at the charge-transfer effect in photoionization.[320] After photoionization of the electrons of Ni 2p, the lowest final state is $3d^{9}L^{-1}$, which is formed through the electron transfer from ligand L to the Ni 3d orbital.[320] Here, L^{-1} in $3d^{9}L^{-1}$ denotes a hole generated on the nearest ligand due to the transfer of one electron from the ligand to the 3d orbital of Ni atom. This $3d^{9}L^{-1}$ electronic state gives the main photoemission peak at 853.8 eV (Figure 20c5). In addition, two electrons of the nearest oxygen atoms could be transferred to the photoionized Ni atom, creating another electronic state ($d^{10}L^{-2}$), which gives a satellite peak at 861.0 eV for NiO particles. In addition, the photoionized Ni atom can be neutralized by transferring an electron from one of the oxygen atoms of the second-nearest Ni atoms, Ni*-O(L_1)-Ni(L_2)-O(L_{far})-Ni(L_4)-O(L_5), forming a different final state labelled as $3d^{9}LL_{far}{}^{-1}$, which corresponds to the strong satellite peak at 856.0 eV of NiO particle (Figure 20c5). The absence of the $3d^{9}LL_{far}{}^{-1}$ at 856.0 eV and $3d_{10}L^{-2}$ at 861.0 eV in the Ni 2p photoemission feature of the 10wt% Ni-ZSM-5 in Figures 19c2-19c4 clearly shows the lack of long-range crystal structure of NiO. Thus, XPS studies clearly show the lack of lattice of NiO nanoparticles in the 2.5wt%Ni-ZSM-5. The XPS peak intensity in Figures 19c2-19c4 was contributed from singly dispersed Ni atoms anchored in these micropores near to surface of a ZSM-5 particle although these Ni atoms were singly dispersed in deep pores of ZSM-5 could not be observed by XPS.

The existence of Ni-O-Ni bonds in the micropores was confirmed with in situ studies of Ni K-edge of 5 wt % Ni-ZSM5. As shown in Figure 20e1, the peak contributed from Ni-O-Ni was observed in the Ni-ZSM-5 which was activated with O_2 at 400°C. The Ni-O-Ni species was marked with Ni-Ni in Figure 20e for the convenience of showing the direct distance of Ni to Ni although there is an oxygen atom bonding with the two Ni atoms. The fitting of r-space spectrum of Ni K-edge of Ni-ZSM-5 at 350°C in CH_4 (Figure 20f) shows that the coordination number of O atoms to Ni is 3.0±0.3. Thus, the in situ EXAFS studies suggests that the

performed structure is bent mono(μ-oxo)dinickel (Figures 19e and 19f).

This Ni-ZSM-5 exhibits activity in activation and oxidation CH_4 to CH_3OH, HCOOH and $HOCH_2CH_2OH$. The activity originated at the bent mono(μ-oxo)dinickel since microporous aluminosilicate without bent mono(μ-oxo)dinickel is inert for formation of these product molecules.

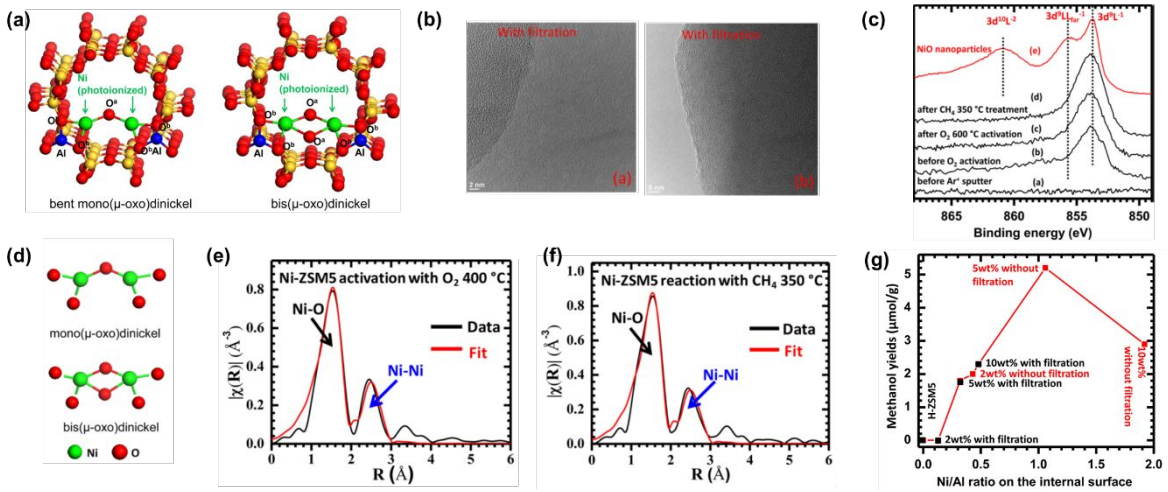

Figure 20. *Representation of structure and characterizations of Ni-ZSM5 catalysts consisting of bent mono(μ-oxo) dinickel.*[319] *(a) Structural mode [a1: bent mono(μ-oxo)dinickel; a2: bis(μ-oxo)dinickel], (b) TEM images,(c) Ni 2p photoemission feature of 10wt%Ni-ZSM-5, (d) Bonding environment of Ni atoms, (e) Ni K-edge of 5 wt % Ni-ZSM-5, (f) Menthol yields on Ni/ZSM-5. Reproduced from Ref. 319, copyright 2014, with permission from ACS.*

9.7 Necessity of parallel studies of different metal atoms anchored in zeolite

Activation of C-H of CH_4 with a following oxidization to form CH_3OH and even products of deep oxidation was studied by several types of catalysts which are mainly Fe and Cu-anchored in ZSM-5 and MOR. Significant insights on oxidization of CH_4 to CH_3OH on this type of catalysts were achieved although complexity in environment of this catalysis and in structure of a catalyst was suggested. Inspired by the systematic studies of activation and oxidation of CH_4 on free-standing MO^+ clusters of 3d transition metals, parallel studies of a type of $M_aO_a^{2+}$ such as $[M_2(\mu\text{-}O)_2]^{2+}$ of different transition metals such as Mn, Fe, Co, Ni, Cu, Zn anchored in the same zeolite such as ZSM-5 or MOR could provide valuable insights for uncovering descriptor for reactivity in oxidation of CH_4 to CH_3OH. Another set of parallel studies could be M atoms in $[M_3(\mu\text{-oxo})_3]^{2+}$ anchored in ZSM-5; here M is a transition metal such as Mn, Fe, Co, Ni, Cu, Zn. By replacing ZSM-5 with MOR, systematic studies of $[M_2(\mu\text{-}O)_2]^{2+}$ anchored in MOR and $[M_3(\mu\text{-oxo})_3]^{2+}$ anchored in MOR would be valuable. Notably, the complexity in catalyst preparation and challenges in characterization could make these

comparisons quite challenging. To save the cost of these exploration, a specific suggestion is to perform parallel computational studies on $M_2(\mu\text{-}O)_2]^{2+}$ anchored in MOR and $[M_3(\mu\text{-oxo})_3]^{2+}$ anchored in MOR (=Mn, Fe, Co, Ni, Cu, or Zn) to obtain a list of prioritized metals before any experimental explorations are planned. We expect that these sets of proposed parallel studies can provide profound knowledge for developing zeolite-based catalysts for oxidative transformation of CH_4 to CH_3OH.

10. Activation and oxidation of CH_4 with anchored oxygen atoms bonding to Cu in zeolite to form acetic acid

Acetic acid is an important intermediate compound for production of high-value chemicals. It is produced from catalytic carboxylation of CH_3OH at industrial scale. CH_3OH is produced from high-temperature processes of syngas production from CH_4 or coal and then synthesis of CH_3OH from syngas or mixture of CO, CO_2 and H_2 as shown in Figure 2. It was reported recently that Cu-H-MOR is reactive for formation of acetic acid through tandem reactions in terms of first formation of a methoxy species and then coupling between the methoxy species and CO at 200^{o}C although the reported formation of acetic acid is not a catalytic cycle.[321] Correspondingly, the role of Cu-H-MOR in the formation of acetic acid is the oxidant instead of a catalyst. Oxygen atoms anchored on Cu clusters in Cu-H-MOR oxidizes CH_4 to form methoxy species and then the formed methoxy species on Cu-H-MOR can couple with CO through carboxylation, forming acetic acid. Notably, Cu-Na-MOR with Cu/Al=0.22 is also active for production of acetic acid. But its activity is much lower than Cu-H-MOR. The observed formation of acetic acid in the tandem reactions suggests that the $Cu_xO_y^{n+}$ clusters are active for formation of acetic acid from CH_4 although the chemical and coordination environments of Cu atoms of the $Cu_xO_y^{n+}$ clusters of the Cu-H-MOR and Cu-Na-MOR were not reported.[321]

Cu/Al ratio of Cu-Na-MOR is an important factor in determining whether a Cu-Na-MOR has activity in formation of acetic acid or not. Notably, Cu-Na-MOR with Cu/Al>0.36 is not active for formation of acetic acid although Cu-Na-MOR with Cu/Al ≤0.36 is active for formation of acetic acid. However, Cu/Al ratio is not a factor in determining activity in formation of acetic acid for Cu-H-MOR. Cu-H-MORs in both ranges of Cu/Al >0.36 and Cu/Al≤0.36 are active for formation of acetic acid. Thus, the mechanisms for carboxylation of methoxy to acetic acid on Cu-Na-MOR is different from Cu-H-MOR. The difference in reaction mechanisms between Cu-Na-MOR and Cu-H-MOR was supported by UV-vis

spectroscopy. For Cu-H-MOR upon being activated in O_2, the d-d transition at 9600 cm^{-1} was observed before introduction of CH_4; more importantly, the intensity of this *d-d* transition decayed upon simultaneous reaction with CH_4 at 200°C for 2 hrs; this coherent observation clearly shows that the species contributed to 9600 cm^{-1} is responsible for the formation of acetic acid on Cu-H-MOR.

Parallel studies were performed on Cu-H-MOR and Cu-Na-MOR for further understanding their different reaction mechanisms. Cu-H-MOR (Cu/Al=0.35) and Cu-Na-MOR (Cu/Al=0.36) have the same Cu/Al ratio but obviously Cu-H-MOR (Cu/Al=0.35) produced larger amount of acetic acid with Cu-Na-ZSM-5 (Cu/Al=0.36). The high activity in transformation of CH_4 to acetic acid on Cu-H-MOR (Cu/Al=0.35) suggests that Bronsted acid sites of Cu-H-MOR (Cu/Al=0.35) can enhance the formation of acetic acid.[321] Since Bronsted acid sites in Cu-H-MOR play a significant role in carbonylation of methoxy and Cu_xO_y sites are reactive in activation of CH_4 to form methoxy, methoxy formed on Cu_xO_y sites must be transferred from Cu_xO_y sites to Bronsted acid sites so that the methoxy could be carbonylated to form acetic acid. Upon the consumption of oxygen atoms of Cu_xO_y clusters for formation of acetic acid, Cu-H-MOR and Cu-Na-MOR can be regenerated a few times through pre-treatment in O_2 at 600°C although the reported tandem reactions are not a catalytic cycle.

11. Catalytic oxidation of CH_4 with O_2 at low temperature in aqueous solution

Different from the oxidation of CH_4 with O_2 catalysed by molecular catalysts,[225] Oisuka et al reported one exciting catalytic oxidation of CH_4 with molecular O_2 at 40°C by their unique catalytic system consisting of Zn powder, $EuCl_3$, and $CF_3CO_2CH_3$.[322, 323] Although the preparation of this catalyst is not intricate, there has been definitely lack of specific understanding on the reaction mechanism of this amazing catalytic oxidation of CH_4 with *inexpensive* molecular O_2 by inexpensive catalyst at near room temperature. The hypothesized mechanism is the following.[322, 323] Eu^{2+} is a key reductant which is generated in situ through reduction of Eu^{3+} with metallic Zn powder. Then, Eu^{2+} activates molecular O_2 to form a type of active oxygen species O*. The active oxygen species O* is expected to exhibit a strong electrophilicity. It activates CH_4 to form CH_3OH. The choice of Zn power to reduce Eu^{3+} is that its redox potential $\psi(Zn^{2+}/Zn)$ (-0.77 V) is lower than $\psi(Eu^{3+}/Eu^{2+})$ (-0.35 V). In addition, the use of a strong acid CF_3COOH to stabilize product CH_3OH through formation of ester CF_3COOCH_3 drove the thermodynamics of $CH_4 + O_2 \rightarrow CH_3OH$ to the direction favourable

for the production of CH_3OH since oxidation of CH_4 to CH_3OH is only weak exothermic at 298 K (ΔH^o=-26 kcal/mol). Another hypothesis could be that catalytic transformation of CH_3OH from CH_4 is due to the oxidation of CH_4 by H_2O_2. This hypothesized path us feasible since H_2 can be readily formed by reduction of H^+ with Zn and then H_2 can couple with O_2 to form H_2O_2. However, it is not clear how the formation of H_2O_2 from H_2 and O_2 was catalysed. Fundamental understanding of this fascinating catalysts is expected to be necessary for providing insights to design active catalysts for catalytic oxidation of CH_4 to CH_3OH under mild conditions.

12. Catalytic oxidation coupling of CH_4, CO and O_2 to synthesize acetic acid

Compared to the oxidation of CH_4 with an oxidant such as H_2O_2 or O_2 to be reviewed in Section 13, the reaction of coupling CH_4 with CO and O_2 is a quite different path of utilizing CH_4 to generate high value chemicals. It uses inexpensive oxidant, O_2 or even cost-free air as oxidant instead of costly H_2O_2. This coupling is a carbon-addition reaction, different from other reactions reported in literature. Different from the tandem reactions in Cu-MOR, the coupling of CH_4 with CO and O_2 on Rh_1O_5 clusters anchored in ZSM-5 is a catalytic reaction which continuously transforms CH_4 to acetic acid with high activity at 150^{o}C.[188]

12.1 Advantage of direct conversion of CH_4 to acetic acid under mild conditions

Acetic acid is an important intermediate compound used for production of high value chemicals. Currently, acetic acid is produced from CH_3OH carbonylation, in which CO reacts with CH_3OH to form acetic acid. As shown in Figure 2, CH_3OH is synthesized from CO/CO_2 and H_2 at a relatively high temperature, 250-300^{o}C; the mixture of CO/CO_2 and H_2 is produced from steam reforming of either coal or CH_4 at quite high temperatures, 600-800^{o}C. Unfortunately, high-temperature reforming of coal or CH_4 has made the synthesis of acetic acid become a high energy-demanded, high-cost process. It would be ideal if a catalytic reaction could directly transform CH_4 to acetic acid through a one-step catalysis instead of the current three-step synthesis, under mild condition instead of high-temperature harsh condition, through heterogeneous catalysis instead of the current homogeneous catalysis, using a reusable catalyst instead of current Ir or Rh-based molecular catalyst without recycle.

Motivated by these expected advantages, a carbon-addition reaction was used for the purpose of direct transformation of CH_4 to acetic acid. Inspired by the use of precious metal catalyst in the Badische Anilin und Soda Fabrik (BASF) process developed in 1960's and

Monsanto process developed in 1990's, a Rh-based single atom catalytic sites anchored in microporous aluminosilicate was reported recently.[188] It was used for synthesis of acetic acid through a carbon-addition reaction under a mild condition in terms of 150°C and lower.[188]

12.2 Direct conversion of CH_4 to acetic acid on a Rh_1-based single-atom site in microporous aluminosilicate

Single-atom catalyst was used for catalysing this carbon addition reaction.[188] For a reliable and repeatable preparation of a catalyst with singly dispersed metal atoms, microporous aluminosilicate with isolated protons was used as a support to anchor the specific catalytic sites Rh_1O_5.[188] Through ion-exchange and followed calcination, a catalyst with singly dispersed Rh_1 atoms was prepared. In the micropores, Rh coordinates with 5 oxygen atoms (Figure 21a).[188] This site is highly active for synthesis of acetic acid molecules from CH_4 through carbon addition and oxidation using O_2 at 150°C Extensive isotope experiments confirmed the participation of the three reactants in the catalytic cycle of formation of acetic acid. The Rh-O bond protruding to centre of a micropore shown in Figure 21a acts as the site to activate the first C-H bond of CH_4 with an activation barrier of 124 kJ/mol, which is the rate-determining step among the 18 elementary steps of synthesis of two acetic acid molecules from two CH_4, two CO and one O_2 molecules, $2CH_4+2CO+O_2 \rightarrow 2CH_3COOH$ (Figure 21b). The second rate-determining step is the coupling of CH_3CO and OH adsorbed on Rh_1 to form a weakly adsorbed acetic acid through a barrier of 107kJ/mol.

Parallel studies show that single atom sites of precious metals supported on open surface of reducible oxide Rh_1/Co_3O_4,[324] Rh_1/TiO_2[188] and inert oxide Rh_1/SiO_2[325] and Rh_1/Al_2O_3 are neither active for this carbon addition reaction to produce acetic acid nor for oxidation of CH_4 to CH_3OH although literature claimed that very small amount of methanol was produced from Rh/TiO_2 at the level of lower limit of measurement.[326] Close comparison between single-atom sites anchored in the micropore and ones supported on open surface of oxide nanoparticles suggests the significance of micropore in terms of confinement of molecules for providing distorted molecules which was briefed in Section 9.1. The capability of micropore in forcing reactant molecules to distort structurally was further evidenced by the observed activity on other types of microporous aluminosilicates encapsulating singly dispersed precious metal atoms.[60, 269] The structural confinement effect of micropores on this reaction is supported by DFT calculation of activation of CH_4 by ZSM-5 which suggests the sub-nanometer pores of

ZSM-5 exert an effect to destabilize the adsorption and thus decrease the activation barrier for C-H cleavage in the pore.[261]

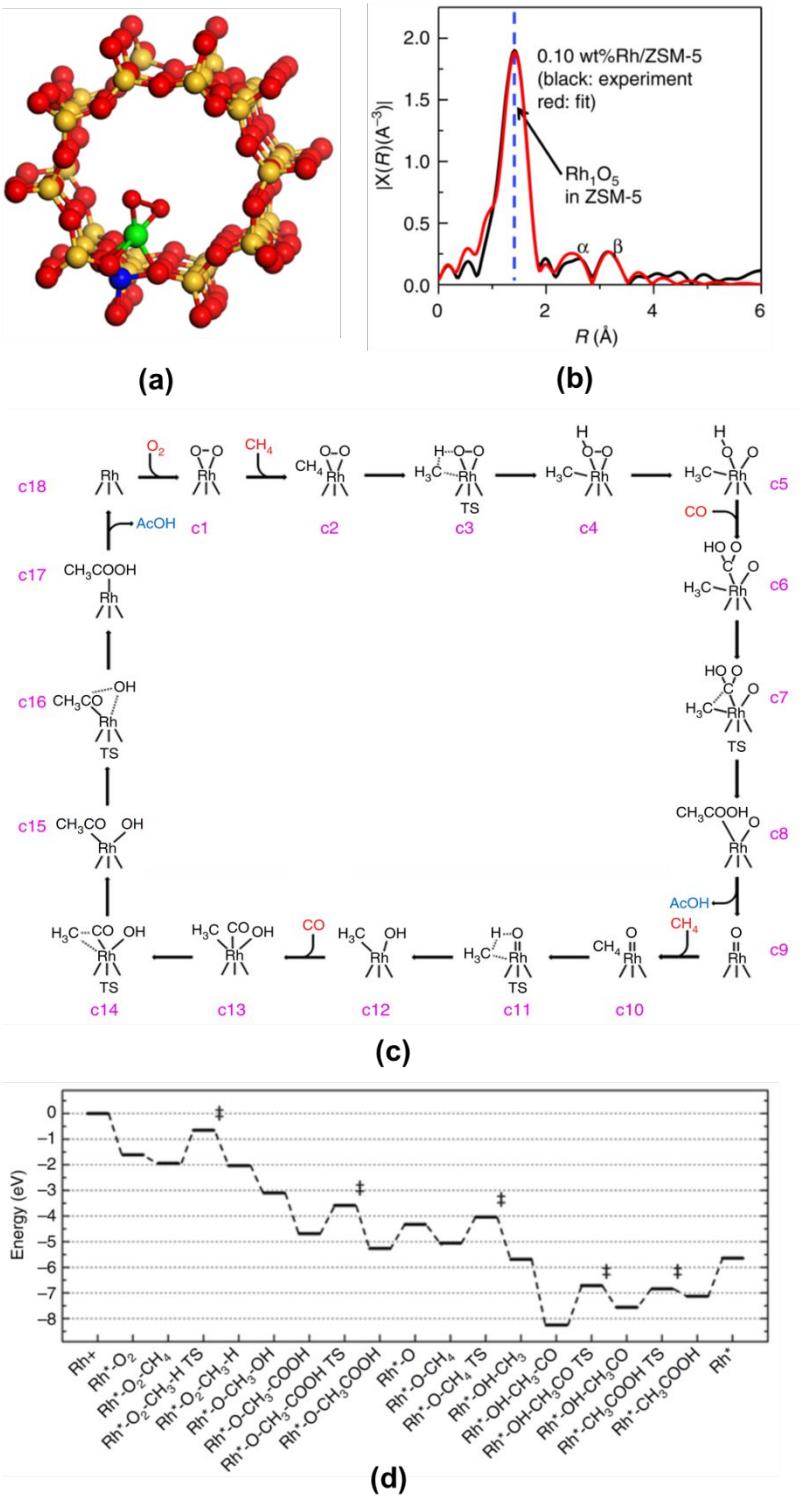

Figure 21. *Representation of EXAFS characterization of Rh_1O_5 anchored in ZSM-5 and results of computational studies for catalytic transformation of CH_4, CO and O_2 to acetic acid molecules.[188] (a) Structural model of microporous aluminosilicate with anchored Rh_1O_5 sites. (b) EXAFS studies of Rh*

K-edge. (c) Catalytic cycle consisting 18 elementary steps for $2CH_4+2CO+O_2 \rightarrow CH_3COOH$. (d) Energy profile of the catalytic cycle in (c). Reproduced from Ref. 188, copyright 2018, with permission from Springer Nature.

12.3 Mechanistic understanding of this catalytic carbon-addition transformation of CH_4

Few catalytic reactions involve three reactants. The direct participation of the three reactants CH_4, CO and O_2 for production of acetic acid was confirmed through extensive isotope experiments.[188] Based on the stoichiometry of this carbon-addition reaction, $2CH_4+O_2+2CO \rightarrow 2CH_3COOH$, a complete catalytic cycle requests the participation of five molecules. Computational studies suggest that this catalytic cycle involves 18 elementary steps. Interestingly, the two CH_4 molecules were activated through two different sites, Rh_1O_5 (c1 in Figure 21b) and Rh_1O_4 (c9 in Figure 21b). Compared to Rh_1O_5, Rh_1O_4 is highly under coordinated. Rh_1O_4 is generated after the formation of the first acetic acid molecule. Compared to the formation of the first acetic acid molecule (c1-c8 in Figure 21b), the pathway for formation of the second acetic acid molecule (c9-c17) is different. In the formation of the first acetic acid molecule, CO was inserted to Rh-O of Rh-OH species as Rh atom has fully coordinated with six atoms (c4), forming a COOH group on Rh_1. A subsequent coupling between HOOC- and CH_3-forms an acetic acid molecule (c8). Upon the desorption of the first acetic acid molecule, Rh_1O_4 site was formed (c9). On the Rh_1O_4, CH_4 was activated through Rh=O bond (c10-c12). As Rh atom in c12 only bonds with five atoms, CO can directly bond with the Rh_1 atom and then couple with its adjacent CH_3 to form an acetyl, $-COCH_3$ (c16), which subsequently couples with a hydroxyl group, forming the second acetic acid molecule (c17). The energy profile of the proposed pathway shows the rate-determining steps are activation of C-H of the first CH_4 molecule by Rh-O bond and the coupling of CO and CH_3 to form CH_3CO- intermediate (c15).

Cleary, catalytic oxidation of CH_4 and coupling with CO to form acetic acid has been successfully demonstrated.[188] Computational studies suggested that Rh-O bond of the anchored single atom site plays a key role. Although TOF of Rh_1O_5 is quite high, Rh is a precious metal. It would be ideal if 3d transition metal could replace Rh to catalyse this reaction. Thus, it is highly valuable to explore which early transition metals could replace Rh. However, due to the complexity of catalyst preparations of this type of catalysts, an inappropriate preparation of a hypothesized catalyst could easily invalidate a good idea. Thus, here we suggest to perform computational studies first to pre-screen in-expensive transition metal atoms which are in a

cluster with the same structure as Rh_1O_5.. A shortlist proposed by computational studies would be tested by experimentalists. It is expected that such an approach could develop a cost-effective catalyst with high activity and selectivity in synthesis of acetic acid through coupling of CH_4, CO and O_2 in aqueous at 150°C or lower temperature.

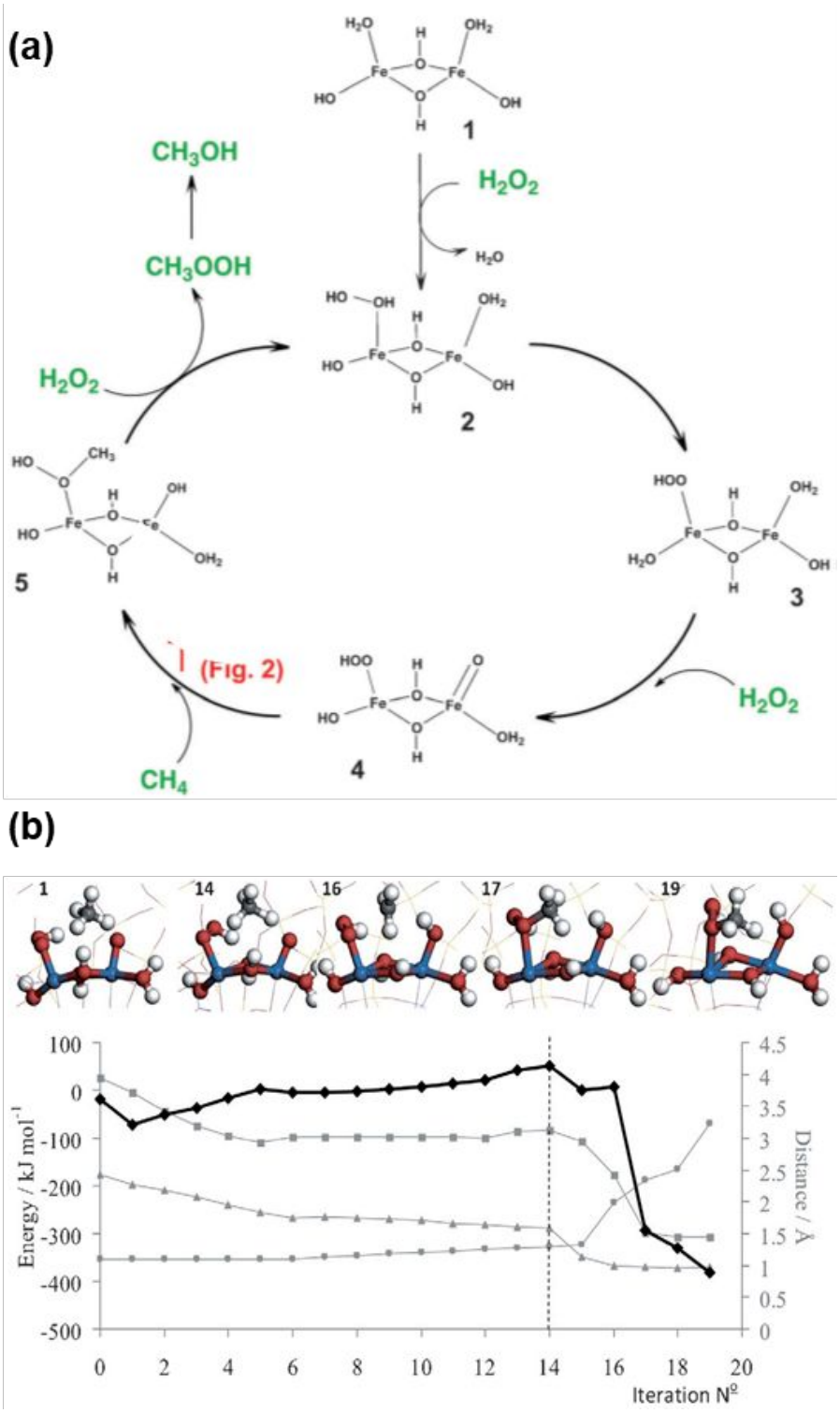

Figure 22. *Representation of catalytic oxidation of CH_4 with H_2O_2 with di-iron complex anchored in*

ZSM-5.[288] (a) Proposed catalytic cycle of oxidizing CH_4 to CH_3OOH with H_2O_2. (b) DFT calculation for elementary steps of transforming CH_4 to CH_3COOH on $[Fe_2(m^2\text{-}OH)_2(OH)_2(HCOO)(=O)]$. Reproduced from Ref. 288, copyright 2012, with permission from John Wiley and Sons.

13. Catalytic oxidation of CH_4 with H_2O_2

Although H_2O_2 is some pricey, it is one of the most active oxidants. The main products of oxidation of CH_4 with H_2O_2 are CH_3OH and formic acid. A number of catalysts active in catalytic oxidation of CH_4 with H_2O_2 were reported. They are mainly singly dispersed Pd, Rh and other metal atoms coordinating with certain number of oxygen atoms in micropores of zeolite.

13.1 Catalytic oxidation of CH_4 to CH_3OH over Fe sites anchored in ZSM-5 with H_2O_2

Hucthings *et al* first reported the high activity of Fe-ZSM-5 in catalytic oxidation of CH_4 to CH_3OH through H_2O_2 under mild conditions.[288] In addition, although TS-1 is not active for this oxidation, TS-1 or silicaliate-1 with anchored Fe exhibits high activity for catalytic oxidation of CH_4 to CH_3OH through H_2O_2 at 50^{o}C.[288] These studies show that Fe species formed in MFI is the key player of the catalytic oxidation of CH_4 with H_2O_2. For instance, 27 mg of 0.014wt%/ZSM-5 convert 10% of dissolved CH_4 in aqueous solution of H_2O_2 with 96% selectivity for producing oxygenates including CH_3OH, CH_3OOH, HCOOH. ^{13}C and ^1H NMR spectra confirmed that CH_4 is the sole carbon source of these products. The observation of Si-O-Fe bond at 700-710 cm^{-1} in FT-IR of the catalyst shows that Fe atoms incorporated into tetrahedral framework sites before calcination.[327] Ex situ EXAFS studies suggest that Fe atoms exist in the form of di-iron species, similar to structures reported in in late literature.[328-330] Structure 1 in Figure 22a, $[Fe_2(m2\text{-}OH)_{2(}OH)_2(H_2O)_2]^{2+}$ anchored in ZSM-5, is the structure closest to the structural parameters of EXAFS studies of the catalyst. It catalyses the synthesis of methanol from CH_4 under mild condition (50^{o}C) with a TOFs >0.6 s^{-1} which are three orders of magnitude greater activity in catalytic oxidation of CH_4 to CH_3OH on these catalysts reported before this work.[288] The significance of this work is that production of CH_3OH from CH_4 can be performed in a continuous flow fixed bed stainless steel reactor with a close catalytic cycle.[331, 332]

Time-on-line analysis suggested that CH_3OOH is the primary product and CH_3OH is formed consecutively. Thus, it is proposed that the H_2O_2 replaces one H_2O molecule bound to di-iron site (1 in Figure 22a), forming OCHO-Fe (2 in Figure 22a). A following transfer of H^+

forms HOO bound to one Fe ion (3 in Figure 22a). Replacement of another H_2O molecule bound to Fe^{2+} by H_2O_2 forms a Fe^{4+}=O site (4 in Figure 22a) based on a reported redox to produce a ferryl ion in Fenton's reagent.[333, 334] Fe^{4+}=O of species 4 activates C-H of CH_4, forming CH_3 and Fe-OH (5 in Figure 22a). The CH_3 couple with oxygen atoms of HOO-, forming a CH_3OOH-like species on one Fe ion (5 in Figure 22a). Figure 22c presents the transformation of CH_3OOH to CH_3OH. CH_3OH releases a HO·, forming CH_3O bound to the Fe ion (6 in Figure 22a). Other than the first report in literature,[288] this catalyst and catalytic oxidation of CH_4 to CH_3OH were extensively studied with respect to identification of active component,[335] kinetics studies,[332] and influence of Si/Al ratio of H-ZSM-5 on catalytic performance.[336]

Catalytic selectivity for production of CH_3OH on Fe-ZSM-5 can be obviously increased by the introduction of Cu^{2+} as a part of the catalyst to reduce over-oxidation process of CH_3OH to other oxygenates.[288] For instance, by mixing Fe-1-silicate with Cu-1-silicate, high selectivity of 93% for producing CH_3OH from CH_4 can be achieved.[288] In addition, it was found that presence of strong acidity is favourable for the formation of formic acid instead of CH_3OH.[337]

13.2 Catalytic oxidation of CH_4 to CH_3OH over Fe sites incorporated in graphene lattice with H_2O_2 at room temperature

Bao et al reported a room temperature catalysis of oxidizing CH_4 to CH_3OH with H_2O_2.[338] This catalysis is performed on a unique catalyst FeN_4/GN consisting of catalytic sites -FeN_4-. Here GN denotes graphene. This catalyst was prepared by high-energy ball milling of mixture of iron precursor, iron phthalocyanine cite.[338] 50 mg of FeN_4/GN can catalyse the oxidation of CH_4 with a yield of CH_3OH of nearly 120 μmol at room temperature in a period of time of 10 hr. The selectivity for C_1 oxygenated products is as high as 94%.

Evolutions of different C1 oxygenate products were tracked with operando TOF-MS method which extracts products during reaction and analyses them in real time.[338] This operando study suggested CH_4 is oxidized to CH_3OH and CH_3OOH at beginning and then further oxidized into HCOOH and $HOCH_2OOH$. The deep oxidation of CH_4 to HCOOH and $HOCH_2OOH$ upon CH_3OH is formed as an intermediate compound was supported by isotope-labelled ^{13}C-NMR experiments.[338]

Fundamental understanding of this room temperature catalysis of CH_4 to CH_3OH on the unique catalyst of FeN_4/GN was achieved by DFT calculations.[338] As shown in Figure 23,

H_2O_2 can readily adsorb on a FeN_4 site to decompose into atomic O and H_2O (Figure 23a). Atomic O is absorbed to Fe atom of the FeN_4 site. As the FeN_4 is incorporated into the graphene lattice, each FeN_4 can chemisorb two O atoms, forming a O-FeN_4-O structure. Compared to bare -FeN_4-, density of electronic states near to Fermi level of O-FeN_4-O is largely increased upon binding to two O atoms at two sides of -FeN_4- (Figure 23b). This difference shows that O-FeN_4-O is more active for electrophilic attack. Reaction pathway of oxidizing CH_4 to CH_3OH was computationally simulated (Figure 23c). DFT calculations suggests that C-H activation of CH_4 is performed through a radical pathway instead of a concerted mechanism.[338] Figure 23C represents the reaction pathway and the corresponding energy profile. The rate-determining step is the C-H bond cleavage with a barrier of 0.79 eV. The generated CH_3· can coulee with OH or OOH groups, forming CH_3OH and CH_3OOH respectively. In addition, DFT calculation shows that the O-FeN_4-O incorporated in graphene lattice exhibits high activity than free standing O-FePc-O (FePc: iron phthalocyanine), suggesting that the graphene lattice enhances activity in oxidation of CH_4 to CH_3OH.[338]

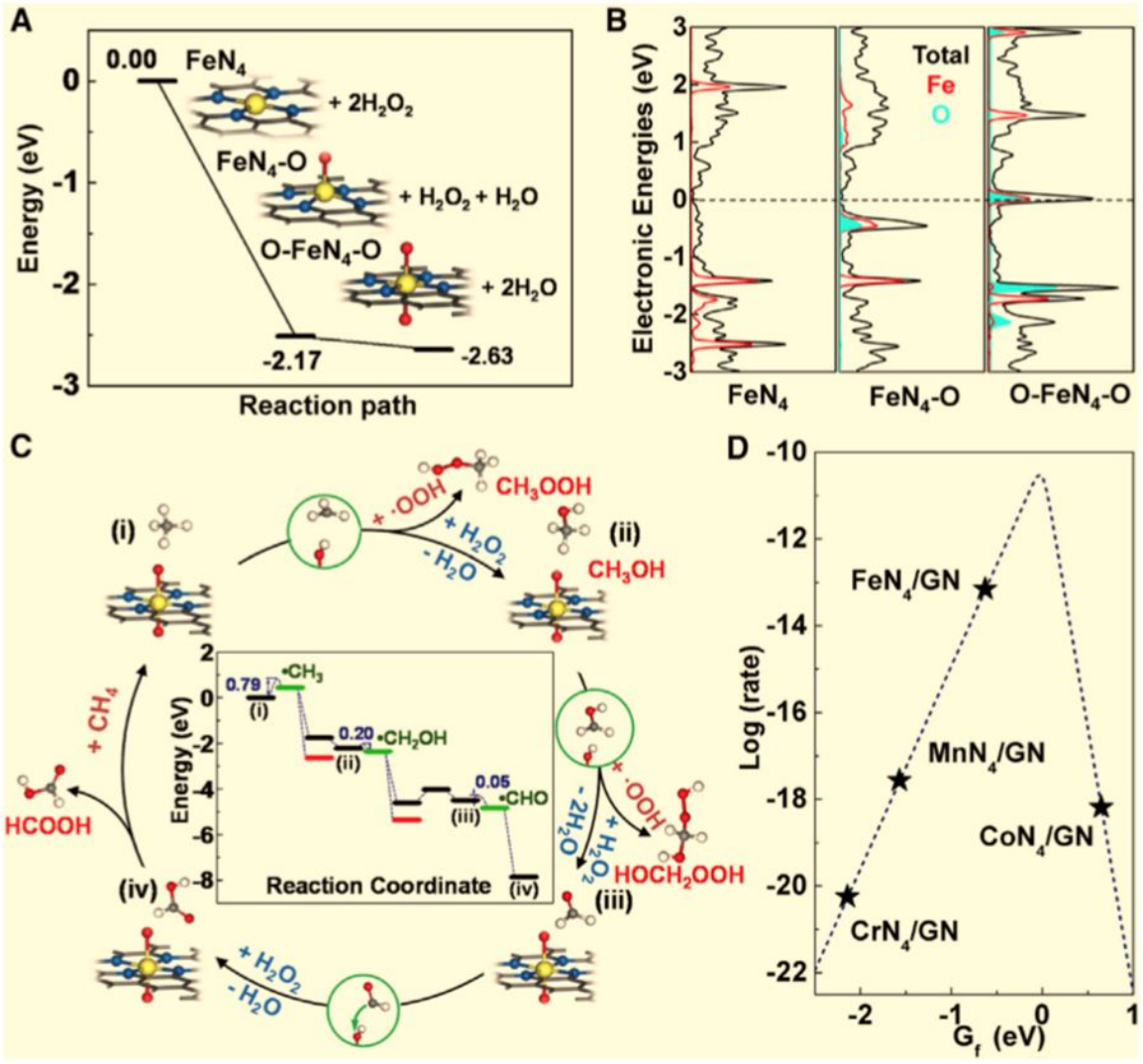

Figure 23. *Representation of theoretical simulation of reaction pathway for oxidation of CH_4 to form CH_3OH on -FeN_4- sites and other similar sites.[338] (a) Thermodynamic calculation of the decomposition of H_2O_2 and binding of oxygen atoms to -FeN_4- to form O-FeN_4-O. (b) Density of states of FeN_4, FeN_4-O and O-FeN_4-O. (c) Suggested reaction pathway of oxidation of CH_4 to CH_3OH, CH_3OOH, $HOCH_2OOH$, and HCOOH on O-FeN_4-O and the corresponding energy profile. (d) Correlation of rate of activation of C-H of CH_4 in Log(rate) with formation energy of O-MN_4-O. Reproduced from Ref. 338, copyright 2018, with permission from Elsevier.*

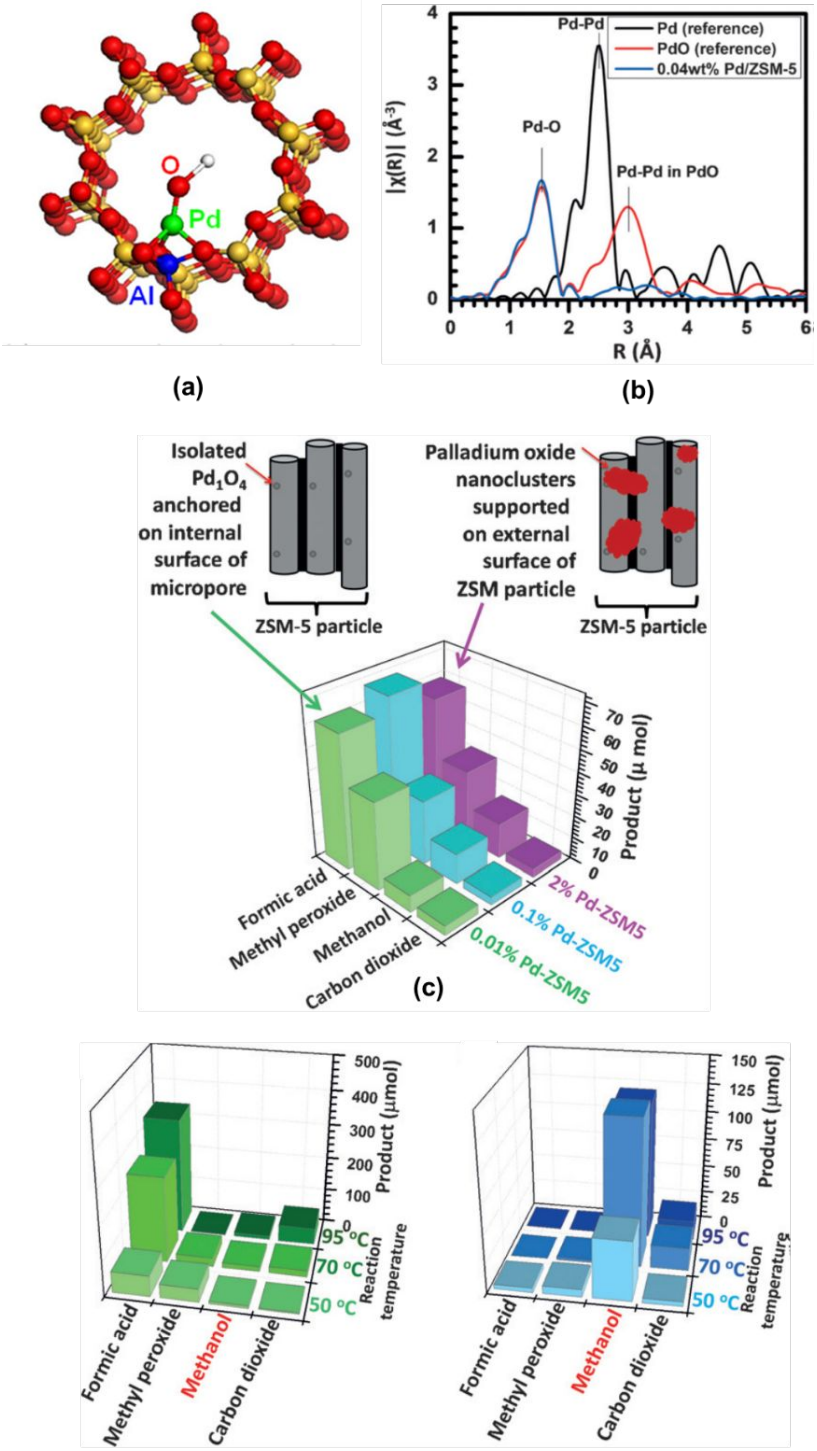

Figure 24. *Representation of structural characterisation and catalytic performance for catalytic oxidation of CH_4 with H_2O_2 to CH_3OH under mild condition.[339] (a) Structural model of microporous aluminosilicate with anchored Pd_1O_4 sites. (b) EXAFS. (c) Catalytic performances of oxidizing CH_4 to CH_3OH with H_2O_2. (d) Increase of selectivity for producing CH_3OH by adding CuO to supress oxidation of CH_3OH. Reproduced from Ref. 339, copyright 2016, with permission from John Wiley and Sons.*

DFT calculations were performed on similar sties (O-MN_4-O) but different metal center (M=Cr, Mn, Co, Ni, Cu). Based on the formation energy of O-MN_4-O structure, only O-CrN_4-O, O-MnN_4-O, O-FeN_4-O, and O-CoN_4-O can be formed. The activation rates of C-H of CH_4 by the four catalysts were calculated (Figure 23d). Bao et al found a volcano-like correlation *between* activation rate of C-H of CH_4, Log (rate) *and* formation energy of the four catalysts, O-MN_4-O (Figure 23d).[338] Thus, these computational studies suggested that the formation energy of O-MN_4-O can be taken as a descriptor for the catalytic oxidation of CH_4 to CH_3OH on this type of catalysts (O-MN_4-O).[338]

13.3 Catalytic oxidation of CH_4 to CH_3OH over Pd sites with H_2O_2

Through ion-exchange between Pd cations and protons in microporous aluminosilicate, Pd_1O_4 clusters anchored in the micropore (0.01wt%Pd) were prepared (Figures 23a and 23b).[339] Although the loading of Pd is extremely low, its role is crucial in the oxidation of CH_4 to CH_3OH and other oxygenates in the temperature range of 50-95^{o}C. As shown in Figure 24c, even at 50^{o}C, CH_3OH can be produced from the catalytic oxidation of CH_4 with H_2O_2. The role of the singly dispersed Pd_1 sites, Pd_1O_4 anchored in micropores was confirmed by the fact that the same microporous aluminosilicate but without Pd atoms under the same catalytic condition exhibit much lower activity. Notably, the increase of loading of Pd to the microporous aluminosilicate from 0.01wt% to 0.1wt% and 2wt% does not increase the yields of oxygenates, suggesting that the crucial role of the singly dispersed single-atom Pd_1 sites in the catalytic oxidation of CH_4 to CH_3OH with H_2O_2. Due to the available significant excess of H_2O_2, products of deep oxidation including formic acid and even carbon dioxide were clearly observed.[339] Thus, control of selectivity for product CH_3OH is a challenging issue for catalytic oxidation using H_2O_2 as an oxidant. Compared to the catalytic oxidation of CH_4 using H_2O_2, the oxidation of CH_4 with metal atoms anchored in zeolite without using H_2O_2 forms CH_3OH with much higher activity. As shown in Figure 24d, by co-loading 2.0wt% CuO to surface of the microporous aluminosilicate consisting of Pd_1O_5 sites, selectivity for producing CH_3OH was obviously increased. The promotion of selectivity by using CuO suggests CuO can catalyse

the decomposition of H_2O_2 to H_2O and O_2 and thus supressed the further oxidization of CH_3OH to products of deep oxidation.

13.4 Catalytic oxidation of CH_4 to CH_3OH over Cu sites with H_2O_2

Catalysts containing the same amount of Cu (1.2wt%) and Fe (0.09wt%) were prepared through different methods including ion exchange between Cu^{2+} and H^+ of H-ZSM-5 by Yashnik *et al*[340, 341]. Similar to Fe-ZSM-5,[288] the main products of CH_4 oxidation with H_2O_2 on Cu-ZSM-5 are CH_3OOH and CH_3OH. After an induction period of oxidation, more formic acid and CO_2 were formed. The role of the anchored Cu^{2+} was confirmed by careful parallel experiments performed on a series of catalysts including catalyst 1 which is H-ZSM-5 originally containing 0.09wt% Fe in lattice, and catalyst 2 which is H-ZSM-5 originally containing both Fe (0.09wt%) and the lately anchored Cu (1.2wt%) by ion exchange between Cu^{2+} of precursor and H^+ of H-ZSM-5 with a followed calcination at 500°C in air.[342] Compared to the catalyst 1 (H-ZSM-5 with 0.09wt% Fe but no Cu) the introduction of Cu^{2+} to ZSM-5 led to an increase of conversion of both CH_4 and H_2O_2. It is suggested that Cu peroxo complexes in ZSM-5 participates into the formation of CH_3OH from CH_3OOH.[342] When concentration of Fe(III) in H-ZSM-5 is high, the role of Cu(II) peroxo complexes is less important. Notably, some of the anchored Cu^{2+} in ZSM-5 leached to aqueous solution during catalysis. It is reported that even half of anchored Cu^{2+} cations were leached in the first half hour of catalysis. Compared to the Cu^{2+} introduced to the cation exchange positions of H-ZSM-5, the Fe (III) cations introduced to the lattice of ZSM-5 in the synthesis of H-ZSM-5 are much more stable during catalysis.[342]

As reviewed in sections 13.1-13.4, ZSM-5 anchored with Fe, Pd, and Cu are active for catalysing oxidation of CH_4 to CH_3OH with H_2O_2. Similar to the proposals in other sections, there are lack of systematic, parallel studies for ZSM-5 anchored with other transition metals including 3d and 4d metals. Coordination environment of metal atoms is crucial for catalytic performance in oxidation of CH_4 with H_2O_2. However, it is challenging to prepare a series of catalysts of different metals which have the same coordination environment such as M_1O_4 (M=Zr, Nb, Mo, Ru, Rh, Pd, Ag). Thus, here computational "experiments" were suggested to perform parallel studies on these catalysts ZSM-5 anchored with M_1O_4 sites (M=Zr, Nb, Mo, Ru, Rh, Ag). By applying the same reaction pathway on these catalysts, rate determining steps and their corresponding activation barriers can be uncovered through computational studies. With this piece of information, a correlation of activation barriers of these catalysts and electronic factors of the active site M_1O_4 of these catalysts such as Bader charge, orbital

contribution can be established. With this correlation, active catalysts can be proposed on the basis of these computational studies for experimental tests. Through these computational studies-driven experimental studies, catalysts with high activity and selectivity are expected to develop.

13.5 Catalytic oxidation of CH_4 to CH_3OH with H_2O_2 over Rh single atom sites anchored on open surface of oxide support

As reviewed in Sections 13.1-13.3, the encapsulated metal atoms in zeolites are active in catalysing oxidation of CH_4 with H_2O_2. Recently, it is reported *that single atoms Rh* (SAs Rh) anchored on CeO_2 nanowires (*SAs Rh-CeO_2 NWs*) can catalyse oxidation of CH_4 with H_2O_2 at 50°C.[343] SAs Rh-CeO_2 NWs was prepared through impregnating Na_3RhCl_6 on the as-prepared CeO_2 NWs through a conventional wet impregnation method.[343] The formation of single atoms Rh on CeO_2 NWs was suggested by the lack of peak of Rh-O-Rh in r-space of Rh K-edge. For comparison, *Rh NPs* supported on commercial CeO_2 NWs (*Rh/CeO_2-com*) were prepared through impregnation of Rh to commercial CeO_2. Although chemical and coordination environments of Rh atoms of Rh/CeO_2-com catalysts were not reported, Rh 3d 5/2 of Rh/CeO_2-com is 308.9 eV which is obviously higher than 307.4 eV of metal Rh nanoparticles. It suggests that Rh atoms of Rh/CeO_2-com are in the form of RhO_x nanoclusters supported on commercial CeO_2.

Compared to Rh/CeO_2-com, SAs Rh-CeO_2 NWs exhibits much higher catalytic activity and selectivity in production of CH_3OH and CH_3OOH through oxidation of CH_4 with H_2O_2 at 50°C. This significant difference was attributed to the distinctly different electronic states of Rh atoms in the two catalysts in terms of projected density of states (PDOSs) of surfaces of the two catalysts. For SAs Rh-CeO_2 NWs, its Rh 4d occupation near the Fermi level is sharp. However, the Rh 4d occupation of Rh/CeO_2-com is quite broad. Different from SAs Rh-CeO_2 NWs, the significant overlap among Rh 4d, O 2p and Ce 4f suggests a strong coupling between RhO_x cluster and support CeO_2 particle. This strong coupling in Rh/CeO_2-com results in over-binding effects, consequently increasing activation barrier of dehydrogenation of CH_4 on Rh/CeO_2-com.

Other than single atoms Rh anchored on CeO_2,[343] Rh anchored on ZrO_2, TiO_2, SiO_2 were chosen to explore potential oxidation of CH_4 with H_2O_2.[344] Single atoms Rh anchored on ZrO_2 exhibit high activity in catalytic oxidation of CH_4 to CH_3OH. However, no CH_3OH was produced from 0.3wt%Rh/TiO_2 under a catalytic condition of 30 mg catalyst, 0.5 M H_2O_2, at

70°C with a reaction time of 0.5 hr under 30 bars of CH_4.

13.6 Catalytic oxidation of CH_4 to CH_3OH over Au-Pd alloy nanoparticles

Hutchings et al found that 5wt% Au-Pd/TiO_2 exhibits high activity and selectivity for oxidation of CH_4 to CH_3OH with H_2O_2.[345] Notably, their studies also showed that no any product could be observed from a bare TiO_2 under the same condition as 5%Au-Pd/TiO_2, concluding that the activity for oxidation of CH_4 with H_2O_2 on 5wt% Au-Pd/TiO_2 results from Au-Pd nanoparticles instead of TiO_2. Their time-on-line studies of products showed that CH_3OOH is the intermediate compound formed first and then it is transformed to CH_3OH;[345] subsequently, CH_3OH is oxidized to formic acid or even CO_2, dependent on catalysis temperature and concentration of H_2O_2. The feature of sequential reactions including transforming CH_4 to CH_3OOH first, then CH_3OH and finally formic acid and CO_2 ,[345] is similar to oxidation of CH_4 with H_2O_2 on Fe-ZSM-5.[288] The catalysis for formation of CH_3OH from CH_3OOH was confirmed by using isotope-labelled $^{13}CH_3OH$ as a reactant. In addition, the oxidation of CH_3OH to HCOOH was evidenced by observation of $H^{13}COH$ and $H^{13}COOH$ when $^{13}CH_3OH$ was used as a reactant.

Deep understanding of the catalytic mechanisms for oxidation of CH_4 on Au-Pd/TiO_2 was achieved through electron paramagnetic resonance (EPR) studies under catalytic conditions.[345] Both $\cdot CH_3$ and ·OH were tracked with 5,5'-Dimethyl-1-pyrroline-N-oxide (DMPO) in EPR studies, uncovering that $\cdot CH_3$ and ·OH are formed during catalytic oxidation of CH_4 with H_2O_2. Thus, it is concluded that the catalytic oxidation of CH_4 with H_2O_2 on Au-Pd/TiO_2 must involve $\cdot CH_3$ radicals. Then, the formed $\cdot CH_3$ can couple with the intermediate O_2 or ·OOH in-situ formed from decomposition of H_2O_2, formingCH_3OOH which is the intermediate compound for formation of CH_3OH. Notably, this catalysis mechanism is different from oxidation of CH_4 with H_2O_2 on Fe-ZSM-5 where no $\cdot CH_3$ was observed.[288]

Other than the catalytic synthesis of CH_3OH from oxidation of CH_4 with H_2O_2 on Au-Pd/TiO_2, Au-Pd/TiO_2 is active for synthesis of $_{CH3OH}$ from CH_4, H_2 and O_2.[346] This is understandable since Au-Pd/TiO_2 can catalyse the synthesis of H_2O_2 and catalyse the oxidation of CH_4 to CH_3OH with H_2O_2 under mild condition. In other words, a possible path for synthesis of CH_3OH from CH_4, H_2, and O_2 on Au-Pd/TiO_2 is that Au-Pd/TiO_2 first catalyses the synthesis of H_2O_2 from H_2 and O_2 and then catalyse the synthesis of CH_3OH from oxidation of CH_4 with H_2O_2.[346, 347]

13.7 Catalytic oxidation of CH_4 to CH_3OH catalysed by an engineered nanocomposite catalyst AuPd@ZSM-5-R

The feature of high activity of Au-Pd nanoparticles in catalysing oxidation of H2 by O2 to form H_2O_2 at room temperature or even low temperature and the capability of H-ZSM-5 in catalysing oxidation of CH_4 with H_2O_2 to form CH_3OH under mild conditions were intelligently mingled in a recent work, creating a catalyst with high activity and selectivity in synthesis of CH_3OH from CH_4, H_2 and O_2.[348] In this work, Jin et al reported that AuPd@ZSM-5-C_{16} exhibits high activity and selectivity for oxidation of CH_4 to CH_3OH at 70°C.[348] As shown in Figure 25a, this is a nanocomposite catalyst with a MFI framework encapsulated with Au-Pd nanoparticles internally supported with molecular fence of C_3-C_{16} on external surface of the ZSM-5 particle. Conversions and yields on catalysts with a fence such as AuPd@ZSM-5-C_3 (or C_6, C_{16}) are obviously higher than AuPd@ZSM-5 without a molecular fence (Figure 25b). The external organic layer anchored on the ZSM-5 particle is hydrophobic and thus prevents the emigration of H_2O_2 formed on surface of AuPd which was encapsulated in the ZSM-5 particle. This is evidenced by the quantitative analyses of the amount of H_2O_2 in zeolite and that in liquid. As shown in Figure 25c, there is a distinct difference in the distribution of H_2O_2 in ZSM-5 *between* a catalyst with a molecular fence such as AuPd@ZSM-5-C_3 *and* a catalyst without any molecular fence such as AuPd@ZSM-5. With the protection of this molecular fence, H_2O_2 formed through catalysis on AuPd nanoparticles encapsulated in ZSM-5 particles is mainly remained in the micropores of ZSM-5; but without such a fence, majority of H_2O_2 in the micropores emigrated to liquid which is the external environment of AuPd@ZSM-5 particles. Clearly, the hydrophobic nature of the organic layer (C_3, C_6, or C_{16}) on the external surface of the ZSM-5 particle has stopped the emigration of H_2O_2 efficiently. Thus, contributed from the hydrophobic nature of the organic fence, the high local concentration of H_2O_2 in ZSM-5 near to the catalyst sites of CH_4 oxidation largely increased reaction rate of CH_4 oxidation by H_2O_2 on surface of Au-Pd nanoparticles. Notably, this hydrophobic layer on external surface of ZSM-5 does not hinder the diffusion of hydrophobic, nonpolar CH_4 from liquid to micropores of AuPd@ZSM-5.[348]

CH_3OH was considered as an intermediate product for further oxidation to form HCHO and formic acid.[62, 349] As discussed in Section 13.3, one disadvantage of catalytic oxidation of CH_4 with H_2O_2 by catalytic sites, M_xO_y clusters anchored in micropores of zeolites is the further oxidation of CH_3OH by excess oxidant, H_2O_2. The work of Jin et al shows that CH_3OH on Au-Pd can readily emigrate from micropores of ZSM-5 to solvent although H_2O_2 cannot.

The efficient separation of CH_3OH from region of high concentration H_2O_2 in ZSM-5 prevents CH_3OH from being further oxidized to HCHO and HCOOH, leading to a high selectivity for production of CH_3OH. Thus, such a smart catalyst with a molecular fence, AuPd@ZSM-5-C_{16} can catalyse the conversion of CH_4 to CH_3OH with a selectivity of 60%-90%, higher than selectivity for production of CH_3OH through oxidation of CH_4 with H_2O_2 on other catalysts.[348]

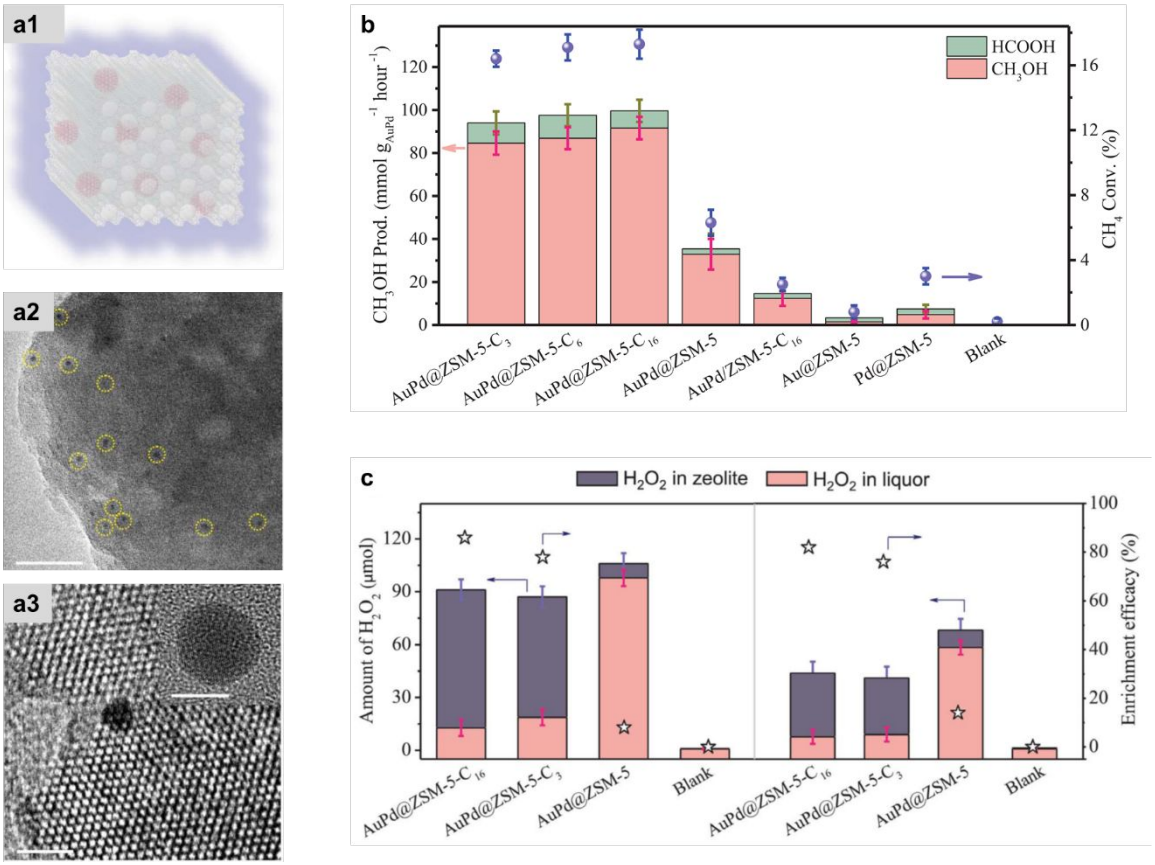

Figure 25. *Representation of AuPd@ZSM-5-R and their catalytic performance and molecular fence effect of external layer of* C_n.[348] *(a) Models (a1) and TEM images (a2 and a3) of AuPd@ZSM-5-R. (b) Activity of* CH_3OH *and conversion of* CH_4 *on AuPd@ZSM-5-R, AuPd@ZSM-5 and other related catalysts; here R denotes the organic layer of molecular fence. (c) Molecular-fence effect investigation; it shows a distinct difference in distribution of* H_2O_2 *in ZSM-5 between a catalyst with molecular fence such as AuPd@ZSM-5-*C_3 *and a catalyst without a fence such as AuPd@ZSM-5. Reproduced from Ref. 348, copyright 2020, with permission from AAAS.*

13.8 Catalytic oxidation of CH_4 to C_1 oxygenates on vanadium-based complexes

Vanadium-based complexes are active in catalytic oxidation of organic compounds with H_2O_2.[350, 351] It is reported that the acetonitrile solution of $[NBu_4]VO_3$ (or $NaNO_3$) and pyrazine-2-carboxylic acid (PCA) is active in catalytic oxidation of CH_4 with H_2O_2 and O_2 by groups in Russia and Switzerland.[352, 353] It produces methyl hydroperoxide, formaldehyde and formic acid. Based on control experiments using cyclohexane to substitute for CH_4, it is

claimed that H_2O_2 is only a promoter and molecular O_2 is the actual oxidant. They proposed that HO· radical is formed from H_2O_2 and then it attacks alkane including CH_4 to form alkyl radicals such as CH_3·. The formed CH_3· can rapidly react with molecular O_2 to form peroxyl radicals ROO· such as CH_3OO·. ROO· is transformed to ROOH such as CH_3OOH.[352, 354-356] In terms of active sites, there was no any indication in this literature although it is sure that the active sites must be vanadium-based species.

Another group independently reported that $H_{3+x}PV_xMo_{12-x}O_{40}$ catalyst (x=0, 1, 2, and 3) in $(CF_3CO)_2O$ solvent at 353 K can catalyse oxidation of CH_4 with H_2O_2 under inert gaseous environment.[357] $H_4PVMo_{II}O_{40}$ gave the highest conversion of CH_4. Majority of the products is $HCOOCH_3$. HCOOH and CH_3OH are minor products.[357] $H_{3+x}PV_xMo_{12-x}O_{40}$(x=0-3) Keggin-type heteropoly acid was used as precursor. Among the used solvents $(CF_3CO)_2O$, CH_3CN, H_2O, and $(CH_3)_2SO$, $(CF_3CO)_2O$ has the highest solubility of CH_4,[357] resulting in highest conversion among the same catalyst in different solvents. Although there was no any information on the active sites for this oxidation, it seems that vanadium is a necessary element of the unknown active sites.

Other than the above two types of Vanadium-based catalysts, vanadyl oxysulate was found being active for oxidizing CH_4 with H_2O_2 at 60°C.[358] The main product is formic acid. Their UV-Vis spectroscopy measurements suggest that $VOSO_4$ is oxidized to oxoperoxo $VO(O_2)^+$ species by H_2O_2. Thus, the V^{5+} species formed under catalytic condition was proposed to be active sites of the oxidation of CH_4.

13.9 Catalytic oxidation of CH_4 by H_2O_2 to form oxygenates in solution of transition metal chloride

A series of transition metal chlorides ($FeCl_3$, $CoCl_2$, $CuCl_2$, $RuCl_3$, $RhCl_3$, $PdCl_2$, $OsCl_3$, $IrCl_3$, H_2PtCl_6, and $HAuCl_4$) were studies in parallel for catalytic oxidation of CH_4 with H_2O_2 in aqueous solution.[359] Obvious difference in catalytic activity in oxidation of CH_4 was found. $FeCl_3$, $CoCl_2$, $CuCl_2$, $RhCl_3$, $PdCl_2$, $OsCl_3$, $IrCl_3$, H_2PtCl_6 and $HAuCl_4$ are active for oxidation of CH_4 with H_2O_2. Active sites in terms of authentic player of the catalytic reactions under mild condition were not identified in literature.[359]

Among these chlorides, $OsCl_3$ is the most active catalyst for oxidation of CH_4. Compared to other chlorides, the high activity for catalytic oxidation of CH_4 with H_2O_2 on $OsCl_3$ is probably correlated with the high activity of OsO_4 in selective oxidation of alkenes[360, 361] although likely OsO_4 is not the real player of this catalysis. UV-Vis spectra studies of $OsCl_3$,

$OsCl_3$+H_2O_2 before catalysis, $OsCl_3$+H_2O_2 after catalysis, Na_2OsCl_6 and OsO_4 suggested that the nominal catalyst $OsCl_3$ was evolved into a species with high oxidation state (+IV) of Os during catalysis. Compared to the spectral feature of OsO_4, the UV-Vis spectrum of the catalyst ($OsCl_3$+H_2O_2) after catalysis is distinctly different. Thus, OsO_4 could be the active sites formed during catalysis and evolved into other species after catalysis. Definitely, more studies are necessary for elucidation of the active site of this oxidation.

At initial period of catalysis, methyl hydroperoxide was observed.[360, 361] Analysis of products as a function of time suggests that methyl hydroperoxide is an intermediate product. In addition, oxidation of CH_4 ceased once the radical scavenger hydroquinone was added to the system, showing that this catalysis is performed through a radical-based pathway. It is suggested that the active radical, HO· or HOO· activates CH_4 by abstracting a H atom, forming CH_3· radical. Then, coupling CH_3· radical with HO· or HOO· forms products.

13.10 Catalytic oxidation of CH_4 with H_2O_2 to CH_3OH over M_1O_n cluster in complex encapsulated in second coordination shell

One type of well-studied catalysts are μ-nitrido diiron phthalocyanine[362-365] and porphyrin[366] which are active for catalytic oxidation of CH_4 with H_2O_2. These Fe- or Cu-contained catalysts exhibit high selectivity for formic acid but low for CH_3OH.

Complexes including Fe^{II}(TPA), and V(TKA) shown in Figures 25a and 25b exhibit low activity for oxidation of CH_4 with H_2O_2 and low selectivity for producing CH_3OH. These complexes are soluble in aqueous solution. Upon encapsulating such a complex into a hydrophobic hemicryptophane cage, a new catalyst was formed as shown in Figures 25c-25e.[367] These cage-like catalysts can accommodate CH_4 molecules and make them physically proximal to the oxidation site of these complexes.[367] Notably, this cage structure obviously improved catalytic activity and selectivity. For instance, Fe^{II}(Hm-TPA) and V(Hm-TKA) having cages (Figures 25c and 25d) exhibit much higher catalytic activity in terms of TOF than Fe^{II}(TPA) and V(TKA) without cages (Figures 25a and 25b). Covering TPA-iron (II) active centre with a hydrophobic cage, Fe^{II}(Hm-TPA) promotes the yield of mono-oxidized products (CH_3OH and CH_3OOH) on Fe^{II}(TPA) by a factor or about 4. Such a promotion of selectivity results from the physical proximity between the adsorbed CH_4 and the Fe-based active site of the complex Fe^{II}(TPA) in the cage, and the preferential release of hydrophilic products (CH_3OH and CH_3OOH) by the hydrophobic cage.

The promotion of selectivity by caging a molecule was also supported by the increased

yields of CH_3OH and CH_3OOH on V(Hm-TKA) (Figure 26d) compared to V(TKA) (Figure 26b). By replacing phenyl spacers of the cage (Hm) of V(Hm-TKA) with biphenyl groups, a different catalyst was formed (Figure 26e). Catalytic activity of V(Hm-BINOL-TKA) increased by 2 times due to the increase of capability of recognition of hydrophobic substrates. Thus, obviously encapsulation of molecular catalyst in an organic shell is a strategy to improve catalytic performance of oxidation of CH_4 with H_2O_2 under mild conditions. It is expected that the encapsulation approach could be used in other catalyst systems for promotion of catalysis activity.

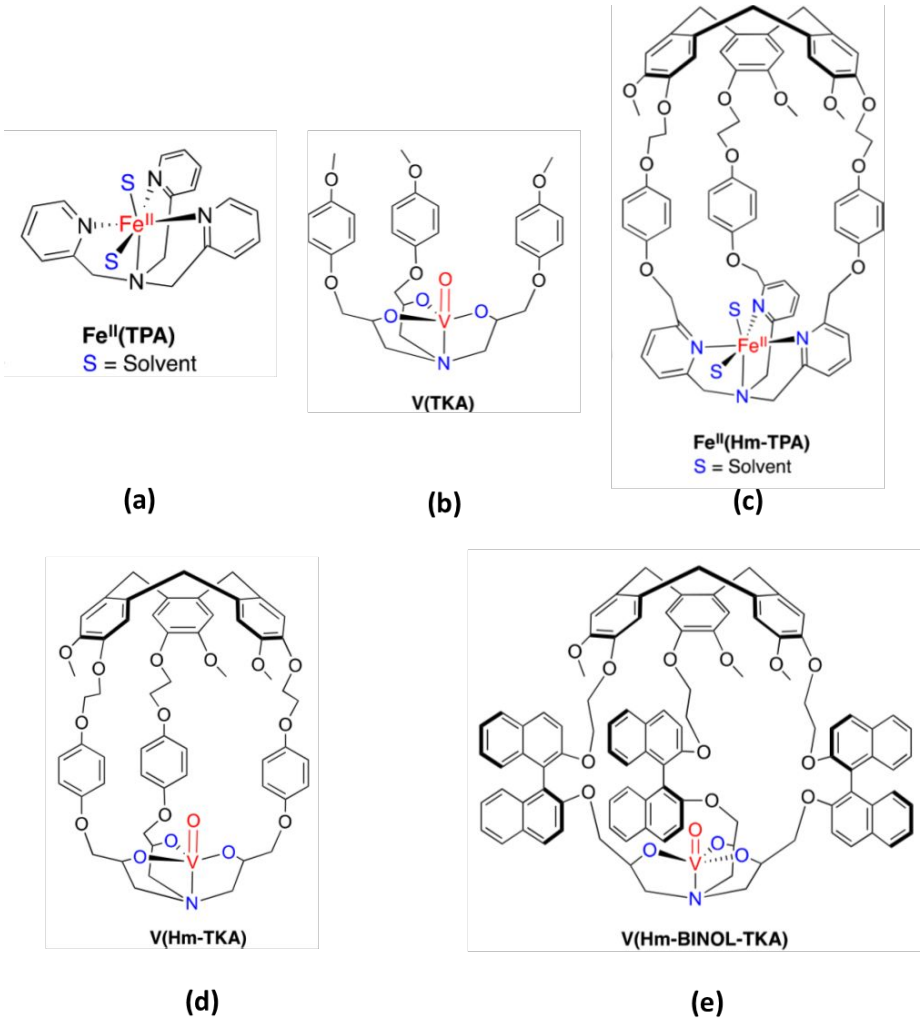

Figure 26. *Representation of structure of Fe, V and Cu complexes without second coordination shell (a and b) and with second coordination shell (c-e).*[367] *(a) FeII(TPA), (b) V(TKA), (c) FeII(Hm-TPA), (d) V(Hm-TKA), and (e)V(Hm-BINOL-TKA). Reproduced from Ref. 367, copyright 2019, with permission from ACS.*

14. Facing challenges

Direct transformation of CH_4 to value-added chemicals under mild conditions has been one of the most challenging tasks in the field of catalysis. Compared to the well-studied high temperature processes of catalytic transformation of CH_4, there is no formation of coke and much less extent of decay of catalysts in transformation of CH_4 under mild conditions. However, transformations under mild conditions rely on specific catalytic sites which need to be designed and prepared with atomic precise. These sites are typically metal oxide nanocluster-like structures with specific composition and specific coordination environment of metal atoms. In many cases, they need to be anchored some "protective" environment such as microporous silica since the confinement effect of micropores is significant for performing many transformations under mild conditions. Although significant progress has been done in the field of activation and catalytic transformation of CH_4 under mild conditions, the following challenges still remain.

Challenges in preparation with atomic precision and ready duplication. Majority of catalysts active for transforming of CH_4 to value-added chemicals are catalysts consisting of single-atom sites or sub-nanometer clusters encapsulated in micropores of zeolites. The chemical and coordination environments of these metal atoms are essential for catalysis under mild conditions. Compared to the preparation of conventional catalysts such as supported oxide or oxide nanoparticles, repeatedly preparation of these catalysts brought into great challenges. From this point of view, development of precise preparation including new preparation protocol and integration of other preparation techniques could be a solution to tackle this challenge. For instance, atomic layer deposition technique can be used to homogenously introduce metal precursor to micropores, making a catalyst consisting of homogeneous sites toward repeatable syntheses of catalysts active for transformation of CH_4 under mild conditions.

Challenges in characterization of catalytic sites during catalysis. It has been well acknowledged that establishment of a correlation between structure of active sites and its corresponding catalytic performance is a key approach to achieve fundamental understanding of catalytic mechanism at a molecular level. As the catalyst consisting of active sites is dispersed in liquid which is under a high-pressure gas phase, it is quite challenging to characterize these catalytic sites *during catalysis* since most electron-excitation or electron-generation-related analytical methods of solid materials such as TEM and XPS were developed

for characterizing catalyst nanoparticles in high vacuum or in gas phase instead of a liquid phase. Development of analytical methods with capability of characterizing catalysts in liquid during catalysis is significant but a challenging task.

Access to the chemical and coordination environments of atoms of authentic active sites anchored in micropores during catalysis is challenging even for catalysis performed at solid-gas interface. Unfortunately, most transformations of CH_4 to value-added chemicals under mild conditions are performed at solid-liquid or solid-liquid-gas interfaces. It is extremely challenging for accessing chemical and coordination environments of metal atoms of catalyst sites of catalysts working in liquid. There are the following challenges. (1) Due to the much higher density of molecules in liquid environment around the catalyst particles than gas phase, most electron-based techniques are limited in probing the surface of a catalyst particles in liquid. (2) Most reactions request high pressure reactant gas above liquid since gas molecules can only access surface of catalyst in liquid by molecular diffusion in liquid; thus, the pressure of gas above the liquid is 10 bar or higher. (3) Many of the reactions and catalysis are performed on active sites embedded in micropores of zeolite. The thickness of wall of silicate limits the access of electron or light to the active sites encapsulated in pores and also prevents the generated electrons or photons from escaping for detection. (4) The preservation of products in micropores after reaction could make characterization of active sites in zeolite at the atomic scale challenging; for instance, the adsorption of CH_3OH molecules on or near to the active sites in the zeolite prevents the EXAFS from distinguishing the coordination environment of Cu atoms of active sites from the coordination environment of Cu bound to product molecules.

Al Kα X-ray photoelectron spectroscopy (XPS) is an appropriate analytical method for characterizing chemical environment of most elements. Due to its high surface sensitivity in terms of short inelastic scatting mean free path (λ), it is extremely challenging if not impossible to study metal sites anchored in micropore of zeolite in liquid phase. In addition, although AP-XPS has been widely used in observation of chemical state of metal atoms in gas phase,[78] the working pressure of reactant gas is still quite low in terms of a pressure range of sub-Torr or Torr. Many efforts have made with the goal of having Al Kα or soft X-ray AP-XPS for working at a pressure higher than 25 Torr. Unfortunately, scientists failed in these efforts. These challenges have made elucidation of chemical states of metal elements of catalysts functioning in liquid phase quite difficult. Alternatively, XANES and EXAFS are appropriate spectroscopies probing metal atoms in gas phase up to a few tens of bar or in liquid phase although it is lack of surface sensitivity.

To tackle this challenge, there are some possible approaches. Attenuated total reflection (ATR) spectroscopy could be used to track adsorbate of active site and measure the concentration of stable intermediates or products near to catalyst particles as long as the catalyst power can be immobilized on IGE crystal robustly.

Challenge in establishing a correlation between a catalytic performance and their corresponding chemical and coordination environments. DFT calculations have been a significant approach to provide understanding of catalytic mechanism at a molecular level. In most cases, a reaction pathway can be proposed and rate-determining step can be identified. A deep analysis of participations of orbitals of atoms of a catalytic site in transition states allows to propose a descriptor of catalyst structure at an atomic scale. Finding out the authentic chemical and coordination environments of atoms of a catalytic site responsible for the reported catalytic performance is a primary task before establishing a door-to-door structure-property intrinsic correlation. Unfortunately, this is a challenging task in fundamental studies of catalytic reaction performed at solid-liquid or solid-liquid-gas interface. A possible solution to tackle this challenge is to design a catalysis-XAS reaction system which can perform both catalytic oxidation of CH_4 on catalyst particles dispersed in liquid under high-pressure gas phase and XAS experiments during catalysis. We have designed a reactor for tracking catalyst nanoparticle dispersed in liquid at high temperature up to 350^{o}C under a gas phase with a pressure up to 50 bars by using XAS spectroscopy. Through modification of this type of reactor, a catalysis-XAS system could be developed, in which the liquid in the reaction cell can be periodically injected to HPLC for analysis in line.

Challenges in prompting catalytic selectivity for production of value-added chemical. In terms of transformation of CH_4 to high volume chemicals, by-products are observed due to different extents of catalytic oxidation. For instance, in most cases formic acid and CO_2 are produced upon the formation of ideal product, CH_3OH in catalytic oxidation of CH_4. One reason for formation of these by-products is that a deep oxidation is thermodynamically favourable compared to selective oxidation to form an idea product. Suppression of deep oxidation is a challenging task in obtaining selective oxidation of CH_4 to form CH_3OH. A possible solution is to add certain amount of scarifying agent to consume the extra oxidant, preventing CH_3OH from being further oxidized.

Challenges in achieving high yield of ideal product. Most of the yields of high-value chemicals such as CH_3OH, ethanol and acetic acid reported in literature are lower than 10%; typically, they are in the range of 0.1%-5%; many of them are in fact lower than 1%. From measurement point of view, low yield achieved under mild conditions could result in large

error bar in analysis of products. The limited yield results from several aspects. One is the limited density of active sites on a support. For example, the maximum number of Rh_1O_5 and Pd_1O_4 sites anchored to one gram of microporous aluminosilicate is limited by the slow diffusion of metal precursor in the micropore of zeolite. In addition, the thermodynamic at low temperature limits the potentially achievable conversion of CH_4. To increase conversion, separation of products from the liquid environment of reactants and catalyst could be a necessary step other than catalysis for gaining a high kinetics. More importantly, the low yield has been the bottleneck toward any potential production of value-added chemicals at large scale. So far, there has not been catalysts reported for production at large scale.

Challenges in fair comparison of catalytic activities among reported catalysts. Most references in literature reported catalytic performances in the unit of the number of μmol CH_3OH produced through catalysis by **1 gram** of a catalyst per hr although most of them never used 1 gram of a catalyst in their experiments. The reported number is typically 1-50 μmol CH_3OH formed on 1 gram of catalyst per hr. This is a value derived from the result of measurement like x μmol CH_3OH formed on y gram of catalyst. Again, in most case the weight of catalysts used in experiments is only 0.020-0.050 gram instead of 1.0 gram. Thus, the amount of measured CH_3OH from a sample is in fact in the range of 0.02-2.5 μmol of CH_3OH. If the volume of the solution used in test of NMR of other technique is 2 ml, the concentration of CH_3OH in water is only 0.46-57.5 ppm. However, most studies did not report the original concentration of ideal products in their solutions used for measurements with NMR, GC, mass spectrometer or other instrument. This makes evaluation of the uncertainty and reliability of measurements impossible. Error bar for quantitative analysis of a solute with a concentration of 0.46-57.5 ppm is in fact quite large for many analytical techniques. To have a fair comparison and a reasonable evaluation, it is necessary to provide concentration of methanol of the solution used for analysis. To reflect the accuracy of catalytic performances, it is suggested to include the following three pieces of information. (1) The concentration of the products in the solution used for measurements of NMR or other spectroscopies in each test sample and the mass of the catalyst in each patch should be reported simultaneously although the yield in μmol in one gram of catalyst can be reported as a supplementary message; (2) the amount of product in μmol in a blank experiment without using any catalyst must be reported; (3) the absolute error bar of each measurement of NMR, mass spectrometry, or other techniques must be reported.

15. Summary and prospect

Transformations of CH_4 to value-added chemicals under mild conditions have driven the development of significant new chemistries in activation of CH_4, oxidative transformation of CH_4, and catalytic oxidation of CH_4 to value-added chemicals through biocatalysis, molecular catalysis and heterogeneous catalysis. Significant progress in fundamental understanding of these chemistries at a molecular level has been achieved. Compared to extensively studied metal catalysis in the last several decades, the topic of transformation of CH_4 to oxygenates with high activity and selectivity under mild conditions is still at its incubation period although important achievements have been made. Due to the complexity in transformation chemistry of CH_4 under mild conditions, no catalysts and catalytic processes exhibit feasibility of production at a large scale. Future development of catalysts for catalytic transformations of CH_4 under mild conditions will definitely benefit from these insights achieved in the last two decades. The ultimate goal of transformation of CH_4 through catalysis under mild condition is to develop catalysts and CH_4-based catalytic processes which can replace the current high-temperature catalytic processes. To realize this goal, a library of durable, cost-effective catalysts with high activity and selectivity for formation of ideal products under mild conditions need to be developed.

Development of an efficient catalyst replies on fundamental understanding of the profound chemistry in the transformation of CH_4 to an ideal oxygenate. Such understanding has to be established on appropriate characterizations of active sites at an atomic scale during catalysis. Different from the exposure of catalytic sites on external surface of supported metal or oxide catalysts widely used under high temperature conditions, catalytic sites of many catalysts active for transformation of CH_4 under mild conditions are embedded in micropores at solid-liquid or solid-liquid-gas interfaces under high pressure of reactant gas. In contrast to catalysis performed at solid-gas interface at high temperature, transformations of CH_4 to ideal oxygenates under mild conditions have to be performed at solid-liquid or solid-liquid-gas interfaces since the catalysis temperatures under mild conditions are typically lower than boiling point of products such as methanol, formic acid, and acetic acid under high pressure of reactants . This feature of performing catalysis at solid-liquid or solid-liquid-gas interface under high pressure reactant gases makes characterisations of catalytic sites at atomic scale and during catalysis extremely challenging. In addition, how the existence of solvent molecules around catalyst particles could influence the catalytic activity and selectivity in transformation of CH_4 is an important issue to address. In addition, the lack of kinetic studies of the catalysis

performed at a solid-liquid or solid-liquid-gas interface could have limited our understanding of the catalytic process since molecular diffusion of CH_4 in liquid phase could limit the production of oxygenate and the diffusion of products formed at solid-liquid interface could limit reaction kinetics. Furthermore, compared to the lack of loss of metal atoms of a catalyst while a catalyst is at high temperature in gas phase, another complicated factor is the instability of catalysts resulting from leaching of metal atoms of a catalyst in acidic aqueous solution. Overall, these factors have largely impeded the accomplishment of profound understanding of these catalytical reactions under mild conditions.

Computational studies have been a quite valuable approach in achieving understanding of these low-temperature catalytic processes of CH_4 transformation. Intermolecular interactions, particularly the interactions among reactants in confined space at sub-nanometer scale in micropores, the interaction between reactant molecules and wall of micropores, and interaction between reactants and solvent in confined space, and even interaction between products and solvents, must be considered into computational studies toward proposing the pathway reflecting actual reaction path at a molecular level.

Many characterization techniques of catalysts appropriate for catalysis performed at solid-gas interfaces may not be applicable to low-temperature catalysis at solid-liquid or solid-liquid-gas interface under high pressure gas phase. Development of characterization methods congruous with the catalytic condition of CH_4 transformation under mild conditions is expected to be significant. Due to these challenges, it is expected that continuous endeavours of a couple of decades could be necessary for design of catalysts and development of catalytic processes for transformation of CH_4 to important intermediate compounds or value-added chemicals under mild conditions at a large scale.

16. Acknowledgments

The contribution of Yuting Li and Franklin Tao to this work was supported by the Chemical Catalysis Program of Division of Chemistry, National Science Foundation (NSF Career Award) with project no. NSF-CHE-1462121 and the Catalysis Science Program of the Chemical Sciences, Geosciences and Biosciences Division, Office of Basic Energy Sciences, Office of Science, U.S. Department of Energy under Grant No. DE-SC0014561, and National Science Foundation under the grant No. NSF-OIA 1539105. This review article does not carry on any intellectual properties from institutions of authors. All information reviewed in this article is knowledge and insights of fundamental understanding of catalytic reaction

mechanism published in literature instead of information of any potential applications to any industries.

References

1. D. Pakhare and J. Spivey, *Chemical Society Reviews*, 2014, **43**, 7813-7837.
2. T. V. Choudhary and V. R. Choudhary, *Angewandte Chemie-International Edition*, 2008, **47**, 1828-1847.
3. A. Y. Khodakov, W. Chu and P. Fongarland, *Chemical Reviews*, 2007, **107**, 1692-1744.
4. E. de Smit and B. M. Weckhuysen, *Chemical Society Reviews*, 2008, **37**, 2758-2781.
5. W. Zhou, K. Cheng, J. Kang, C. Zhou, V. Subramanian, Q. Zhang and Y. Wang, *Chemical Society Reviews*, 2019, **48**, 3193-3228.
6. W. Chen, Z. L. Fan, X. L. Pan and X. H. Bao, *J. Am. Chem. Soc.*, 2008, **130**, 9414-9419.
7. Y. Zhu, Y. Ye, S. Zhang, M. E. Leong and F. Tao, *Langmuir*, 2012, **28**, 8275-8280.
8. K. Xu, B. Sun, J. Lin, W. Wen, Y. Pei, S. Yan, M. Qiao, X. Zhang and B. Zong, *Nature Communications*, 2014, **5**, 5783.
9. X. Pan, Z. Fan, W. Chen, Y. Ding, H. Luo and X. Bao, *Nature Materials*, 2007, **6**, 507-511.
10. F. Jiao, J. Li, X. Pan, J. Xiao, H. Li, H. Ma, M. Wei, Y. Pan, Z. Zhou, M. Li, S. Miao, J. Li, Y. Zhu, D. Xiao, T. He, J. Yang, F. Qi, Q. Fu and X. Bao, *Science*, 2016, **351**, 1065-1068.
11. J. P. den Breejen, P. B. Radstake, G. L. Bezemer, J. H. Bitter, V. Froseth, A. Holmen and K. P. de Jong, *J. Am. Chem. Soc.*, 2009, **131**, 7197-7203.
12. R. Liu, R. Liu, X. Ma, B. H. Davis and Z. Li, *Fuel*, 2018, **211**, 827-836.
13. P. Zhai, C. Xu, R. Gao, X. Liu, M. Li, W. Li, X. Fu, C. Jia, J. Xie, M. Zhao, X. Wang, Y.-W. Li, Q. Zhang, X.-D. Wen and D. Ma, *Angewandte Chemie-International Edition*, 2016, **55**, 9902-9907.
14. B. Zhao, P. Zhai, P. Wang, J. Li, T. Li, M. Peng, M. Zhao, G. Hu, Y. Yang, Y.-W. Li, Q. Zhang, W. Fan and D. Ma, *Chem*, 2017, **3**, 323-333.
15. C. Yang, H. Zhao, Y. Hou and D. Ma, *J. Am. Chem. Soc.*, 2012, **134**, 15814-15821.
16. H. M. T. Galvis and K. P. de Jong, *ACS Catalysis*, 2013, **3**, 2130-2149.
17. H. M. T. Galvis, J. H. Bitter, C. B. Khare, M. Ruitenbeek, A. I. Dugulan and K. P. de Jong, *Science*, 2012, **335**, 835-838.
18. J. Wei, Q. Ge, R. Yao, Z. Wen, C. Fang, L. Guo, H. Xu and J. Sun, *Nature Communications*, 2017, **8**, 15174.
19. H. T. Luk, C. Mondelli, D. C. Ferre, J. A. Stewart and J. Perez-Ramirez, *Chemical Society Reviews*, 2017, **46**, 1358-1426.
20. L. Zhong, F. Yu, Y. An, Y. Zhao, Y. Sun, Z. Li, T. Lin, Y. Lin, X. Qi, Y. Dai, L. Gu, J. Hu, S. Jin, Q. Shen and H. Wang, *Nature*, 2016, **538**, 84-87.
21. Y. Chen, B. deGlee, Y. Tang, Z. Wang, B. Zhao, Y. Wei, L. Zhang, S. Yoo, K. Pei, J. H. Kim, Y. Ding, P. Hu, F. F. Tao and M. Liu, *Nature Energy*, 2018, **3**, 1042-1050.
22. C.-j. Liu, J. Ye, J. Jiang and Y. Pan, *Chemcatchem*, 2011, **3**, 529-541.
23. A. Iulianelli, S. Liguori, J. Wilcox and A. Basile, *Catalysis Reviews-Science and Engineering*, 2016, **58**, 1-35.
24. D. A. J. M. Ligthart, R. A. van Santen and E. J. M. Hensen, *Journal of Catalysis*, 2011, **280**, 206-220.
25. L. Barelli, G. Bidini, F. Gallorini and S. Servili, *Energy*, 2008, **33**, 554-570.
26. Y. Tang, Y. Wei, Z. Wang, S. Zhang, Y. Li, L. Nguyen, Y. Li, Y. Zhou, W. Shen, F. F. Tao and P. Hu, *J. Am. Chem. Soc.*, 2019, **141**, 7283-7293.
27. N. A. K. Aramouni, J. G. Touma, B. Abu Tarboush, J. Zeaiter and M. N. Ahmad, *Renewable & Sustainable Energy Reviews*, 2018, **82**, 2570-2585.
28. L. C. Buelens, V. V. Galvita, H. Poelman, C. Detavernier and G. B. Marin, *Science*, 2016, **354**, 449-452.
29. Z. Liu, D. C. Grinter, P. G. Lustemberg, N.-P. Thuy-Duong, Y. Zhou, S. Luo, I. Waluyo, E. J. Crumlin, D. J. Stacchiola, J. Zhou, J. Carrasco, H. F. Busnengo, M. Veronica Ganduglia-Pirovano, S. D. Senanayake and J. A. Rodriguez, *Angewandte Chemie-International Edition*, 2016, **55**, 7455-7459.
30. M. Akri, S. Zhao, X. Li, K. Zang, A. F. Lee, M. A. Isaacs, W. Xi, Y. Gangarajula, J. Luo, Y. Ren, Y.-T. Cui, L. Li, Y. Su, X. Pan, W. Wen, Y. Pan, K. Wilson, L. Li, B. Qiao, H. Ishii, Y.-F. Liao, A. Wang, X. Wang and T. Zhang, *Nature Communications*, 2019, **10**, 5181.
31. Z. Wang, X. M. Cao, J. Zhu and P. Hu, *Journal of Catalysis*, 2014, **311**, 469-480.
32. Y. H. Hu and E. Ruckenstein, *Science*, 2020, **368**.
33. Y. Song, E. Ozdemir, S. Ramesh, A. Adishev, S. Subramanian, A. Harale, M. Albuali, B. A. Fadhel, A. Jamal, D. Moon, S. H. Choi and C. T. Yavuz, *Science*, 2020, **367**, 777-781.
34. T. Margossian, K. Larmier, S. M. Kim, F. Krumeich, A. Fedorov, P. Chen, C. R. Muller and C. Coperet,

J. Am. Chem. Soc., 2017, **139**, 6919-6927.
35. J. Dong, Q. Fu, H. Li, J. Xiao, B. Yang, B. Zhang, Y. Bai, T. Song, R. Zhang, L. Gao, J. Cai, H. Zhang, Z. Liu and X. Bao, *J. Am. Chem. Soc.*, 2020, **142**, 17167-17174.
36. Z. Xie, B. Yan, S. Kattel, J. H. Lee, S. Yao, Q. Wu, N. Rui, E. Gomez, Z. Liu, W. Xu, L. Zhang and J. G. Chen, *Applied Catalysis B-Environmental*, 2018, **236**, 280-293.
37. Y. H. Hu and E. Ruckenstein, *Industrial & Engineering Chemistry Research*, 1998, **37**, 2333-2335.
38. E. Ruckenstein and Y. H. Hul, *Applied Catalysis A: General*, 1999, **183**, 85-92.
39. S. Liu, G. Xiong, H. Dong, W. Yang, S. Sheng, W. Chu and Z. Yu, *Studies in Surface Science and Catalysis*, 2000, **130**, 3567-3572.
40. S. Sengodan, R. Lan, J. Humphreys, D. Du, W. Xu, H. Wang and S. Tao, *Renewable & Sustainable Energy Reviews*, 2018, **82**, 761-780.
41. A. H. Elbadawi, L. Ge, Z. Li, S. Liu, S. Wang and Z. Zhu, *Catalysis Reviews*, 2021, **63**, 1-67.
42. G. Pauletto, N. Libretto, D. C. Boffito, J. T. Miller, A. Jentys, G. S. Patience and J. A. Lercher, *Applied Catalysis B: Environmental*, 2021, **286**, 119849.
43. A. M. Arinaga, M. C. Ziegelski and T. J. Marks, *Angewandte Chemie-International Edition*, 2021, **60**, 10502-10515.
44. S. Liu, S. Udyavara, C. Zhang, M. Peter, T. L. Lohr, V. P. Dravid, M. Neurock and T. J. Marks, *Proceedings of the National Academy of Sciences*, 2021, **118**, e2012666118.
45. S. Zou, Z. Li, Q. Zhou, Y. Pan, W. Yuan, L. He, S. Wang, W. Wen, J. Liu, Y. Wang, Y. Du, J. Yang, L. Xiao, H. Kobayashi and J. Fan, *Chinese Journal of Catalysis*, 2021, **42**, 1117-1125.
46. P. Wang, G. Zhao, Y. Wang and Y. Lu, *Science Advances*, 2017, **3**, e1603180.
47. K. Takanabe, A. M. Khan, Y. Tang, L. Nguyen, A. Ziani, B. W. Jacobs, A. M. Elbaz, S. M. Sarathy and F. Tao, *Angewandte Chemie-International Edition*, 2017, **56**, 10403-10407.
48. F. F. Tao, J. J. Shan, L. Nguyen, Z. Y. Wang, S. R. Zhang, L. Zhang, Z. L. Wu, W. X. Huang, S. B. Zeng and P. Hu, *Nature Communications*, 2015, **6**, 7798.
49. S. Zhang, J. Shan, L. Nie, L. Nguyen, Z. Wu and F. F. Tao, *Surface Science*, 2016, **648**, 156-162.
50. Y.-H. Chin, C. Buda, M. Neurock and E. Iglesia, *J. Am. Chem. Soc.*, 2011, **133**, 15958-15978.
51. Y.-H. Chin, C. Buda, M. Neurock and E. Iglesia, *J. Am. Chem. Soc.*, 2013, **135**, 15425-15442.
52. M. Cargnello, J. J. Delgado Jaen, J. C. Hernandez Garrido, K. Bakhmutsky, T. Montini, J. J. Calvino Gamez, R. J. Gorte and P. Fornasiero, *Science*, 2012, **337**, 713-717.
53. L. Luo, X. Tang, W. Wang, Y. Wang, S. Sun, F. Qi and W. Huang, *Scientific Reports*, 2013, **3**, 1625
54. Y. Gao, J. Bu, Z. Peng and B. Yang, *Journal of Spectroscopy*, 2014, **2014**, 1-10.
55. X. Guo, G. Fang, G. Li, H. Ma, H. Fan, L. Yu, C. Ma, X. Wu, D. Deng and M. Wei, *Science*, 2014, **344**, 616-619.
56. D. C. Upham, V. Agarwal, A. Khechfe, Z. R. Snodgrass, M. J. Gordon, H. Metiu and E. W. McFarland, *Science*, 2017, **358**, 917-920.
57. Y. Q. Su, J. X. Liu, I. A. W. Filot, L. Zhang and E. J. M. Hensen, *ACS Catalysis*, 2018, **8**, 6552-6559.
58. J. R. Zeng, M. Tarazkar, T. Pennebaker, M. J. Gordon, H. Metiu and E. W. McFarland, *ACS Catalysis*, 2020, **10**, 8223-8230.
59. C. Palmer, D. C. Upham, S. Smart, M. J. Gordon, H. Metiu and E. W. McFarland, *Nat. Catal.*, 2020, **3**, 83-89.
60. P. Tomkins, M. Ranocchiari and J. A. van Bokhoven, *Accounts of Chemical Research*, 2017, **50**, 418-425.
61. M. Ravi, M. Ranocchiari and J. A. van Bokhoven, *Angewandte Chemie-International Edition*, 2017, **56**, 16464-16483.
62. M. A. Newton, A. J. Knorpp, V. L. Sushkevich, D. Palagin and J. A. van Bokhoven, *Chemical Society Reviews*, 2020, **49**, 1449-1486.
63. P. Del Campo, C. Martinez and A. Corma, *Chemical Society Reviews*, 2021, **50**, 8511-8595.
64. P. Schwach, X. Pan and X. Bao, *Chemical Reviews*, 2017, **117**, 8497-8520.
65. Alexander, E., Shilov, Georgiy, B. and Shul'pin, *Chemical Reviews*, 1997, **97**, 2879-2932.
66. J. W. M. H. Geerts, J. H. B. J. Hoebink and K. V. D. Wiele, *Catalysis Today*, 1990, **6**, 613-620.
67. G. A. Somorjai and Y. Li, *Introduction to surface chemistry and catalysis*, John Wiley & Sons, 2010.
68. S. Zhang, X.-S. Li, B. Chen, X. Zhu, C. Shi and A.-M. Zhu, *ACS Catalysis*, 2014, **4**, 3481-3489.
69. K. Paredis, L. K. Ono, F. Behafarid, Z. Zhang, J. C. Yang, A. I. Frenkel and B. Roldan Cuenya, *J. Am. Chem. Soc.*, 2011, **133**, 13455-13464.
70. Z. Liang, T. Li, M. Kim, A. Asthagiri and J. F. Weaver, *Science*, 2017, **356**, 298-301.
71. D. Schröder and H. Schwarz, *Angewandte Chemie International Edition*, 1990, **29**, 1433-1434.
72. Y.-M. Chen, D. Clemmer and P. Armentrout, *J. Am. Chem. Soc.*, 1994, **116**, 7815-7826.
73. D. Schröder and H. Schwarz, *Angewandte Chemie International Edition*, 1995, **34**, 1973-1995.
74. M. F. Ryan, A. Fiedler, D. Schroeder and H. Schwarz, *J. Am. Chem. Soc.*, 1995, **117**, 2033-2040.

75. J. Hagen, *Industrial catalysis: a practical approach*, John Wiley & Sons, 2015.
76. F. Tao and M. Salmeron, *Science*, 2011, **331**, 171-174.
77. F. Tao and P. A. Crozier, *Chemical Reviews*, 2016, **116**, 3487-3539.
78. L. Nguyen, F. F. Tao, Y. Tang, J. Doug and X.-J. Bao, *Chemical Reviews*, 2019, **119**, 6822-6905.
79. J. Dou, Z. Sun, A. A. Opalade, N. Wang, W. Fu and F. Tao, *Chemical Society Reviews*, 2017, **46**, 2001-2027.
80. S. Zhang, N. Luan, Y. Zhu, S. Zhan, C.-K. Tsung and F. Tao, *Accounts of Chemical Research*, 2013, **46**, 1731-1739.
81. F. Tao, S. Zhang, N. Luan and X. Zhang, *Chemical Society Reviews*, 2012, **41**, 7980-7993.
82. J. Timoshenko and B. R. Cuenya, *Chemical Reviews*, 2021, **121**, 882-961.
83. D. E. Sayers, E. A. Stern and F. W. Lytle, *Physical Review Letters*, 1971, **27**, 1204.
84. F. Lytle, P. Wei, R. Greegor, G. Via and J. Sinfelt, *The Journal of Chemical Physics*, 1979, **70**, 4849-4855.
85. F. Lytle, G. Via and J. Sinfelt, *The Journal of Chemical Physics*, 1977, **67**, 3831-3832.
86. F. Lytle, G. Via and J. Sinfelt, in *Synchrotron Radiation Research*, Springer, 1980, pp. 401-424.
87. J. H. Sinfelt, *Reviews of Modern Physics*, 1979, **51**, 569.
88. S. Bordiga, E. Groppo, G. Agostini, J. A. van Bokhoven and C. Lamberti, *Chemical Reviews*, 2013, **113**, 1736-1850.
89. I. Ogino, *Chinese Journal of Catalysis*, 2017, **38**, 1481-1488.
90. Y. Iwasawa, K. Asakura and M. Tada, *XAFS techniques for catalysts, nanomaterials, and surfaces*, Springer, 2017.
91. X. Li, X. Yang, J. Zhang, Y. Huang and B. Liu, *ACS Catalysis*, 2019, **9**, 2521-2531.
92. J. Singh, C. Lamberti and J. A. van Bokhoven, *Chemical Society Reviews*, 2010, **39**, 4754-4766.
93. I. Yasuhiro, *X-ray absorption fine structure for catalysts and surfaces*, World Scientific, 1996.
94. J. Sá, *High-resolution XAS/XES: analyzing electronic structures of catalysts*, CRC Press, 2014.
95. J. A. Van Bokhoven and C. Lamberti, *X-ray absorption and X-ray emission spectroscopy: theory and applications*, John Wiley & Sons, 2016.
96. J. Stöhr, *NEXAFS spectroscopy*, Springer Science & Business Media, 2013.
97. H. Kuroda, T. Yokoyama, K. Asakura and Y. Iwasawa, *Faraday Discussions*, 1991, **92**, 189-198.
98. M. W. Small, S. I. Sanchez, N. S. Marinkovic, A. I. Frenkel and R. G. Nuzzo, *ACS Nano*, 2012, **6**, 5583-5595.
99. A. Frenkel and J. Rehr, *Physical Review B*, 1993, **48**, 585.
100. N. Weiher, E. Bus, B. Gorzolnik, M. Möller, R. Prins and J. A. Van Bokhoven, *Journal of Synchrotron Radiation*, 2005, **12**, 675-679.
101. L. Nguyen, Y. Tang, Y. Li, X. Zhang, D. Wang and F. Tao, *Review of Scientific Instruments*, 2018, **89**, 054103.
102. Y. Li, D. Zakharov, S. Zhao, R. Tappero, U. Jung, A. Elsen, P. Baumann, R. G. Nuzzo, E. A. Stach and A. I. Frenkel, *Nature Communications*, 2015, **6**, 7583.
103. P. T. Kristiansen, T. C. R. Rocha, A. Knop-Gericke, J. H. Guo and L. C. Duda, *Review of Scientific Instruments*, 2013, **84**, 113107
104. J. D. Grunwaldt, M. Caravati, S. Hannemann and A. Baiker, *Physical Chemistry Chemical Physics*, 2004, **6**, 3037-3047.
105. I. Pettiti, D. Gazzoli, M. Inversi, M. Valigi, S. De Rossi, G. Ferraris, P. Porta and S. Colonna, *Journal of Synchrotron Radiation*, 1999, **6**, 1120-1124.
106. A. T. Bell, *NMR techniques in catalysis*, CRC Press, 2020.
107. A. A. Lysova and I. V. Koptyug, *Chemical Society Reviews*, 2010, **39**, 4585-4601.
108. W. Zhang, S. Xu, X. Han and X. Bao, *Chemical Society Reviews*, 2012, **41**, 192-210.
109. W. Zhang, D. Ma, X. Liu, X. Liu and X. Bao, *Chemical Communications*, 1999, 1091-1092.
110. J. F. Haw, P. W. Goguen, X. Teng, T. W. Skloss and Z. Wang, *Angewandte Chemie International Edition*, 1998, **37**, 948-949.
111. X. Teng, D. H. Barich, P. W. Goguen, W. Song and J. F. Haw, *J. Am. Chem. Soc.*, 1998, **120**, 4025-4026.
112. J. F. Haw, J. B. Nicholas, W. Song, F. Deng, Z. Wang, T. Xu and C. S. Heneghan, *J. Am. Chem. Soc.*, 2000, **122**, 4763-4775.
113. D. M. McCann, D. Lesthaeghe, P. W. Kletnieks, D. R. Guenther, M. J. Hayman, V. Van Speybroeck, M. Waroquier and J. F. Haw, *Angewandte Chemie International Edition*, 2008, **47**, 5179-5182.
114. M. Xu, K. D. Harris, J. M. Thomas and D. E. Vaughan, *ChemPhysChem*, 2007, **8**, 1311-1313.
115. P. Goguen and J. F. Haw, *Journal of Catalysis*, 1996, **161**, 870-872.
116. M. Hunger, M. Seiler and T. Horvath, *Catalysis Letters*, 1999, **57**, 199-204.
117. J. F. Haw, *Topics in Catalysis*, 1999, **8**, 81-86.
118. G. W. Haddix, A. T. Bell and J. A. Reimer, *Journal of Physical Chemistry*, 1989, **93**, 5859-5865.

119. M. S. Went and J. A. Reimer, *J. Am. Chem. Soc.*, 1992, **114**, 5768-5775.
120. A. Bendada, G. Chinchen, N. Clayden, B. Heaton, J. Iggo and C. Smith, *Catalysis Today*, 1991, **9**, 129-136.
121. M. Hunger and T. Horvath, *Journal of the Chemical Society, Chemical Communications*, 1995, 1423-1424.
122. C. Keeler, J. Xiong, H. Lock, S. Dec, T. Tao and G. E. Maciel, *Catalysis Today*, 1999, **49**, 377-383.
123. L. Baltusis, J. S. Frye and G. E. Maciel, *J. Am. Chem. Soc.*, 1986, **108**, 7119-7120.
124. E. F. Rakiewicz, A. W. Peters, R. F. Wormsbecher, K. J. Sutovich and K. T. Mueller, *Journal of Physical Chemistry B*, 1998, **102**, 2890-2896.
125. P. J. Giammatteo, W. W. Hellmuth, F. G. Ticehurst and P. W. Cope, *Journal of Magnetic Resonance*, 1987, **71**, 147-150.
126. W. Zhang, X. Han, X. Liu and X. Bao, *Journal of Molecular Catalysis A: Chemical*, 2003, **194**, 107-113.
127. J. Zhuang, D. Ma, Z. Yan, F. Deng, X. Liu, X. Han, X. Bao, X. W. Liu, X. Guo and X. Wang, *Journal of Catalysis*, 2004, **221**, 670-673.
128. D. Ma, Y. Shu, W. Zhang, X. Han, Y. Xu and X. Bao, *Angewandte Chemie International Edition*, 2000, **39**, 2928-2931.
129. W. Zhang, D. Ma, X. Han, X. Liu, X. Bao, X. Guo and X. Wang, *Journal of Catalysis*, 1999, **188**, 393-402.
130. K. J. Sutovich, A. W. Peters, E. F. Rakiewicz, R. F. Wormsbecher, S. M. Mattingly and K. T. Mueller, *Journal of Catalysis*, 1999, **183**, 155-158.
131. L. Wang, L. Tao, M. Xie, G. Xu, J. Huang and Y. Xu, *Catalysis Letters*, 1993, **21**, 35-41.
132. H. Zheng, D. Ma, X. Bao, J. Z. Hu, J. H. Kwak, Y. Wang and C. H. Peden, *J. Am. Chem. Soc.*, 2008, **130**, 3722-3723.
133. J. Z. Hu, J. H. Kwak, Y. Wang, C. H. Peden, H. Zheng, D. Ma and X. Bao, *Journal of Physical Chemistry C*, 2009, **113**, 2936-2942.
134. S. Xu, W. Zhang, X. Liu, X. Han and X. Bao, *J. Am. Chem. Soc.*, 2009, **131**, 13722-13727.
135. J. Weitkamp and S. Maixner, *Zeolites*, 1987, **7**, 6-8.
136. J. L. White, N. D. Lazo, B. R. Richardson and J. F. Haw, *Journal of Catalysis*, 1990, **125**, 260-263.
137. J. Huang, Y. Jiang, V. R. Marthala, Y. S. Ooi and M. Hunger, *ChemPhysChem*, 2008, **9**, 1107-1109.
138. M. Xu, W. Wang and M. Hunger, *Chemical Communications*, 2003, 722-723.
139. T. Bürgi and A. Baiker, *Advances in Catalysis*, 2006, **50**, 227-283.
140. J. Ryczkowski, *Catalysis Today*, 2001, **68**, 263-381.
141. T. Bürgi, R. Wirz and A. Baiker, *Journal of Physical Chemistry B*, 2003, **107**, 6774-6781.
142. J. A. Lercher, V. Veefkind and K. Fajerwerg, *Vibrational spectroscopy*, 1999, **19**, 107-121.
143. A. Vimont, F. Thibault-Starzyk and M. Daturi, *Chemical Society Reviews*, 2010, **39**, 4928-4950.
144. G. L. Chiarello, M. Nachtegaal, V. Marchionni, L. Quaroni and D. Ferri, *Review of Scientific Instruments*, 2014, **85**, 074102
145. M. S. Schneider, J. D. Grunwaldt, T. Burgi and A. Baiker, *Review of Scientific Instruments*, 2003, **74**, 4121-4128.
146. J.-M. Andanson and A. Baiker, *Chemical Society Reviews*, 2010, **39**, 4571-4584.
147. C. Lamberti, A. Zecchina, E. Groppo and S. Bordiga, *Chemical Society Reviews*, 2010, **39**, 4951-5001.
148. B. L. Mojet, S. D. Ebbesen and L. Lefferts, *Chemical Society Reviews*, 2010, **39**, 4643-4655.
149. F. Zaera, *Chemical Society Reviews*, 2014, **43**, 7624-7663.
150. P. A. Jacobs and R. A. van Santen, *Zeolites: facts, figures, future*, Elsevier, 1989.
151. E. Stavitski and B. M. Weckhuysen, *Chemical Society Reviews*, 2010, **39**, 4615-4625.
152. M. Nowotny, J. A. Lercher and H. Kessler, *Zeolites*, 1991, **11**, 454-459.
153. M. H. F. Kox, K. F. Domke, J. P. R. Day, G. Rago, E. Stavitski, M. Bonn and B. M. Weckhuysen, *Angewandte Chemie-International Edition*, 2009, **48**, 8990-8994.
154. J. Melsheimer and R. Schlogl, *Berichte Der Bunsen-Gesellschaft-Physical Chemistry Chemical Physics*, 1997, **101**, 733-740.
155. J. Melsheimer and R. Schlogl, *Fresenius Journal of Analytical Chemistry*, 1997, **357**, 397-400.
156. X. T. Gao, J. M. Jehng and I. E. Wachs, *Journal of Catalysis*, 2002, **209**, 43-50.
157. L. J. Burcham, G. Deo, X. T. Gao and I. E. Wachs, *Topics in Catalysis*, 2000, **11**, 85-100.
158. E. V. Kondratenko and M. Baerns, *Applied Catalysis A: General*, 2001, **222**, 133-143.
159. A. Bruckner, *Applied Catalysis A: General*, 2000, **200**, 287-297.
160. M. D. Argyle, K. D. Chen, C. Resini, C. Krebs, A. T. Bell and E. Iglesia, *Chemical Communications*, 2003, DOI: 10.1039/b305264h, 2082-2083.
161. M. D. Argyle, K. D. Chen, C. Resini, C. Krebs, A. T. Bell and E. Iglesia, *Journal of Physical Chemistry B*, 2004, **108**, 2345-2353.

162. A. Bruckner and E. Kondratenko, *Catalysis Today*, 2006, **113**, 16-24.
163. J. Q. Lu, J. J. Bravo-Suarez, A. Takahashi, M. Haruta and S. T. Oyama, *Journal of Catalysis*, 2005, **232**, 85-95.
164. B. F. Sels, D. E. De Vos, P. J. Grobet and P. A. Jacobs, *Chemistry-A European Journal*, 2001, **7**, 2547-2556.
165. M. Schwidder, W. Grunert, U. Bentrup and A. Bruckner, *Journal of Catalysis*, 2006, **239**, 173-186.
166. T. A. Nijhuis, S. J. Tinnemans, T. Visser and B. M. Weckhuysen, *Chemical Engineering Science*, 2004, **59**, 5487-5492.
167. T. X. Nijhuis, S. J. Tinnemans, T. Visser and B. M. Weckhuysen, *Physical Chemistry Chemical Physics*, 2003, **5**, 4361-4365.
168. F. C. Jentoft, in *Advances in Catalysis*, eds. B. C. Gates and H. Knozinger, 2009, vol. 52, pp. 129-211.
169. B. M. Weckhuysen and R. A. Schoonheydt, *Catalysis Today*, 1999, **49**, 441-451.
170. B. M. Weckhuysen, P. Voort and G. Catana, *Spectroscopy of transition metal ions on surfaces*, Leuven University Press, 2000.
171. B. M. Weckhuysen, A. A. Verberckmoes, J. Debaere, K. Ooms, I. Langhans and R. A. Schoonheydt, *Journal of Molecular Catalysis A: Chemical*, 2000, **151**, 115-131.
172. B. M. Weckhuysen, D. Baetens and R. A. Schoonheydt, *Angewandte Chemie-International Edition*, 2000, **39**, 3419-3422.
173. B. M. Weckhuysen, A. Bensalem and R. A. Schoonheydt, *Journal of the Chemical Society-Faraday Transactions*, 1998, **94**, 2011-2014.
174. S. Tinnemans, M. Kox, T. Nijhuis, T. Visser and B. Weckhuysen, *Physical Chemistry Chemical Physics*, 2005, **7**, 211-216.
175. S. Kuba, P. Lukinskas, R. Ahmad, F. C. Jentoft, R. K. Grasselli, B. C. Gates and H. Knözinger, *Journal of Catalysis*, 2003, **219**, 376-388.
176. F. C. Jentoft, *Advances in catalysis*, 2009, **52**, 129-211.
177. L. G. van de Water, J. A. Bergwerff, G. Leliveld, B. M. Weckhuysen and K. P. de Jong, *Journal of Physical Chemistry B*, 2005, **109**, 14513-14522.
178. L. G. van de Water, J. A. Bergwerff, T. A. Nijhuis, K. P. de Jong and B. M. Weckhuysen, *J. Am. Chem. Soc.*, 2005, **127**, 5024-5025.
179. U. Bentrup, A. Brückner, C. Rüdinger and H.-J. Eberle, *Applied Catalysis A: General*, 2004, **269**, 237-248.
180. D. G. Barton, M. Shtein, R. D. Wilson, S. L. Soled and E. Iglesia, *Journal of Physical Chemistry B*, 1999, **103**, 630-640.
181. M. Salmeron and R. Schlogl, *Surface Science Reports*, 2008, **63**, 169-199.
182. D. E. Starr, Z. Liu, M. Haevecker, A. Knop-Gericke and H. Bluhm, *Chemical Society Reviews*, 2013, **42**, 5833-5857.
183. Y. Han, H. Zhang, Y. Yu and Z. Liu, *ACS Catalysis*, 2021, **11**, 1464-1484.
184. F. Tao, *Chemical Communications*, 2012, **48**, 3812-3814.
185. Y. Takagi, T. Uruga, M. Tada, Y. Iwasawa and T. Yokoyama, *Accounts of Chemical Research*, 2018, **51**, 719-727.
186. A. Kolmakov, D. A. Dikin, L. J. Cote, J. Huang, M. K. Abyaneh, M. Amati, L. Gregoratti, S. Guenther and M. Kiskinova, *Nature Nanotechnology*, 2011, **6**, 651-657.
187. N. Luan, P. Tao, H. Liu, M. Al-Hada, M. Amati, H. Sezen, Y. Tang, L. Gregoratti and F. Tao, *Chemical Communications*, 2018, **54**, 9981-9984.
188. L. Nguyen, P. P. Tao, H. Liu, M. Al-Hada, M. Amati, H. Sezen, L. Gregoratti, Y. Tang, S. D. House and F. F. Tao, *Langmuir*, 2018, **34**, 9606-9616.
189. K. Ding, A. Gulec, A. M. Johnson, N. M. Schweitzer, G. D. Stucky, L. D. Marks and P. C. Stair, *Science*, 2015, **350**, 189-192.
190. M. A. Culpepper and A. C. Rosenzweig, *Critical Reviews in Biochemistry and Molecular Biology*, 2012, **47**, 483-492.
191. H. J. Kim, J. Huh, Y. W. Kwon, D. Park, Y. Yu, Y. E. Jang, B. R. Lee, E. Jo, E. J. Lee, Y. Heo, W. Lee and J. Lee, *Nat. Catal.*, 2019, **2**, 342-353.
192. N. R. Hunter, H. D. Gesser, L. A. Morton, P. S. Yarlagadda and D. P. C. Fung, *Applied Catalysis*, 1990, **57**, 45-54.
193. G. Ljunger, P. Adlercreutz and B. Mattiasson, *Biocatalysis*, 1993, **7**, 279-288.
194. M. Urrutigoity and J. Souppe, *Biocatalysis*, 1989, **2**, 145-149.
195. Z. Gou, X.-H. Xing, M. Luo, H. Jiang, B. Han, H. Wu, L. Wang and F. Zhang, *FEMS microbiology letters*, 2006, **263**, 136-141.
196. R. L. Lieberman and A. C. Rosenzweig, *Critical Reviews in Biochemistry and Molecular Biology*, 2004, **39**, 147-164.

197. I. McDonald, H. Uchiyama, S. Kambe, O. Yagi and J. Murrell, *Applied and Environmental Microbiology*, 1997, **63**, 1898-1904.
198. J. Green and H. Dalton, *Journal of Biological Chemistry*, 1985, **260**, 5795-5801.
199. D. Park and J. Lee, *Korean Journal of Chemical Engineering*, 2013, **30**, 977-987.
200. S. Friedle, E. Reisner and S. J. Lippard, *Chemical Society Reviews*, 2010, **39**, 2768-2779.
201. B. Fox, W. Froland, J. Dege and J. Lipscomb, *Journal of Biological Chemistry*, 1989, **264**, 10023-10033.
202. C. E. Tinberg and S. J. Lippard, *Accounts of Chemical Research*, 2011, **44**, 280-288.
203. H. Dalton, in *Advances in Applied Microbiology*, Elsevier, 1980, vol. 26, pp. 71-87.
204. J. Lund, M. P. Woodland and H. Dalton, *European Journal of Biochemistry*, 1985, **147**, 297-305.
205. J. Colby and H. Dalton, *The Biochemical journal*, 1978, **171**, 461-468.
206. J. Colby and H. Dalton, *The Biochemical journal*, 1979, **177**, 903-908.
207. M. P. Woodland and H. Dalton, *Journal of Biological Chemistry*, 1984, **259**, 53-59.
208. R. Balasubramanian and A. C. Rosenzweig, *Accounts of Chemical Research*, 2007, **40**, 573-580.
209. S. I. Chan and S. S.-F. Yu, *Accounts of Chemical Research*, 2008, **41**, 969-979.
210. A. S. Hakemian and A. C. Rosenzweig, *Annual Review of Biochemistry*, 2007, **76**, 223-241.
211. R. L. Lieberman and A. C. Rosenzweig, *Nature*, 2005, **434**, 177-182.
212. K.-Y. Ng, L.-C. Tu, Y.-S. Wang, S. I. Chan and S. S. F. Yu, *Chembiochem*, 2008, **9**, 1116-1123.
213. S. S. F. Yu, L. Y. Wu, K. H. C. Chen, W. I. Luo, D. S. Huang and S. I. Chan, *Journal of Biological Chemistry*, 2003, **278**, 40658-40669.
214. B. Wilkinson, M. Zhu, N. D. Priestley, H. H. T. Nguyen, H. Morimoto, P. G. Williams, S. I. Chan and H. G. Floss, *J. Am. Chem. Soc.*, 1996, **118**, 921-922.
215. P. P. Y. Chen and S. I. Chan, *Journal of Inorganic Biochemistry*, 2006, **100**, 801-809.
216. K. Yoshizawa and Y. Shiota, *J. Am. Chem. Soc.*, 2006, **128**, 9873-9881.
217. S. I. Chan, V. C. C. Wang, J. C. H. Lai, S. S. F. Yu, P. P. Y. Chen, K. H. C. Chen, C.-L. Chen and M. K. Chan, *Angewandte Chemie-International Edition*, 2007, **46**, 1992-1994.
218. S. I. Chan, K. H. C. Chen, S. S. F. Yu, C. L. Chen and S. S. J. Kuo, *Biochemistry*, 2004, **43**, 4421-4430.
219. S. S. F. Yu, K. H. C. Chen, M. Y. H. Tseng, Y. S. Wang, C. F. Tseng, Y. J. Chen, D. S. Huang and S. I. Chan, *Journal of Bacteriology*, 2003, **185**, 5915-5924.
220. M. Martinho, D. W. Choi, A. A. DiSpirito, W. E. Antholine, J. D. Semrau and E. Muenck, *J. Am. Chem. Soc.*, 2007, **129**, 15783-15785.
221. H. H. T. Nguyen, K. H. Nakagawa, B. Hedman, S. J. Elliott, M. E. Lidstrom, K. O. Hodgson and S. I. Chan, *J. Am. Chem. Soc.*, 1996, **118**, 12766-12776.
222. K. H. C. Chen, C. L. Chen, C. F. Tseng, S. S. F. Yu, S. C. Ke, J. F. Lee, H. T. Nguyen, S. J. Elliott, J. O. Alben and S. I. Chan, *Journal of the Chinese Chemical Society*, 2004, **51**, 1081-1098.
223. S. C. Hung, C. L. Chen, K. H. C. Chen, S. S. F. Yu and S. I. Chan, *Journal of the Chinese Chemical Society*, 2004, **51**, 1229-1244.
224. E. A. Lewis and W. B. Tolman, *Chemical Reviews*, 2004, **104**, 1047-1076.
225. N. J. Gunsalus, A. Koppaka, S. H. Park, S. M. Bischof, B. G. Hashiguchi and R. A. Periana, *Chemical Reviews*, 2017, **117**, 8521-8573.
226. J. A. Labinger and J. E. Bercaw, *Nature*, 2002, **417**, 507-514.
227. J. L. Bennett and P. T. Wolczanski, *J. Am. Chem. Soc.*, 1997, **119**, 10696-10719.
228. G. Luinstra, L. Wang, S. Stahl, J. Labinger and J. Bercaw, *Journal of organometallic chemistry*, 1995, **504**, 75-91.
229. A. E. Shilov and G. B. Shul'pin, *Russian Chemical Reviews*, 1987, **56**, 442.
230. M. Lin, C. Shen, E. A. Garcia-Zayas and A. Sen, *J. Am. Chem. Soc.*, 2001, **123**, 1000-1001.
231. M. S. Freund, J. A. Labinger, N. S. Lewis and J. E. Bercaw, *Journal of molecular catalysis*, 1994, **87**, L11-L15.
232. R. A. Periana, D. J. Taube, E. R. Evitt, D. G. Loffler, P. R. Wentrcek, G. Voss and T. Masuda, *Science*, 1993, **259**, 340-343.
233. R. A. Periana, D. J. Taube, S. Gamble, H. Taube, T. Satoh and H. Fujii, *Science*, 1998, **280**, 560-564.
234. J. Allison, *Progress in inorganic chemistry*, 1986, 627-676.
235. P. Watson, J. Liebman and A. Greenberg, *Selective Hydrocarbon Activation*, VCH Publishers, Inc.: New York, 1990.
236. K. Eller and H. Schwarz, *Chemical Reviews*, 1991, **91**, 1121-1177.
237. Y. Shiota and K. Yoshizawa, *J. Am. Chem. Soc.*, 2000, **122**, 12317-12326.
238. A. Gannouni, F. o. Delbecq, M. Saïd Zina and P. Sautet, *Journal of Physical Chemistry A*, 2017, **121**, 5500-5508.
239. V. C.-C. Wang, S. Maji, P. P.-Y. Chen, H. K. Lee, S. S.-F. Yu and S. I. Chan, *Chemical Reviews*, 2017, **117**, 8574-8621.
240. B. Ipek, M. J. Wulfers, H. Kim, F. Göltl, I. Hermans, J. P. Smith, K. S. Booksh, C. M. Brown and R. F.

Lobo, *ACS Catalysis*, 2017, **7**, 4291-4303.
241. M. H. Mahyuddin, A. Staykov, Y. Shiota, M. Miyanishi and K. Yoshizawa, *ACS Catalysis*, 2017, **7**, 3741-3751.
242. T. Jackson, D. Jacobson and B. Freiser, *J. Am. Chem. Soc.*, 1984, **106**, 1252-1257.
243. D. Schröder and H. Schwarz, *Angewandte Chemie International Edition*, 1990, **29**, 1431-1433.
244. D. Schroeder, A. Fiedler, M. F. Ryan and H. Schwarz, *Journal of Physical Chemistry*, 1994, **98**, 68-70.
245. D. Clemmer, Y.-M. Chen, F. A. Khan and P. Armentrout, *Journal of Physical Chemistry*, 1994, **98**, 6522-6529.
246. D. Schröder and H. Schwarz, *Helvetica Chimica Acta*, 1992, **75**, 1281-1287.
247. D. Schrder, H. Florencio, W. Zummack and H. Schwarz, *Helvetica Chimica Acta*, 1992, **75**, 1792-1797
248. H. Becker, D. Schroeder, W. Zummack and H. Schwarz, *J. Am. Chem. Soc.*, 1994, **116**, 1096-1100.
249. M. F. Ryan, A. Fiedler, D. Schroeder and H. Schwarz, *Organometallics*, 1994, **13**, 4072-4081.
250. K. K. Irikura and J. Beauchamp, *J. Am. Chem. Soc.*, 1989, **111**, 75-85.
251. P. B. Grosshans and A. G. Marshall, *Analytical Chemistry*, 1991, **63**, 2057-2061.
252. D. Clemmer, N. Aristov and P. Armentrout, *Journal of Physical Chemistry*, 1993, **97**, 544-552.
253. M. Azzaro, S. Breton, M. Decouzon and S. Geribaldi, *International journal of mass spectrometry and ion processes*, 1993, **128**, 1-20.
254. K. Liu and J. Parson, *Journal of Physical Chemistry*, 1979, **83**, 970-973.
255. J. M. Parnis, R. D. Lafleur and D. M. Rayner, *Chemical physics letters*, 1994, **218**, 544-550.
256. H. Kang and J. Beauchamp, *J. Am. Chem. Soc.*, 1986, **108**, 5663-5668.
257. R. Wesendrup, D. Schroder and H. Schwarz, *Angewandte Chemie-International Edition*, 1994, **33**, 1174-1176.
258. D. Olson, W. Haag and R. Lago, *Journal of Catalysis*, 1980, **61**, 390-396.
259. C. Zicovich-Wilson, A. Corma and P. Viruela, *Journal of Physical Chemistry*, 1994, **98**, 10863-10870.
260. A. Corma, H. García, G. Sastre and P. M. Viruela, *Journal of Physical Chemistry B*, 1997, **101**, 4575-4582.
261. M. H. Mahyuddin, A. Staykov, Y. Shiota and K. Yoshizawa, *ACS Catalysis*, 2016, **6**, 8321-8331.
262. Y. Jin, C. Sun and S. Su, *Physical Chemistry Chemical Physics*, 2015, **17**, 16277-16284.
263. J. Anderson and P. Tsai, *Journal of the Chemical Society, Chemical Communications*, 1987, 1435-1436.
264. V. Sobolev, A. Kharitonov, Y. A. Paukshtis and G. Panov, *Journal of molecular catalysis*, 1993, **84**, 117-124.
265. G. Panov, G. Sheveleva, A. e. a. Kharitonov, V. Romannikov and L. Vostrikova, *Applied Catalysis A: General*, 1992, **82**, 31-36.
266. G. Pannov, V. Sobolev and A. Kharitonov, *Journal of molecular catalysis*, 1990, **61**, 85-97.
267. V. Sobolev, K. Dubkov, O. Panna and G. Panov, *Catalysis Today*, 1995, **24**, 251-252.
268. K. Dubkov, V. Sobolev, E. Talsi, M. Rodkin, N. Watkins, A. Shteinman and G. Panov, *Journal of Molecular Catalysis A: Chemical*, 1997, **123**, 155-161.
269. M. H. Groothaert, P. J. Smeets, B. F. Sels, P. A. Jacobs and R. A. Schoonheydt, *J. Am. Chem. Soc.*, 2005, **127**, 1394-1395.
270. E. M. Alayon, M. Nachtegaal, M. Ranocchiari and J. A. van Bokhoven, *Chemical Communications*, 2012, **48**, 404-406.
271. G. Panov, A. Kharitonov and V. Sobolev, *Applied Catalysis A: General*, 1993, **98**, 1-20.
272. A. M. Volodin, V. A. Bolshov and G. I. Panov, *Journal of Physical Chemistry*, 1994, **98**, 7548-7550.
273. M. Filatov, A. Pelmenschikov and G. Zhidomirov, *Journal of molecular catalysis*, 1993, **80**, 243-251.
274. E. Starokon, K. Dubkov, L. Pirutko and G. Panov, *Topics in Catalysis*, 2003, **23**, 137-143.
275. V. I. Sobolev, O. N. Kovalenko, A. S. Kharitonov, Y. D. Pankrat'ev and G. I. Panov, *Mendeleev Communications*, 1991, **1**, 29-30.
276. K. Dubkov, N. Ovanesyan, A. Shteinman, E. Starokon and G. Panov, *Journal of Catalysis*, 2002, **207**, 341-352.
277. A. Arbuznikov and G. Zhidomirov, *Catalysis Letters*, 1996, **40**, 17-23.
278. L. Que and Y. Dong, *Accounts of Chemical Research*, 1996, **29**, 190-196.
279. K. Yoshizawa, Y. Shiota, T. Yumura and T. Yamabe, *Journal of Physical Chemistry B*, 2000, **104**, 734-740.
280. K. Yoshizawa, Y. Shiota and T. Yamabe, *Chemistry–A European Journal*, 1997, **3**, 1160-1169.
281. K. Yoshizawa, Y. Shiota and T. Yamabe, *J. Am. Chem. Soc.*, 1998, **120**, 564-572.
282. D. E. De Vos, M. Dams, B. F. Sels and P. A. Jacobs, *Chemical Reviews*, 2002, **102**, 3615-3640.
283. R. Hamada, Y. Shibata, S. Nishiyama and S. Tsuruya, *Physical Chemistry Chemical Physics*, 2003, **5**, 956-965.
284. M. Shelef, *Chemical Reviews*, 1995, **95**, 209-225.

285. H. Yahiro and M. Iwamoto, *Applied Catalysis A: General*, 2001, **222**, 163-181.
286. M. H. Groothaert, J. A. van Bokhoven, A. A. Battiston, B. M. Weckhuysen and R. A. Schoonheydt, *J. Am. Chem. Soc.*, 2003, **125**, 7629-7640.
287. E. M. C. Alayon, M. Nachtegaal, A. Bodi and J. A. van Bokhoven, *ACS Catalysis*, 2014, **4**, 16-22.
288. C. Hammond, M. M. Forde, M. H. Ab Rahim, A. Thetford, Q. He, R. L. Jenkins, N. Dimitratos, J. A. Lopez-Sanchez, N. F. Dummer and D. M. Murphy, *Angewandte Chemie International Edition*, 2012, **51**, 5129-5133.
289. A. Itadani, T. Yumura, T. Ohkubo, H. Kobayashi and Y. Kuroda, *Physical Chemistry Chemical Physics*, 2010, **12**, 6455-6465.
290. P. Vanelderen, R. G. Hadt, P. J. Smeets, E. I. Solomon, R. A. Schoonheydt and B. F. Sels, *Journal of Catalysis*, 2011, **284**, 157-164.
291. P. Vanelderen, B. E. Snyder, M.-L. Tsai, R. G. Hadt, J. Vancauwenbergh, O. Coussens, R. A. Schoonheydt, B. F. Sels and E. I. Solomon, *J. Am. Chem. Soc.*, 2015, **137**, 6383-6392.
292. B. Wathen, M. Kuiper, V. Walker and Z. Jia, *J. Am. Chem. Soc.*, 2003, **125**, 729-737.
293. P. J. Smeets, M. H. Groothaert and R. A. Schoonheydt, *Catalysis Today*, 2005, **110**, 303-309.
294. R. A. Himes and K. D. Karlin, *Proceedings of the National Academy of Sciences*, 2009, **106**, 18877-18878.
295. J. S. Woertink, L. Tian, D. Maiti, H. R. Lucas, R. A. Himes, K. D. Karlin, F. Neese, C. Würtele, M. C. Holthausen and E. Bill, *Inorganic Chemistry*, 2010, **49**, 9450-9459.
296. P. J. Smeets, R. G. Hadt, J. S. Woertink, P. Vanelderen, R. A. Schoonheydt, B. F. Sels and E. I. Solomon, *J. Am. Chem. Soc.*, 2010, **132**, 14736-14738.
297. R. A. Himes, K. Barnese and K. D. Karlin, *Angewandte Chemie International Edition*, 2010, **49**, 6714-6716.
298. D. Palagin, A. J. Knorpp, A. B. Pinar, M. Ranocchiari and J. A. van Bokhoven, *Nanoscale*, 2017, **9**, 1144-1153.
299. J. S. Woertink, P. J. Smeets, M. H. Groothaert, M. A. Vance, B. F. Sels, R. A. Schoonheydt and E. I. Solomon, *Proceedings of the National Academy of Sciences*, 2009, **106**, 18908-18913.
300. A. Burkhardt, E. T. Spielberg, H. Görls and W. Plass, *Inorganic Chemistry*, 2008, **47**, 2485-2493.
301. E. I. Solomon, J. W. Ginsbach, D. E. Heppner, M. T. Kieber-Emmons, C. H. Kjaergaard, P. J. Smeets, L. Tian and J. S. Woertink, *Faraday Discussions*, 2011, **148**, 11-39.
302. S. I. Chan, V. C. C. Wang, J. C. H. Lai, S. S. F. Yu, P. P. Y. Chen, K. H. C. Chen, C. L. Chen and M. K. Chan, *Angewandte Chemie International Edition*, 2007, **46**, 1992-1994.
303. G. Li, P. Vassilev, M. Sanchez-Sanchez, J. A. Lercher, E. J. Hensen and E. A. Pidko, *Journal of catalysis*, 2016, **338**, 305-312.
304. S. Grundner, M. A. Markovits, G. Li, M. Tromp, E. A. Pidko, E. J. Hensen, A. Jentys, M. Sanchez-Sanchez and J. A. Lercher, *Nature Communications*, 2015, **6**, 7546.
305. G. Centi and S. Perathoner, *Applied Catalysis A: General*, 1995, **132**, 179-259.
306. Y. Kuroda and M. Iwamoto, *Topics in Catalysis*, 2004, **28**, 111-118.
307. M. H. Groothaert, K. Lievens, H. Leeman, B. M. Weckhuysen and R. A. Schoonheydt, *Journal of Catalysis*, 2003, **220**, 500-512.
308. E. M. C. Alayon, M. Nachtegaal, A. Bodi, M. Ranocchiari and J. A. van Bokhoven, *Physical Chemistry Chemical Physics*, 2015, **17**, 7681-7693.
309. V. A. Veefkind, M. L. Smidt and J. A. Lercher, *Applied Catalysis A: General*, 2000, **194**, 319-332.
310. N. Dietl, M. Schlangen and H. Schwarz, *Angewandte Chemie International Edition*, 2012, **51**, 5544-5555.
311. P. Tomkins, A. Mansouri, S. E. Bozbag, F. Krumeich, M. B. Park, E. M. C. Alayon, M. Ranocchiari and J. A. van Bokhoven, *Angewandte Chemie International Edition*, 2016, **55**, 5467-5471.
312. N. V. Beznis, B. M. Weckhuysen and J. H. Bitter, *Catalysis Letters*, 2010, **138**, 14-22.
313. P. Vanelderen, J. Vancauwenbergh, M. L. Tsai, R. G. Hadt, E. I. Solomon, R. A. Schoonheydt and B. F. Sels, *ChemPhysChem*, 2014, **15**, 91-99.
314. A. A. Verma, S. A. Bates, T. Anggara, C. Paolucci, A. A. Parekh, K. Kamasamudram, A. Yezerets, J. T. Miller, W. N. Delgass and W. F. Schneider, *Journal of Catalysis*, 2014, **312**, 179-190.
315. Z.-J. Zhao, A. Kulkarni, L. Vilella, J. K. Nørskov and F. Studt, *ACS Catalysis*, 2016, **6**, 3760-3766.
316. M. J. Wulfers, S. Teketel, B. Ipek and R. F. Lobo, *Chemical Communications*, 2015, **51**, 4447-4450.
317. N. V. Beznis, B. M. Weckhuysen and J. H. Bitter, *Catalysis Letters*, 2010, **136**, 52-56.
318. N. V. Beznis, A. N. Van Laak, B. M. Weckhuysen and J. H. Bitter, *Microporous and Mesoporous Materials*, 2011, **138**, 176-183.
319. J. Shan, W. Huang, N. Luan, Y. Yu, S. Zhang, Y. Li, A. I. Frenkel and F. Tao, *Langmuir*, 2014, **30**, 8558-8569.
320. A. P. Grosvenor, M. C. Biesinger, R. S. C. Smart and N. S. McIntyre, *Surface Science*, 2006, **600**, 1771-

1779.
321. K. Narsimhan, V. K. Michaelis, G. Mathies, W. R. Gunther, R. G. Griffin and Y. Roman-Leshkov, *J. Am. Chem. Soc.*, 2015, **137**, 1825-1832.
322. I. Yamanaka, M. Soma and K. Oisuka, *Journal of the Chemical Society, Chemical Communications*, 1995, 2235-2236.
323. I. Yamanaka, M. Soma and K. Otsuka, *Research on Chemical Intermediates*, 2000, **26**, 129-135.
324. L. Wang, S. Zhang, Y. Zhu, A. Patlolla, J. Shan, H. Yoshida, S. Takeda, A. I. Frenkel and F. Tao, *ACS Catalysis*, 2013, **3**, 1011-1019.
325. S. Zhang, Y. Tang, L. Nguyen, Y.-F. Zhao, Z. Wu, T.-W. Goh, J. J. Liu, Y. Li, T. Zhu and W. Huang, *ACS Catalysis*, 2018, **8**, 110-121.
326. J. Shan, M. Li, L. F. Allard, S. Lee and M. Flytzani-Stephanopoulos, *Nature*, 2017, **551**, 605-608.
327. P. Ratnasamy and R. Kumar, *Catalysis Today*, 1991, **9**, 329-416.
328. A. Battiston, J. Bitter, W. Heijboer, F. De Groot and D. Koningsberger, *Journal of Catalysis*, 2003, **215**, 279-293.
329. J. Jia, Q. Sun, B. Wen, L. X. Chen and W. M. Sachtler, *Catalysis Letters*, 2002, **82**, 7-11.
330. A. Battiston, J. Bitter and D. Koningsberger, *Journal of Catalysis*, 2003, **218**, 163-177.
331. J. Xu, R. D. Armstrong, G. Shaw, N. F. Dummer, S. J. Freakley, S. H. Taylor and G. J. Hutchings, *Catalysis Today*, 2016, **270**, 93-100.
332. C. Hammond, R. L. Jenkins, N. Dimitratos, J. A. Lopez-Sanchez, M. H. Ab Rahim, M. M. Forde, A. Thetford, D. M. Murphy, H. Hagen and E. E. Stangland, *Chemistry–A European Journal*, 2012, **18**, 15735-15745.
333. B. Ensing, F. Buda, P. E. Blöchl and E. J. Baerends, *Physical Chemistry Chemical Physics*, 2002, **4**, 3619-3627.
334. B. Ensing, F. Buda, M. C. Gribnau and E. J. Baerends, *J. Am. Chem. Soc.*, 2004, **126**, 4355-4365.
335. C. Hammond, N. Dimitratos, R. L. Jenkins, J. A. Lopez-Sanchez, S. A. Kondrat, M. Hasbi ab Rahim, M. M. Forde, A. Thetford, S. H. Taylor and H. Hagen, *ACS Catalysis*, 2013, **3**, 689-699.
336. C. Kalamaras, D. Palomas, R. Bos, A. Horton, M. Crimmin and K. Hellgardt, *Catalysis Letters*, 2016, **146**, 483-492.
337. M. Shahami and D. F. Shantz, *Catalysis Science & Technology*, 2019, **9**, 2945-2951.
338. X. Cui, H. Li, Y. Wang, Y. Hu, L. Hua, H. Li, X. Han, Q. Liu, F. Yang, L. He, X. Chen, Q. Li, J. Xiao, D. Deng and X. Bao, *Chem*, 2018, **4**, 1902-1910.
339. W. X. Huang, S. R. Zhang, Y. Tang, Y. T. Li, L. Nguyen, Y. Y. Li, J. J. Shan, D. Q. Xiao, R. Gagne, A. I. Frenkel and F. Tao, *Angewandte Chemie-International Edition*, 2016, **55**, 13441-13445.
340. S. Yashnik and Z. Ismagilov, *Applied Catalysis B: Environmental*, 2015, **170**, 241-254.
341. S. Yashnik and Z. Ismagilov, *Kinetics and Catalysis*, 2016, **57**, 776-796.
342. S. A. Yashnik, V. V. Boltenkov, D. E. Babushkin, O. P. Taran and V. N. Parmon, *Topics in Catalysis*, 2020, 1-19.
343. S. Bai, F. Liu, B. Huang, F. Li, H. Lin, T. Wu, M. Sun, J. Wu, Q. Shao, Y. Xu and X. Huang, *Nature Communications*, 2020, **11**, 954.
344. Y. Kwon, T. Y. Kim, G. Kwon, J. Yi and H. Lee, *J. Am. Chem. Soc.*, 2017, **139**, 17694-17699.
345. N. Agarwal, S. J. Freakley, R. U. McVicker, S. M. Althahban, N. Dimitratos, Q. He, D. J. Morgan, R. L. Jenkins, D. J. Willock, S. H. Taylor, C. J. Kiely and G. J. Hutchings, *Science*, 2017, **358**, 223-226.
346. J. K. Edwards, B. Solsona, E. Ntainjua, A. F. Carley, A. A. Herzing, C. J. Kiely and G. J. Hutchings, *Science*, 2009, **323**, 1037-1041.
347. J. K. Edwards, B. E. Solsona, P. Landon, A. F. Carley, A. Herzing, C. J. Kiely and G. J. Hutchings, *Journal of Catalysis*, 2005, **236**, 69-79.
348. Z. Jin, L. Wang, E. Zuidema, K. Mondal, M. Zhang, J. Zhang, C. Wang, X. Meng, H. Yang and C. Mesters, *Science*, 2020, **367**, 193-197.
349. H. D. Gesser, N. R. Hunter and C. B. Prakash, *Chemical Reviews*, 1985, **85**, 235-244.
350. A. Butler, M. J. Clague and G. E. Meister, *Chemical Reviews*, 1994, **94**, 625-638.
351. G. Shul'pin, D. Attanasio and L. Suber, *Russian chemical bulletin*, 1993, **42**, 55-59.
352. G. V. Nizova, G. Süss-Fink and G. B. Shul'pin, *Chemical Communications*, 1997, 397-398.
353. G. Süss-Fink, G. V. Nizova, S. Stanislas and G. B. Shul'pin, *Journal of Molecular Catalysis A: Chemical*, 1998, **130**, 163-170.
354. I. Arends, K. Ingold and D. Wayner, *J. Am. Chem. Soc.*, 1995, **117**, 4710-4711.
355. J. Kim, R. G. Harrison, C. Kim and L. Que, *J. Am. Chem. Soc.*, 1996, **118**, 4373-4379.
356. R. H. Fish, M. S. Konings, K. J. Oberhausen, R. H. Fong, W. M. Yu, G. Christou, J. B. Vincent, D. K. Coggin and R. M. Buchanan, *Inorganic Chemistry*, 1991, **30**, 3002-3006.
357. Y. Seki, N. Mizuno and M. Misono, *Applied Catalysis A: General*, 1997, **158**, L47-L51.
358. X. Wei, L. Ye and Y. Yuan, *Journal of natural gas chemistry*, 2009, **18**, 295-299.

359. Q. Yuan, W. Deng, Q. Zhang and Y. Wang, *Advanced Synthesis & Catalysis*, 2007, **349**, 1199-1209.
360. M. Schroeder, *Chemical Reviews*, 1980, **80**, 187-213.
361. H. C. Kolb, M. S. VanNieuwenhze and K. B. Sharpless, *Chemical Reviews*, 1994, **94**, 2483-2547.
362. A. B. Sorokin, E. V. Kudrik and D. Bouchu, *Chemical Communications*, 2008, 2562-2564.
363. Ü. İşci, A. S. Faponle, P. Afanasiev, F. Albrieux, V. Briois, V. Ahsen, F. Dumoulin, A. B. Sorokin and S. P. de Visser, *Chemical Science*, 2015, **6**, 5063-5075.
364. M. G. Quesne, D. Senthilnathan, D. Singh, D. Kumar, P. Maldivi, A. B. Sorokin and S. P. de Visser, *ACS Catalysis*, 2016, **6**, 2230-2243.
365. P. Afanasiev and A. B. Sorokin, *Accounts of Chemical Research*, 2016, **49**, 583-593.
366. E. V. Kudrik, P. Afanasiev, L. X. Alvarez, P. Dubourdeaux, M. Clémancey, J.-M. Latour, G. Blondin, D. Bouchu, F. Albrieux and S. E. Nefedov, *Nature Chemistry*, 2012, **4**, 1024-1029.
367. S. A. Ikbal, C. Colomban, D. Zhang, M. Delecluse, T. Brotin, V. Dufaud, J.-P. Dutasta, A. B. Sorokin and A. Martinez, *Inorganic Chemistry*, 2019, **58**, 7220-7228.